Electronic Supplementary Information

Rational Engineering of Amide Synthetase Enables Bioconversion to Diverse Xiamenmycin Derivatives

Jing-Yi Weng[1], Xu-Liang Bu[2], Bei-Bei He[2], Zhuo Cheng[2], Jun Xu[2], Lin-Tai Da[1]* and Min-Juan Xu[1]*

[1] Key Laboratory of Systems Biomedicine (Ministry of Education), Shanghai Centre for Systems Biomedicine, Shanghai Jiao Tong University, Shanghai 200240, P. R. China

[2] State Key Laboratory of Microbial Metabolism, School of Life Sciences and Biotechnology, Shanghai Jiao Tong University, Shanghai 200240, P. R. China

*Correspondence and requests for materials should be addressed to L. D. (darlt@sjtu.edu.cn), M. X. (minjuanxu@sjtu.edu.cn)

KEYWORDS: *rational design, amide synthetase, bioconversion, catalytic promiscuity, structural diversity*

Experimental section

Materials

All chemicals and reagents used for biochemical and molecular assays were purchased from standard commercial sources. The PrimeSTAR Max DNA Polymerase and pET vector were purchased from TaKaRa (Dalian, China), while restriction endonucleases and T4 DNA ligase were purchased from Thermo Fisher Scientific (Waltham, MA, USA). Malachite Green Phosphate Assay Kit was bought from Bioassay System and the inorganic pyrophosphatase was bought from Sigma-Aldrich (Switzerland).

Strains and Plasmids

E. coli DH5α was used as the host for cloning and *E. coli* Rosetta (DE3) was used as the host for protein expression. Plasmid pET28a was purchased from Novagen (United States). All the strains and plasmids used in this study are listed in the Table S6.

Construction of expression vectors for XimA and site-directed mutants

The *ximA* gene was amplified from genomic DNA of *S. xiamenensis* 318 using the primer pair XimA-F/XimB-R and inserted into pET28a. Point mutations were introduced into XimA to obtain mutant proteins (L185A, F244A, F270A, T295A, V304A, F201A, Y296A, T299A, D375A, R390A, K492A, F201C, F201M, F201N, F201Q, F201S, F201T and N490A), by engineering the above mentioned XimA-expressing plasmid using primers listed in Table S7 by overlap extension PCR. The PCR fragments were cloned into the pET28a expression vector using the restriction sites of *Bam*HI and *Hind*III. Plasmid constructions were confirmed by restriction enzyme digestions and DNA sequencing, the positive plasmids were transformed into *E. coli* Rosetta (DE3).

Protein expression and purification

The recombinant *E. coli* Rosetta (DE3) cells were grown in 2 L Luria-Bertani broth (LB) containing 34 μg/mL chloramphenicol and 50 μg/mL kanamycin at 37 °C, 220 rpm. When the

OD_{600} reached 0.6 - 0.8, isopropyl β-D-thiogalactoside (IPTG) was added at the final concentration of 0.1 mM and the cells were cultured at 16 °C for 20 h, 180 rpm.

For purification, the cells were harvested by centrifugation (8,000 rpm, 10 min, 4 °C), resuspended in 50 mL of lysis buffer (20 mM Tris-HCl, 300 mM NaCl, 2 mM $MgCl_2$, 10% glycerol and 1mM dithiothreitol, pH 8.0), and lysed by sonication in ice bath. The insoluble material was separated by centrifugation (10,000 rpm, 1 h, 4 °C), and the soluble fraction was incubated with 2 mL nickel-nitrilotriacetic acid-agarose resin (Sangon Biotech, P. R. China) in a gravity flow column. The column was washed with 50 mL of wash buffer (20 mM Tris-HCl, 300 mM NaCl, 2 mM $MgCl_2$, 10% glycerol, 1 mM dithiothreitol and 50 mM imidazole, pH 8.0), and eluted by elution buffer (20 mM Tris-HCl, 300 mM NaCl, 2 mM $MgCl_2$, 10% glycerol, 1 mM dithiothreitol and 500 mM imidazole, pH 8.0). The protein fractions were concentrated using Amicon Ultra filters (10 K) and further purified by size-exclusion chromatography using a Superdex 200 increase 10/300 column (GE Healthcare) in a buffer containing 10 mM Tris-HCl, 150 mM NaCl, and 5% glycerol, pH 7.5. The obtained proteins were greater than 95% pure as assessed by SDS-PAGE and stored at -80 °C for later use after a flash freezing in liquid nitrogen. The protein concentrations were measured using the Bradford method with bovine serum albumin (BSA) as standard.

The ATP-PP_i/ATP-P_i release assay

The PP_i or P_i released from ATP by XimA was measured using the Malachite Green Phosphate Assay Kit (Sigma-Aldrich, Switzerland).[1] The reaction contained 1 μM XimA, 0.25 mM xiamenmycin B (or 5 mM $_L$-threonine), 2 mM ATP, 5 mM $MgCl_2$, and 0.4 units/ml of inorganic pyrophosphatase in Tris-HCl buffer, pH 7.5. Each reaction was initiated by adding 2 mM ATP and carried out at 30 °C for 0, 3, 6, 10, 15, 20, and 30 min on a 96-well plate. The reaction mixtures were 20-fold diluted, and 80 μL diluents were added into wells pre-containing 20 μL of malachite green. Upon an incubation at room temperature for 30 min, the absorbance was monitored at 620 nm by Epoch Multi-Volume Spectrophotometer System (BioTek, USA). All PP_i/P_i releasing reactions were carried out in triplicate and the negative control was set up by using boiling inactivated XimA.

Enzymatic assay of XimA

To test the substrate selectivity of XimA, the reaction mixture, containing 1 μM XimA, 1 mM xiamenmycin B, 2 mM ATP, 5 mM different amino acids ($_{L}$-threonine and three stereoisomers of $_{L}$-threonine, as well as nineteen native $_{L}$-type and eighteen $_{D}$-type amino acids), and 5 mM $MgCl_2$ in 100 μL Tris-HCl buffer (pH 7.5) was incubated at 30 ℃ for 12 h. To explore the effects of predicted active sites, an appropriate amount of purified mutant enzymes were incubated with 1 mM xiamenmycin B, 2 mM ATP and 5 mM $MgCl_2$ towards 5 mM different amino acids in 100 μL Tris-HCl buffer (pH 7.5) at 30 ℃ for 12 h. The reaction was stopped by adding an equal volume of methanol and the mixture was separated by centrifugation (12,000 rpm, 5 min). Then the supernatant was analyzed by HPLC (Shimadzu, Japan) on an Extend-C18 reverse phase column (Agilent, 150 × 4.6 mm). The mobile phases were solvent A (water, containing 0.05% TFA) and solvent C (acetonitrile, containing 0.05% TFA). The conditions of gradient elution were as followings: 0 - 4 min, 30% C; 4 - 27 min, 30% - 80% B; 27 - 30 min, 30% B; flow rate: 1 mL/min; monitoring wavelength: 254 nm.

Analyses of kinetic parameters

XimA or F201A activity was separately measured at 30 °C in a 50 μL reaction volume, comprising xiamenmycin B, ATP, different amino acids, 82.5 μg protein, 5 mM $MgCl_2$ and 50 mM Tris-HCl (pH 7.5). Kinetic parameters for xiamenmycin B were determined when the concentration of ATP and amino acids maintained at 2 mM and the concentration of xiamenmycin B varied from 0 to 500 μM. Kinetic parameters for ATP were determined when the concentration of xiamenmycin B and amino acids maintained at 2 mM and the concentration of ATP varied from 0 to 400 μM. Kinetic parameters for different amino acids were successively determined by varying the concentration of amino acid from 0 to 4000 μM. Each reaction was initiated by adding ATP and carried out at 30 °C for 1 h, and stopped by adding an equal volume of methanol. The mixture was separated and detected as described above. Reaction velocities and substrates concentrations were fitted to Michaelis-Menten equation by GraphPad Prism 7 (GraphPad Software, Inc., California) under the default parameters to obtain K_m and K_{cat} values.

Multiple sequence alignment and phylogenetic analysis

Multiple sequence alignment of XimA (AGY49247), BCL_M (2V7B_A), FadD22 (PIG31850), AcsA (BAD90933) and GrsA (NP_721708) was performed using MEGA7[2] and then analyzed by ESPript 3.0 (http://espript.ibcp.fr/ESPript/ESPript/). Phylogenetic analyses were conducted in MEGA7. The evolutionary history was inferred by the Maximum Likelihood method based on the JTT matrix-based model. The bootstrap consensus tree inferred from 100 replicates is taken to represent the evolutionary history of the taxa analyzed. The phylogenetic tree was further edited by EvolView.[3] Proteins in the tree include: GH3.6, *Arabidopsis thaliana* (AAX12878); GH3.8, *Oryza sativa Indica Group* (ABN13880); GH3.1, *Vitis vinifera* (XP_002283886); FtpA, *Aspergillus fumigatus* (ALO65124); DltA, *Bacillus velezensis* FZB42 (ABS75900); TycA, *Brevibacillus brevis* (AWX56246); ColD1, *S. aureus* (AIL50191); AsuD1, *S. nodosus* subsp. asukaensis (ADI58645); Orf33, *S. aizunensis* (AAX98208); SimL, *S. antibioticus* (AAL15599); BafY, *S. lohii* (ADC79614); CouL, *S. rishiriensis* (AAG29784); CloL, *S. roseochromogenus* subsp. oscitans DS 12.976 (AAN65228); NovL, *S. niveus* (AAF67505) ; YwfE, *Bacillus atrophaeus* UCMB-5137 (AKL86946); BacD, *Bacillus velezensis* SQR9 (AHZ17788); RizA, *Bacillus subtilis* (BAG72134).

Construction of xiamenmycin B-AMP bound XimA complex

The WT XimA structure was firstly constructed using the homology modeling strategy by employing the structure of a benzoate CoA ligase BCL_M (PDB id: 2V7B) as a homology template that shares a sequence identify of 26% with XimA. The SWISS-MODEL software was adopted for the model construction.[4] Based on the modeled XimA structure, we then docked the xiamenmycin B-AMP intermediate into the potential substrate-binding pocket according to one former obtained benzoate-AMP bound CoA ligase complex (PDB id: 4zjz).[5] The molecular docking was performed using the AutoDock 4.2.6 software package with the default scoring function,[6] and the docking box size was set to 50 Å. The docking complex with the highest binding affinity was used as the final binding complex for the following structural analysis.

Equilibration of different intermediate-bound XimA complexes using MD simulations

To evaluate the mutational effects of the F201 site on protein dynamics, we conducted one

100-ns MD simulation for each of the WT, F201M, and F201A XimA in complex with xiamenmycin B-AMP intermediate. Based on the above WT intermediate-bound XimA model, the initial structures of the F201M and F201A variants were obtained using the PyMol software (www.pymol.org/). All the MD simulations were conducted using GPU-accelerated version of Gromacs-5.1 package.[7] The AMBER99SB fore field was employed to describe the protein structure.[8] The amber force fields of xiamenmycin B-AMP were generated using the Antechamber module implemented in the AmberTools package,[9-10] and the RESP charges were calculated after a full optimization of each base using the Hartree-Fork methods under the basis set of 6-31G*. Each XimA complex was centered in SPC-water box,[11] and 13 Na^+ ions were added to neutralize the protein charges. The cutoff values for the Van der Waals and short-range electrostatic interactions were set as 12Å, and the long-range electrostatic interactions were treated by the Particle-Mesh Ewald (PME) summation method.[12] All the chemical bonds were constrained using the LINCS algorithm.[13] Each complex was firstly subject to energy minimization using the steepest decent method, followed by a 500-ps NVT MD simulation by restraining the heavy atoms of the solute with an aim to fully relax the water molecules. Then, we gradually increased the system temperature from 50 K to 310 K within 200-ps NVT MD simulation. Finally, we conducted the equilibration 100-ns MD simulation at 310 K using the velocity rescaling thermostat.[14]

Obtaining various reactant-bound XimA complexes using molecular docking

We then attempt to obtain the amino acid-bound XimA complexes for the WT and F201A systems by performing molecular docking using the AutoDock 4.2.6 software package.[6] The receptor XimA structures were derived from the equilibrated conformation from each above MD simulations. For the WT system, the docking grid box size was confined in 30 × 30 × 30 Å and the box center was located at the O3 atom of xiamenmycin B-AMP in the XimA complex. The PDBQT parameters of both receptor and ligand $_L$-Thr were obtained by the AutoDock Tools-1.5.6 package.[6] One hundred docking poses were finally collected for clustering analyses and structural visualization by PyMol. In comparisons, we docked 11 amino acids with the F201A variants using the same docking setup as the above WT system, including $_L$-Thr, $_L$-Trp, $_L$-*allo*-Thr, $_L$-Ser, $_L$-Gly, $_L$-Ala, $_L$-Tyr, $_L$-Val, $_L$-Ile, $_L$-Phe and $_L$-Leu.

Identification of new compounds

The products were purified by semi-preparative HPLC under the following conditions: ZORBAX SB-C18 column (Agilent, 150 x 9.4 mm); olvent A: water, containing 0.05% TFA; solvent B: methanol, containing 0.05% TFA. The conditions of gradient elution were as followings: 0 - 5 min, 48% B; 5 - 30 min, 48% - 80% B; 30 - 34 min, 48% B; flow rate: 2 mL/min; monitoring wavelength: 254 nm.

UPLC-QTOF-MS was performed using a Waters Acquity UPLC system equipped with a Micromass Q-TOF Premier mass spectrometer (Waters MS Technologies, Manchester, UK). Chromatographic separations were performed on a 2.1 × 100 mm (1.7 μm) Acquity BEH C18 chromatography column. The column temperature was set at 45 °C, and the gradient elution program started from 5% B, changed to 30% B within 2 min, to 60% B within 2.5 min, to 100% B within 7.5 min, and was finally held at 100% B for 2 min (solvent A: aqueous solution of 0.1% formic acid; solvent B: ACN containing 0.1% formic acid). The flow rate was 0.40 mL/min. The eluate was directed to the mass spectrometer without splitting. Mass analysis was performed using a Q-TOF mass spectrometer equipped with an ESI source operating in the positive and negative ion modes.

^{1}H, ^{13}C NMR and 2D NMR spectra were acquired with an Avance III 600 MHz NMR spectrometer (Bruker, Germany). The NMR spectra were mostly recorded in DMSO-d_6 referenced to residual solvent signals with resonances at δ_H 2.49/δ_C 39.5 ppm.

Circular dichroism analysis

Circular dichroism (CD) spectra were obtained at room temperature by a spectropolarimeter (JASCO, Japan, Model J-815) in a quartz cuvette of 1 mm optical path length. Scanning of CD spectra occurred in Far UV region (190-260 nm) at 100 nm/min with a bandwidth of 0.5 nm. The secondary structures of XimA and its mutants, including α-helix, β-sheet, β-turn and random coil, were predicted by CDpro software online.

Surface Plasmon Resonance (SPR) assay

All binding kinetic experiments were performed at 25 ºC using Biacore T200 instrument equipped with a CM5 sensor chip (GE Healthcare, USA). The surface of the CM5 chip was pre-

activated with a 1:1 mixture of 0.05 M *N*-hydroxysuccinimide (NHS) and 0.2 M *N-ethyl-N'*-(3-dimethylaminopropyl) carbodiimide (EDC). For analysis of the interaction between XimA and three substrates, the protein XimA diluted to 90 μg/mL in 10 mM sodium acetate (pH 4.5) and three substrates were sequentially diluted with running buffer to different concentrations (xiamenmycin B: 0 - 50 μM; $_{L}$-threonine: 0 - 50 μM; ATP: 0 - 25 μM). The estimated K_D was obtained by fitting the association and dissociation signals with a 1:1 interaction model using the Biacore T200 Evaluation Software.

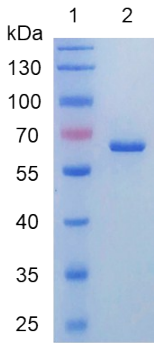

Figure S1. SDS-PAGE analysis of purified recombinant protein XimA.

Lane 1: protein maker, Thermo Scientific PageRuler Prestained Protein Ladder #26616;

lane 2: purified N-terminal 6 × His tagged XimA.

Protein	Substrate	K_m (μM)	K_{cat} (min^{-1})	$k_{cat}/K_m \times 10^{-3}$ ($\mu M^{-1}\ min^{-1}$)
WT	xiamenmycin B	144.7 ± 18.35	3.11 ± 0.16	21.51
	ATP	156.6 ± 23.16	2.66 ± 0.17	17.01
	L-Thr	768.2 ± 97.20	1.97 ± 0.14	2.57
F201A	xiamenmycin B	18.07 ± 1.59	0.70 ± 0.01	38.74
	ATP	21.25 ± 1.40	0.67 ± 0.01	31.53
	L-Thr	190.4 ± 21.49	0.39 ± 0.01	2.04

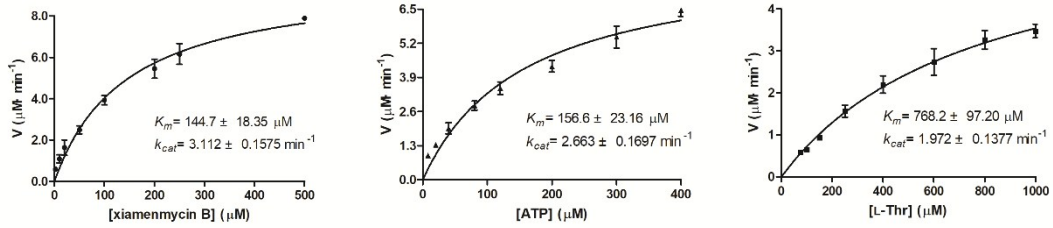

Figure S2. Kinetic parameters determination of XimA using xiamenmycin B, ATP and $_{L}$-Thr as substrates. Kinetic parameters for one substrate were determined when the concentrations of other two substrates remained unchanged.

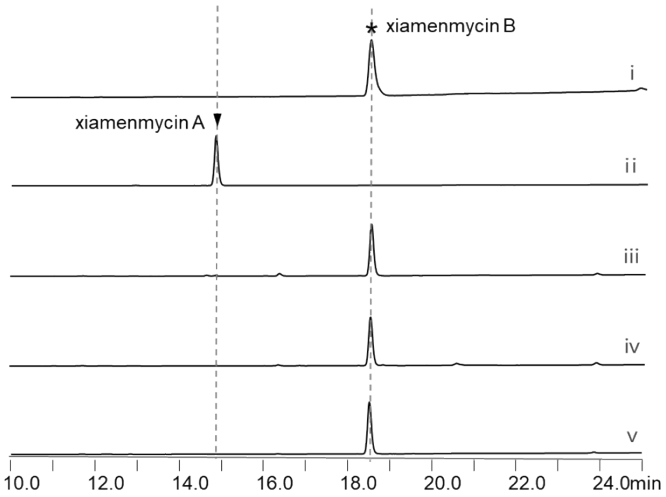

Figure S3. HPLC analysis (UV at 254 nm) of XimA catalytic reactions towards different substrates.

Trace: no amino acid as negative control (i), $_{L}$-Thr (ii), the mixture of $_{D}$-Thr, $_{L}$-*allo*-Thr, $_{D}$-*allo*-Thr (iii), nineteen native $_{L}$-type amino acids mixture (iv) and eighteen $_{D}$-type amino acids mixture (v). The reaction mixture contains 1 μM XimA, 1 mM xiamenmycin B, 2 mM ATP, 5 mM amino acid, and 5 mM $MgCl_2$ in 100 μL Tris-HCl buffer (pH 7.5) at 30 ℃ for 12 h.

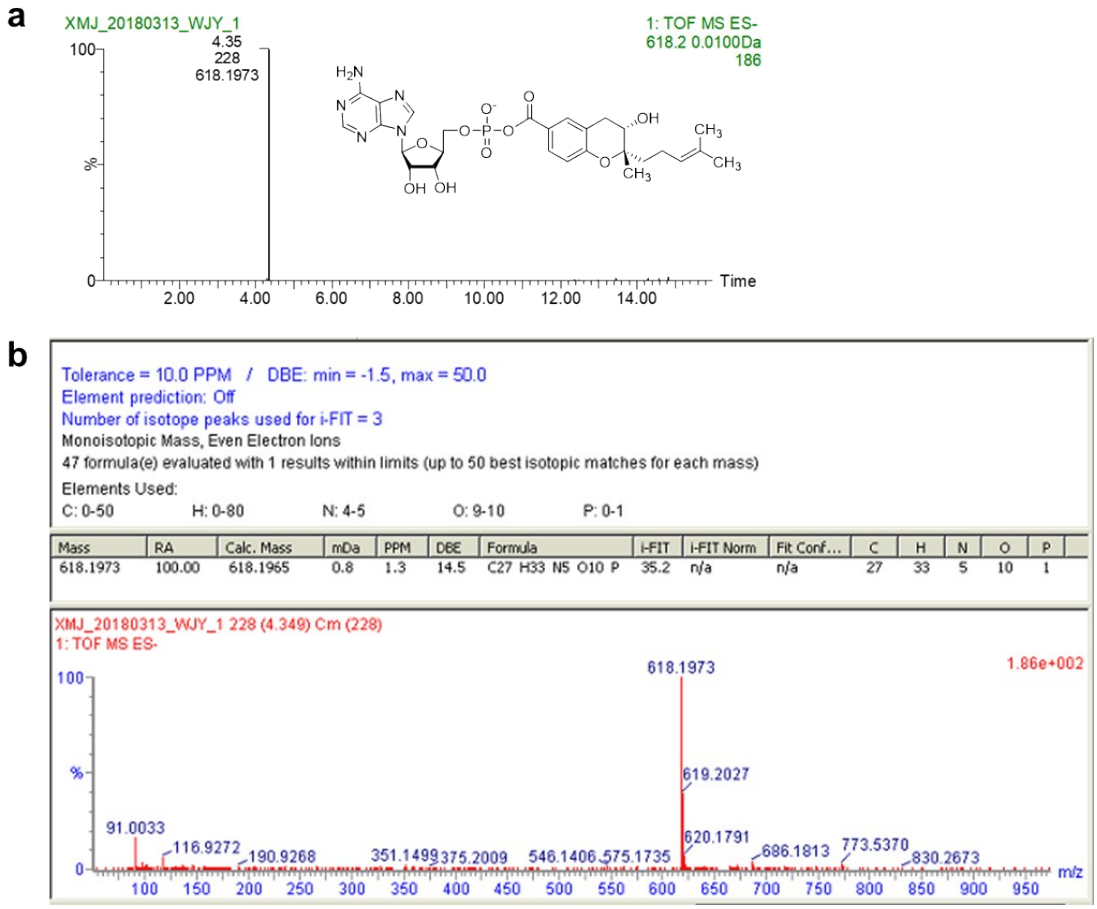

Figure S4. UPLC-QTOF-MS analysis of xiamenmycin B-AMP. (a) Extracted ion chromatogram of xiamenmycin B-AMP. (b) Elemental composition analysis of xiamenmycin B-AMP.

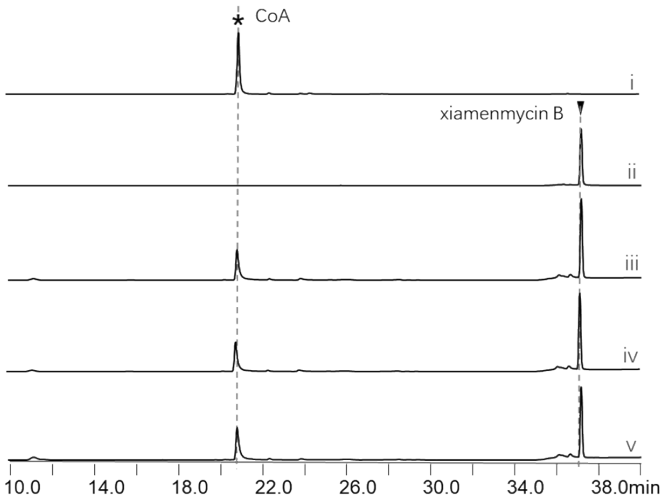

Figure S5. HPLC analysis (UV at 254 nm) of XimA catalytic reactions towards CoA.

(ⅰ) and (ⅱ) are authentic samples of CoA and xiamenmycin B, respectively. The reaction (ⅴ) contains 1 μM XimA, 2 mM xiamenmycin B, 2 mM ATP, 1 mM CoA, and 5 mM $MgCl_2$ in 100 μL Tris-HCl buffer (pH 7.5), at 30 ℃ for 12 h. Control reactions contain (ⅲ) without XimA and (ⅳ) with boiled XimA.

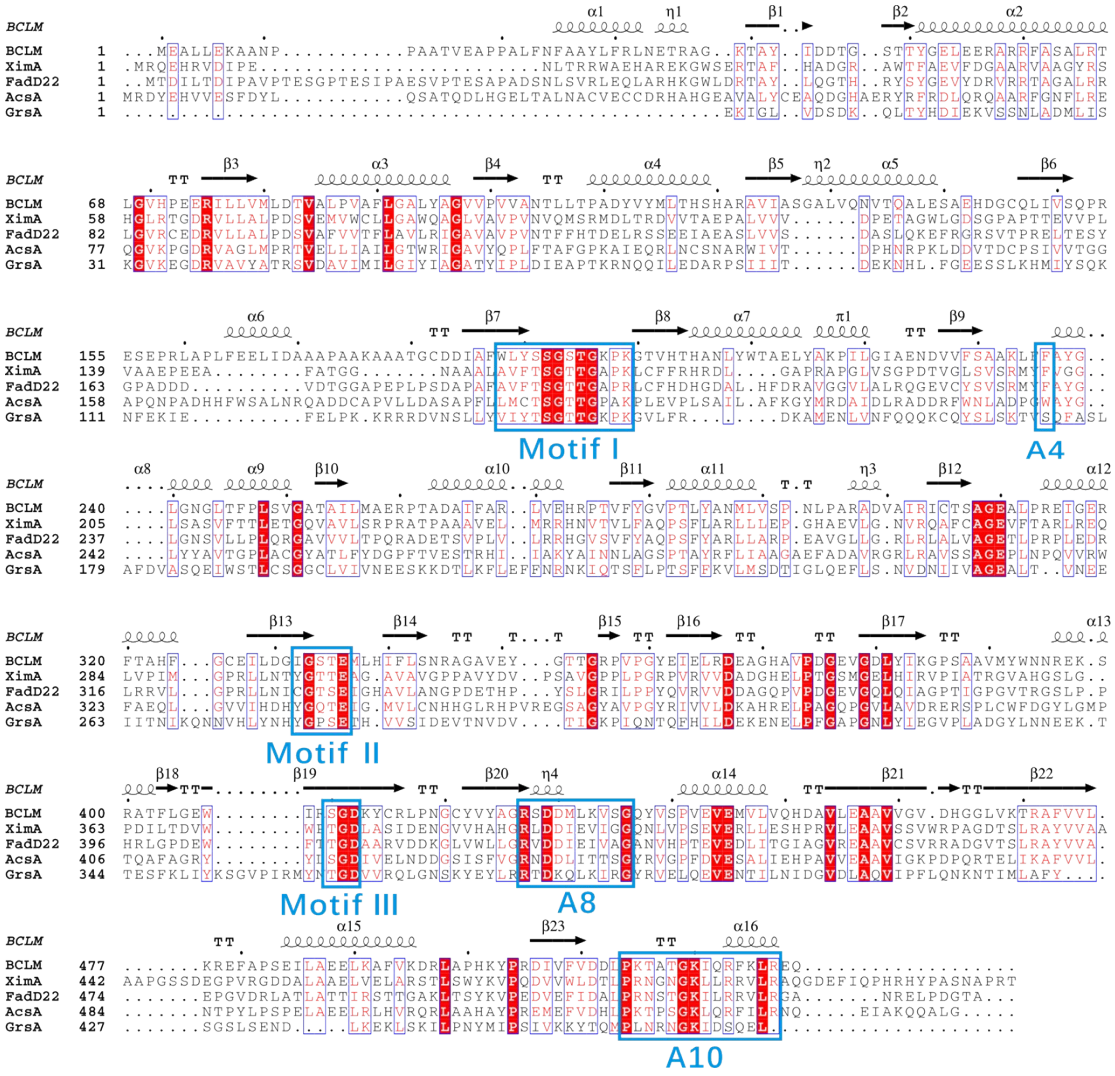

Figure S6. Multiple sequence alignment and secondary structure prediction of XimA with adenylating enzymes of ANL family.

Residues highlighted in white on a red background share a sequence identity of 100% homology; residues colored in red and framed in blue share a sequence identity of 80% - 100% homology. Conserved motifs, i.e., I, II, III, A4, A8, and A10 are underlined. The following proteins are used for the sequence analysis (accession numbers are given in parentheses): BCL_M (PDB ID: 2V7B), *Burkholderia xenovorans* Lb400 (2V7B_A); XimA, *Streptomyces xiamenensis* 318 (AGY49247); FadD22, *Streptomyces* sp. 93 (PIG31850); AcsA, *Pseudomonas chlororaphis* B23 (BAD90933); GrsA, *Streptococcus mutants* UA159 (NP_721708).

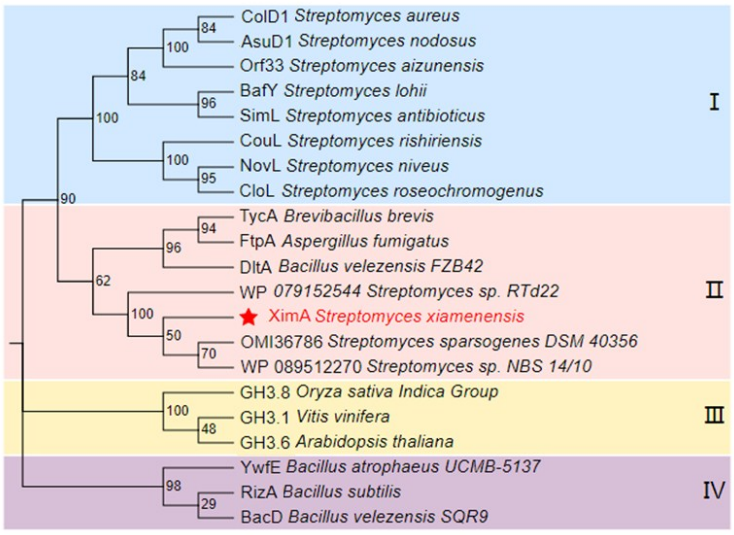

Figure S7. Phylogenetic analysis of XimA with its homologues and known amide synthetases.

The tree was divided into four distinct clades (I, II, III, and IV) and XimA is marked by a solid red star.

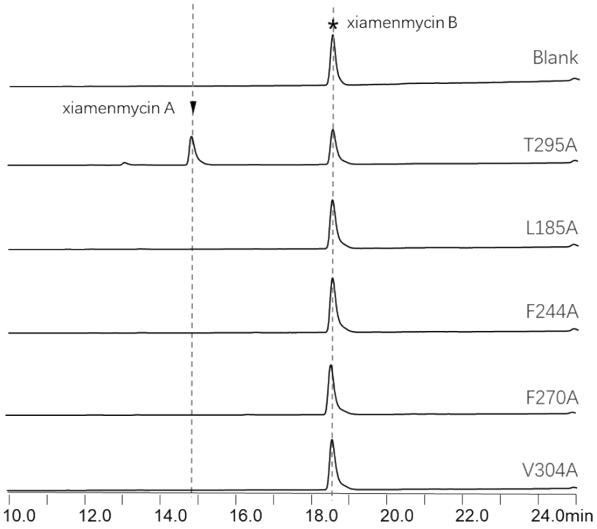

Figure S8. HPLC analysis (UV at 254 nm) of L185A, F244A, F270A, T295A, and V304A catalytic reactions.

The reaction contains 1 μM pure mutant protein, 1 mM xiamenmycin B, 2 mM ATP, 5 mM $_L$-Thr, and 5 mM $MgCl_2$ in 100 μL Tris-HCl buffer (pH 7.5) at 30 ℃ for 12 h. The reaction without enzyme was used as blank.

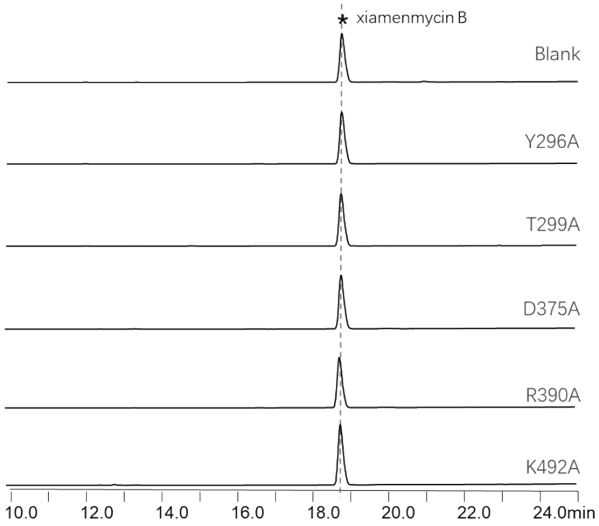

Figure S9. HPLC analysis (UV at 254 nm) of Y296A, T299A, D375A, R390A, and K492A catalytic reactions.

The reaction contains 1 μM enzyme, 1 mM xiamenmycin B, 2 mM ATP, 5 mM $_L$-Thr, and 5 mM $MgCl_2$ in 100 μL Tris-HCl buffer (pH 7.5) at 30 ℃ for 12 h. The reaction without enzyme was used as blank.

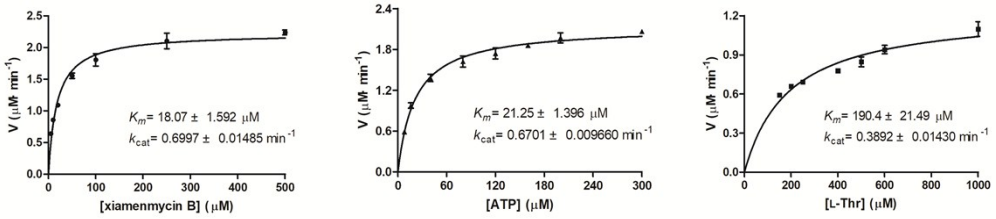

Figure S10. Kinetic parameters determination of F201A using xiamenmycin B, ATP and $_L$-Thr as substrates. Kinetic parameters for one substrate were determined when the concentrations of other two substrates remained unchanged.

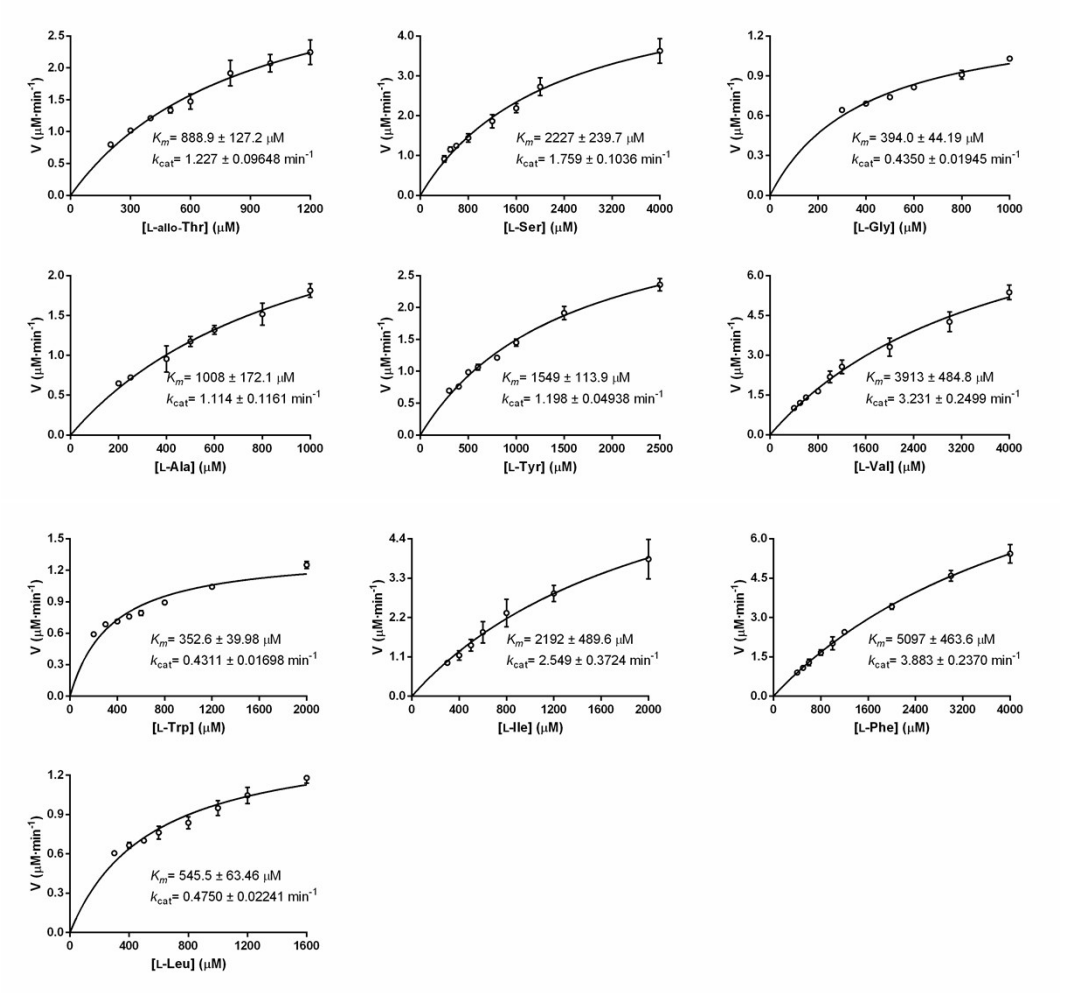

Figure S11. Kinetic parameters determination of F201A using different amino acids as substrates. Kinetic parameters for each amino acid were determined when the concentrations of xiamenmycin B and $_{L}$-Thr remained unchanged.

protein	amino acids can be utilized
F201A	$_{L}$-Phe, $_{L}$-Ala, $_{L}$-Ile, $_{L}$-Leu, $_{L}$-Trp, $_{L}$-Val, $_{L}$-Gln, $_{L}$-Gly, $_{L}$-Ser, $_{L}$-Tyr
F201C	$_{L}$-Phe, $_{L}$-Ala, $_{L}$-Ile, $_{L}$-Leu, $_{L}$-Trp, $_{L}$-Val, $_{L}$-Gln, $_{L}$-Gly, $_{L}$-Ser, $_{L}$-Tyr
F201M	$_{L}$-Phe, $_{L}$-Ala, $_{L}$-Ile, $_{L}$-Trp, $_{L}$-Val, $_{L}$-Gln, $_{L}$-Ser, $_{L}$-Tyr, $_{D}$-Ala, $_{D}$-Tyr, $_{D}$-Met, $_{D}$-Phe
F201N	$_{L}$-Phe, $_{L}$-Ala, $_{L}$-Ile, $_{L}$-Leu, $_{L}$-Trp, $_{L}$-Val, $_{L}$-Gln, $_{L}$-Gly, $_{L}$-Ser, $_{L}$-Tyr
F201Q	$_{L}$-Phe, $_{L}$-Ala, $_{L}$-Ile, $_{L}$-Trp, $_{L}$-Val, $_{L}$-Gly, $_{L}$-Ser, $_{L}$-Tyr
F201S	$_{L}$-Phe, $_{L}$-Ala, $_{L}$-Ile, $_{L}$-Trp, $_{L}$-Val, $_{L}$-Gln, $_{L}$-Gly, $_{L}$-Ser, $_{L}$-Tyr
F201T	$_{L}$-Ile, $_{L}$-Val, $_{L}$-Gln, $_{L}$-Ser

Figure S12. Substrate scope of position 201 mutants.

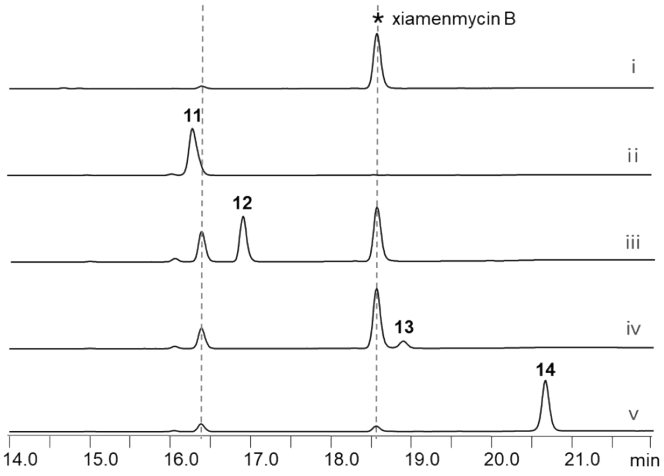

Figure S13. HPLC analysis (UV at 254 nm) of F201M catalytic reactions towards different amino acids.

Different amino acids, i.e., $_{D}$-Ala (ii), $_{D}$-Tyr (iii), $_{D}$-Met (iv) and $_{D}$-Phe (v) were used as substrates. The reaction contains 1 μM F201M, 1 mM xiamenmycin B, 2 mM ATP, 5 mM different amino acids, and 5 mM $MgCl_2$ in 100 μM Tris-HCl buffer (pH 7.5) at 30 ℃ for 12 h. The reaction without amino acid was used as blank (i).

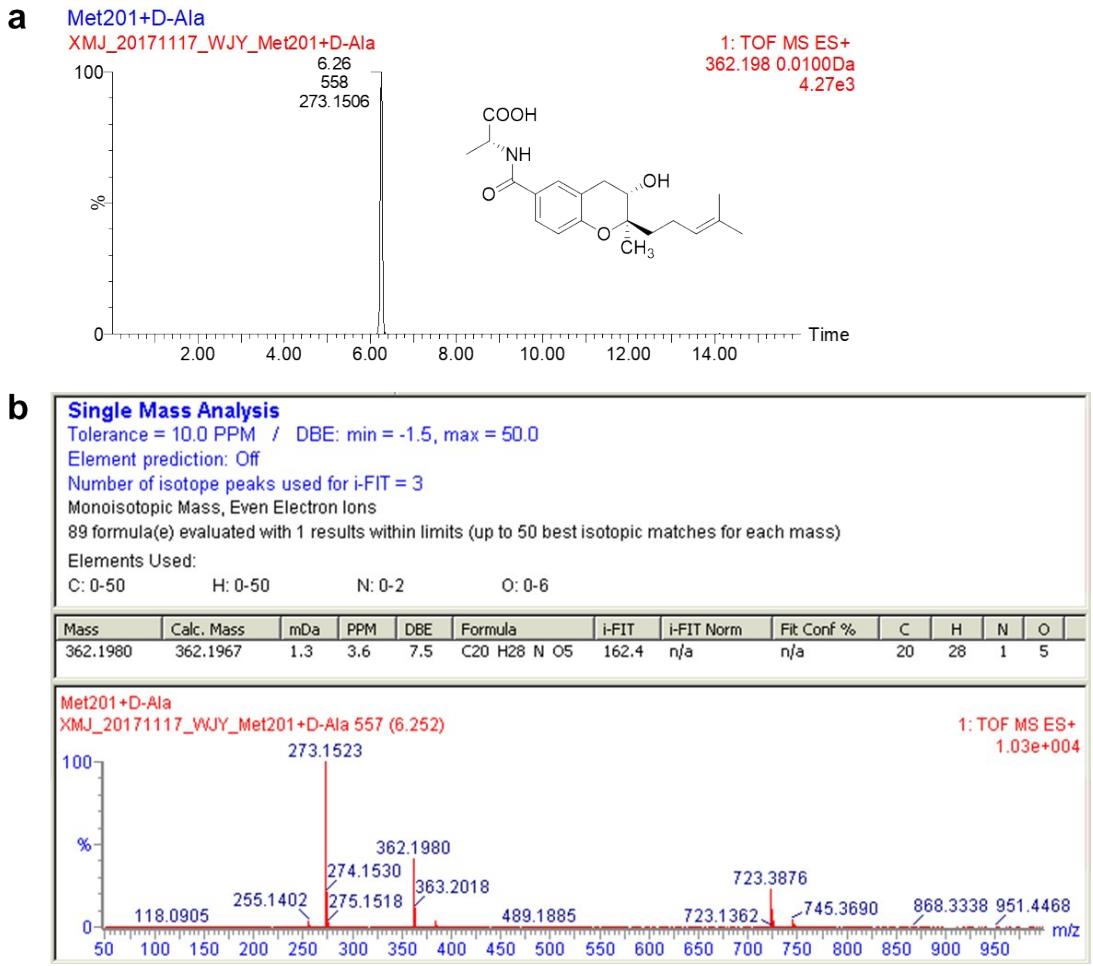

Figure S14. UPLC-QTOF-MS analysis of **11**. (a) Extracted ion chromatogram of **11**. (b) Elemental composition analysis of **11**.

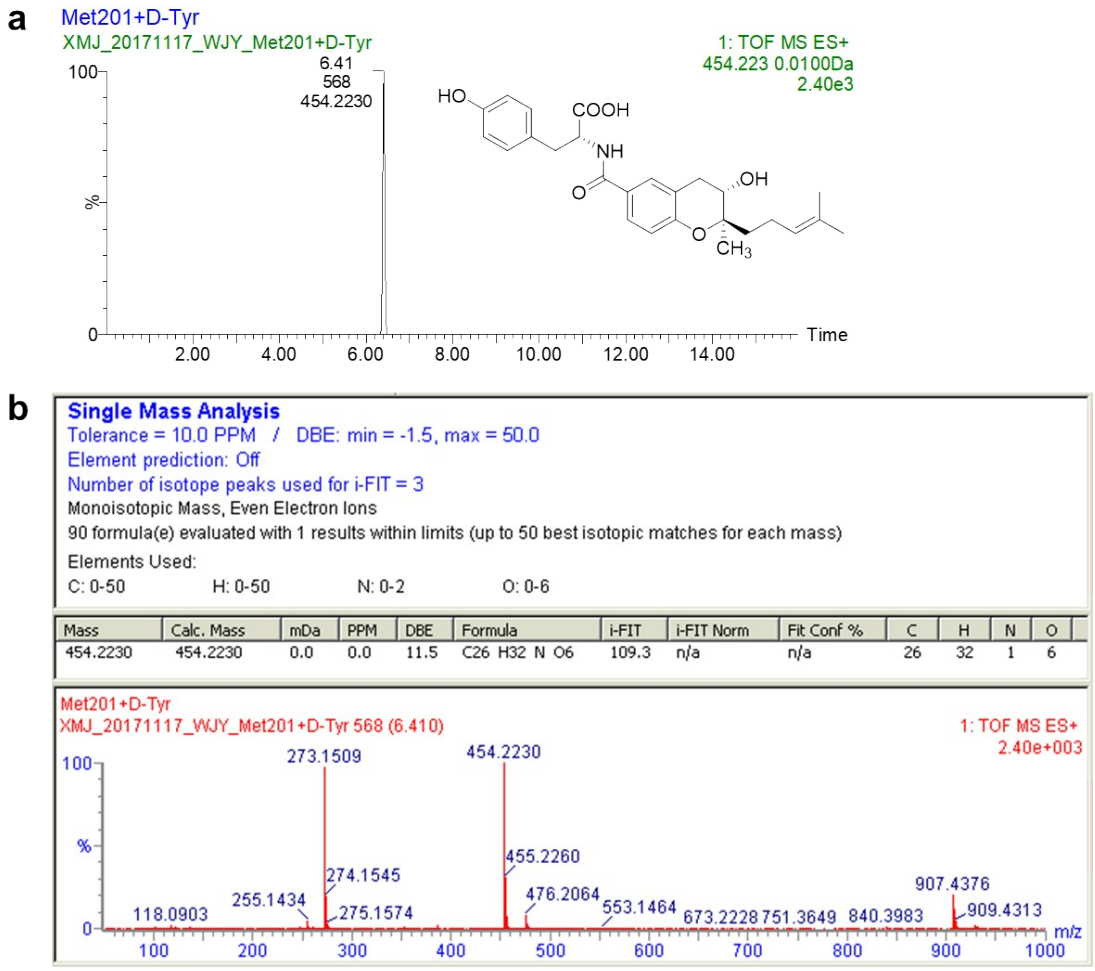

Figure S15. UPLC-QTOF-MS analysis of **12**. (a) Extracted ion chromatogram of **12**. (b) Elemental composition analysis of **12**.

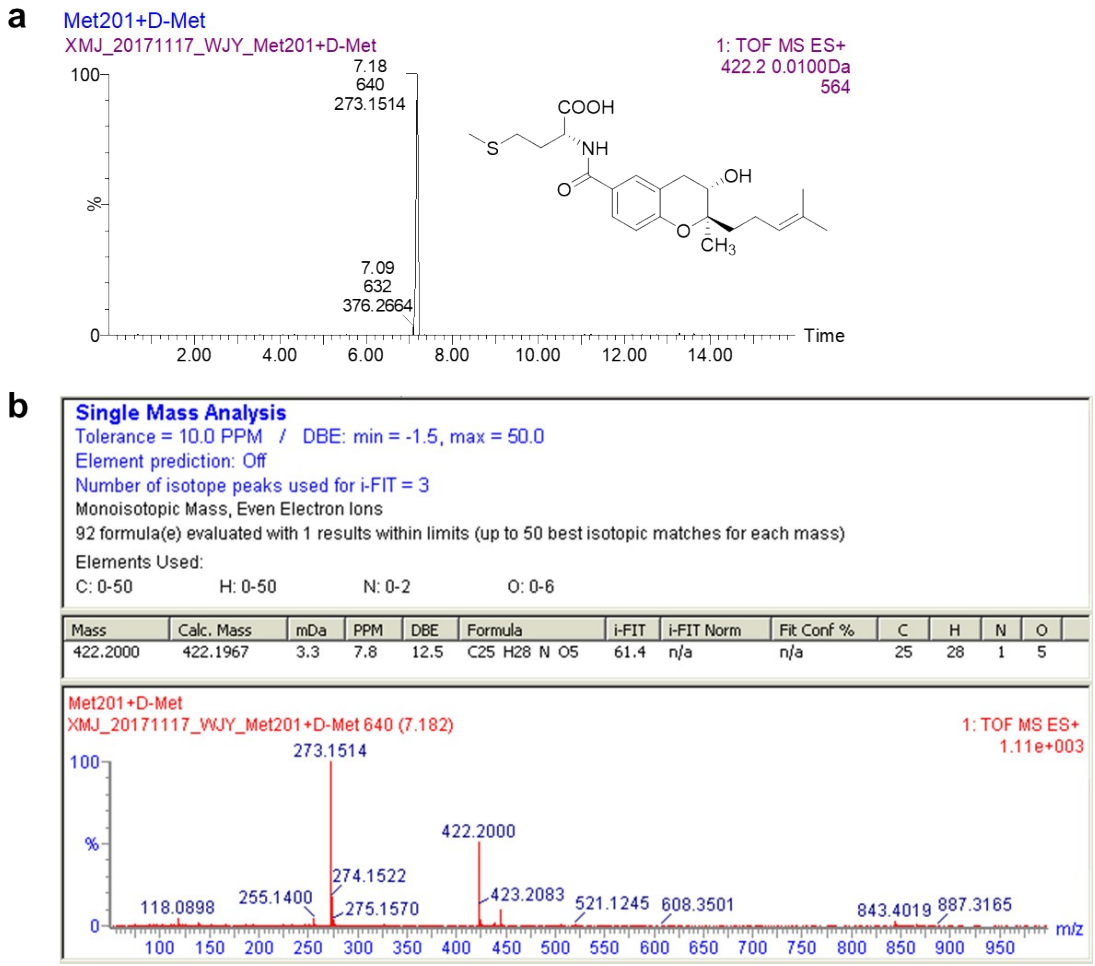

Figure S16. UPLC-QTOF-MS analysis of **13**. (a) Extracted ion chromatogram of **13**. (b) Elemental composition analysis of **13**.

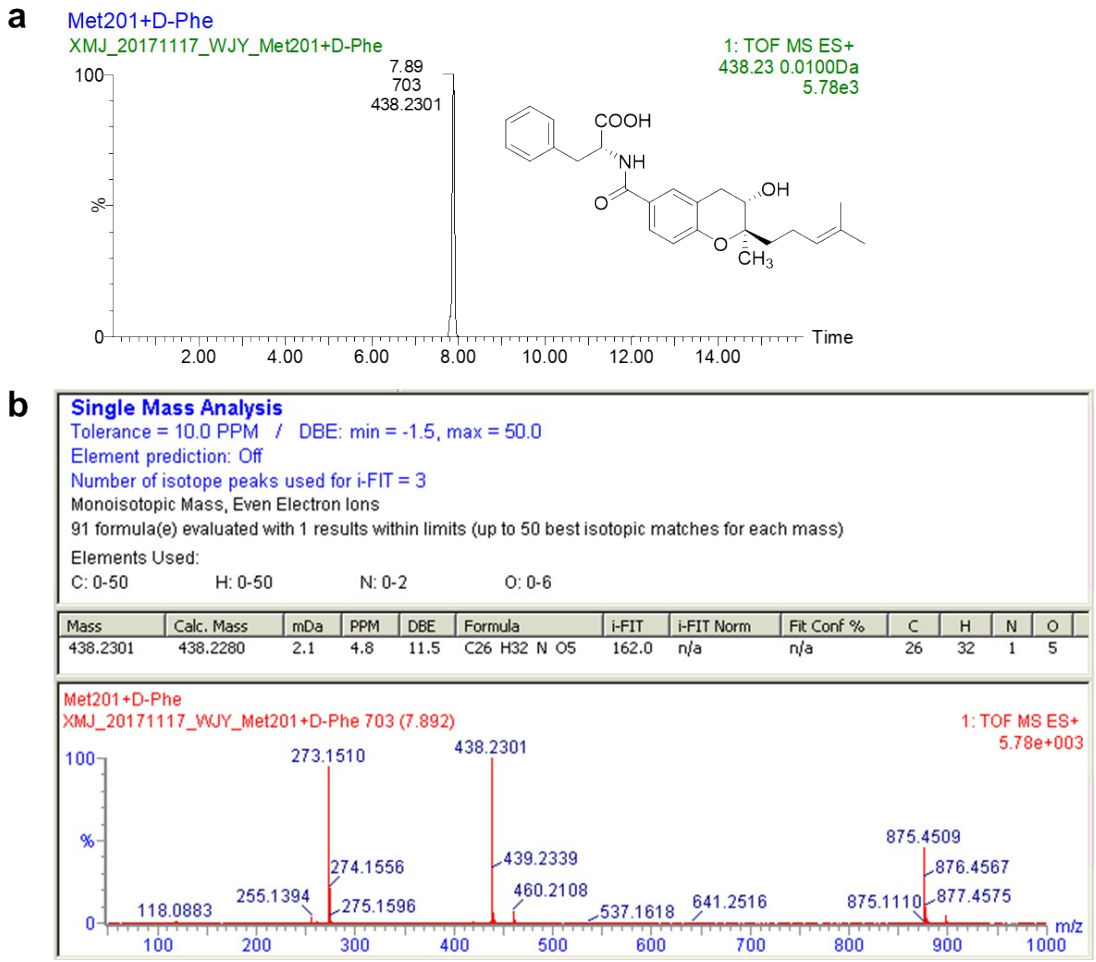

Figure S17. UPLC-QTOF-MS analysis of **14**. (a) Extracted ion chromatogram of **14**. (b) Elemental composition analysis of **14**.

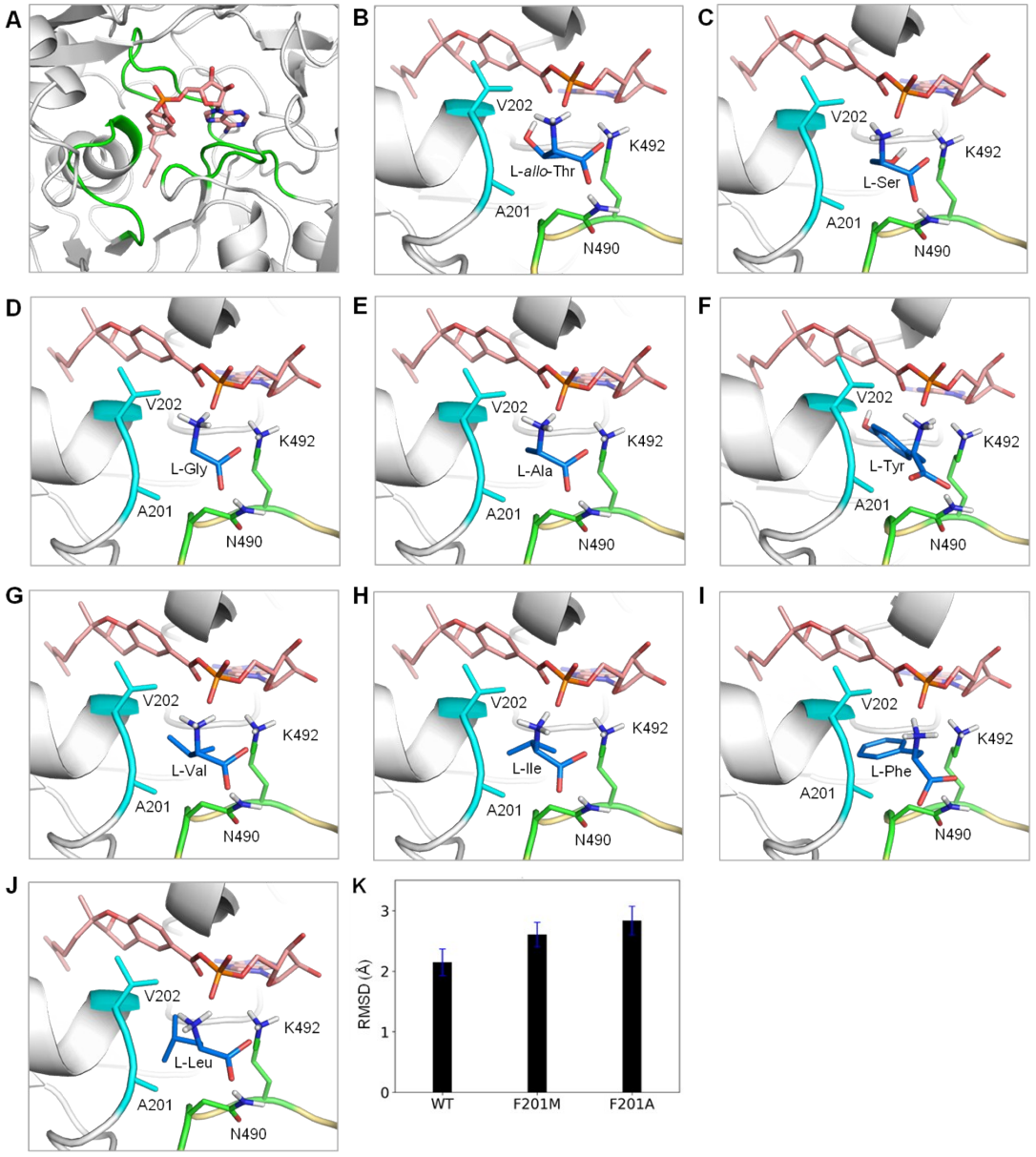

Figure S18. Docking models of various amino acids with the F201A variants.

(A) Residues 195-203, 271-276, 295-303, 490-493, which are colored in green, are used for RMSD calculation. Xiamenmycin B-AMP is represented as sticks with its carbon atoms colored in pink. Docking models of F201A complex using L-*allo*-Thr (B), L-Ser (C), L-Gly (D), L-Ala (E), L-Tyr (F), L-Val (G), L-Ile (H), L-Phe (I) and L-Leu (J) as ligands. The different amino acid ligands are all colored in blue, and the residues N490 and K492 around are colored in green. 201 site is shown in cyan. In all panels, the oxygen, nitrogen, and phosphorus atoms are colored in red, blue, and orange, respectively. (K) Root mean square deviation (RMSD) differences for the WT, F201M, and F201A complexes. The RMSD values were calculated for the regions surrounding the active site, and averaged over the last 80-ns simulation data for each system.

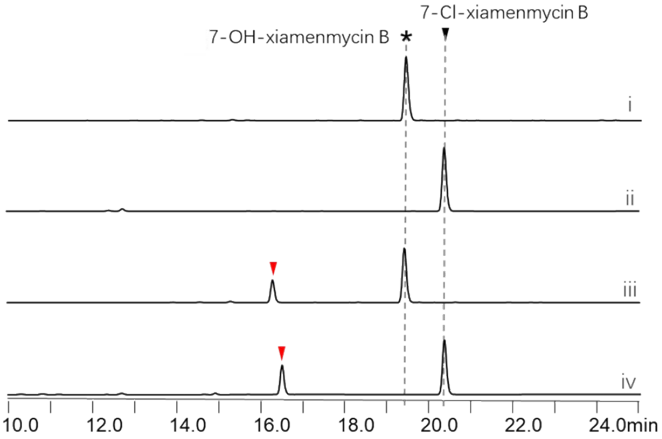

Figure S19. HPLC analysis (UV at 254 nm) of XimA catalytic reactions towards xiamenmycin B analogues.

7-OH-xiamenmycin B (iii) or 7-Cl-xiamenmycin B (iv) were used as substrates. The reaction contains 1 μM XimA, 1 mM xiamenmycin B analogue, 2 mM ATP, 5 mM $_L$-Thr, and 5 mM $MgCl_2$ in 100 μL Tris-HCl buffer (pH 7.5) at 30 ℃ for 12 h. (i) and (ii) are corresponding control reactions with no enzyme.

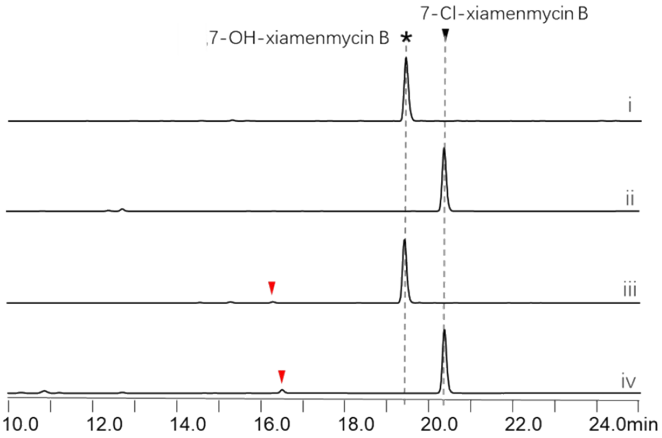

Figure S20. HPLC analysis (UV at 254 nm) of F201A catalytic reactions towards xiamenmycin B analogues.

7-OH-xiamenmycin B (iii) or 7-Cl-xiamenmycin B (iv) were used as substrates. The reaction contains 1 μM F201A, 1 mM xiamenmycin B analogue, 2 mM ATP, 5 mM $_L$-Thr, and 5 mM $MgCl_2$ in 100 μL Tris-HCl buffer(pH 7.5) at 30 ℃ for 12 h. (i) and (ii) are corresponding control reactions with no enzyme.

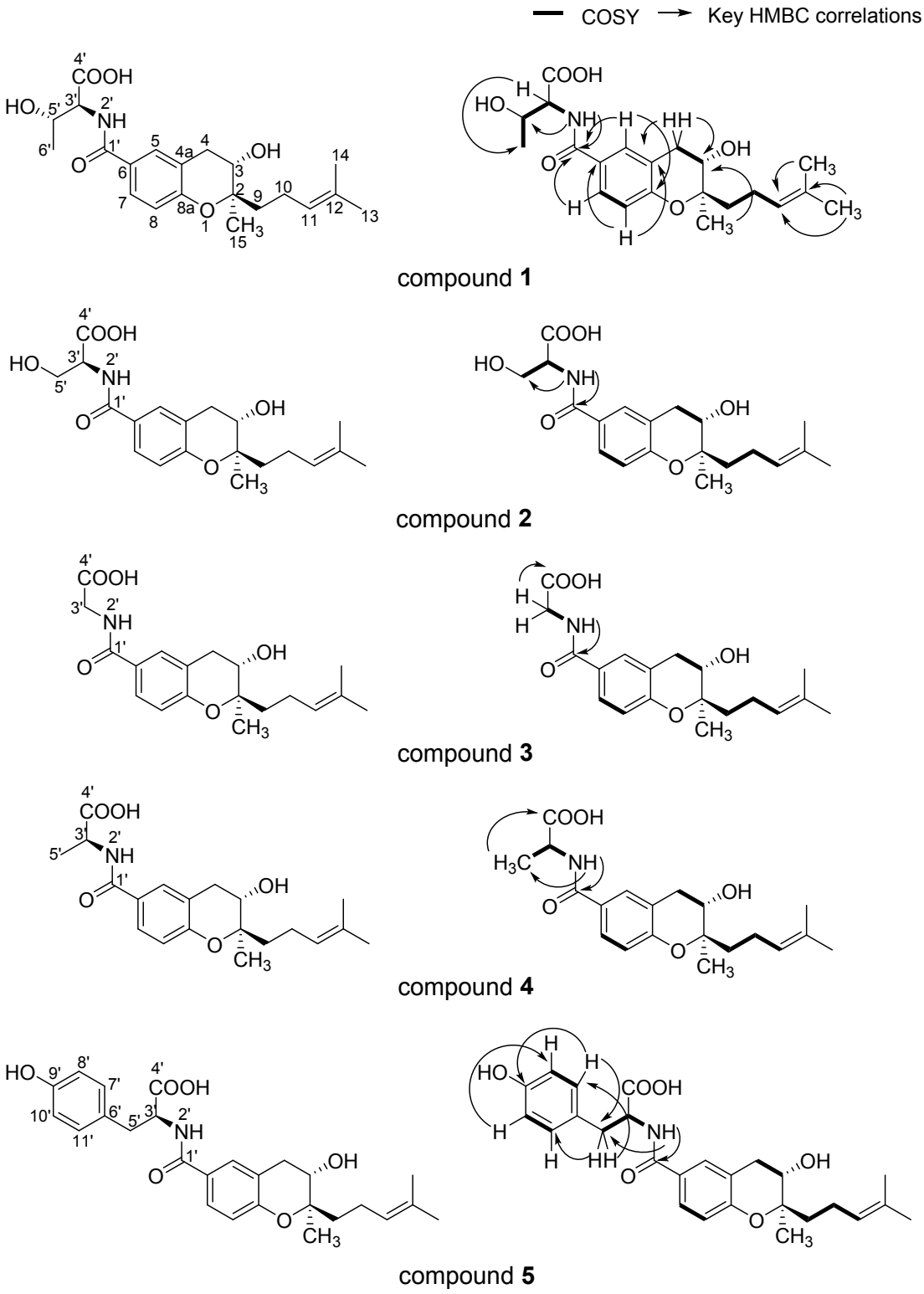

Figure S21. Key HMBC correlations of **1**-**5**.

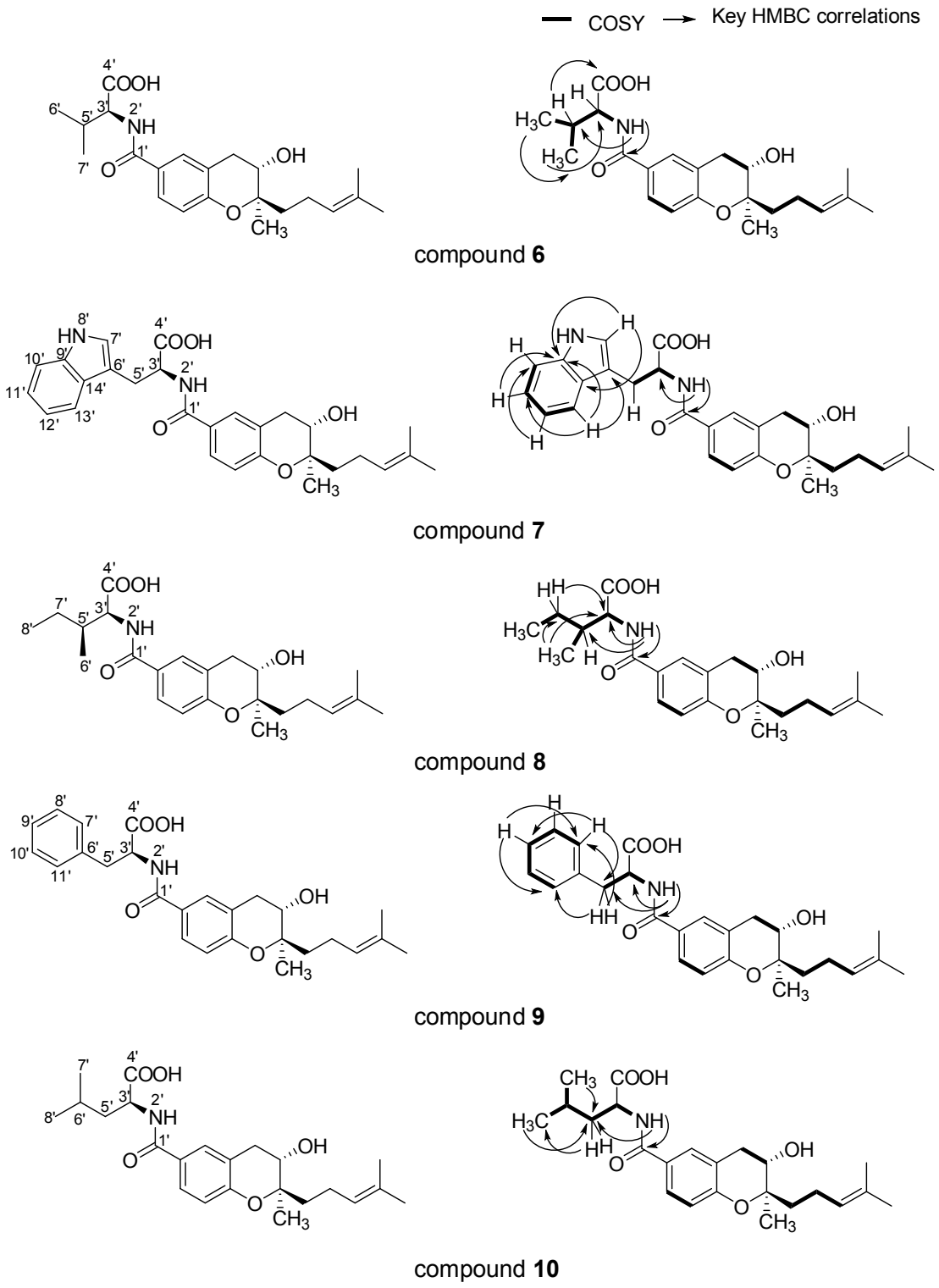

Figure S22. Key HMBC correlations of **6**-**10**.

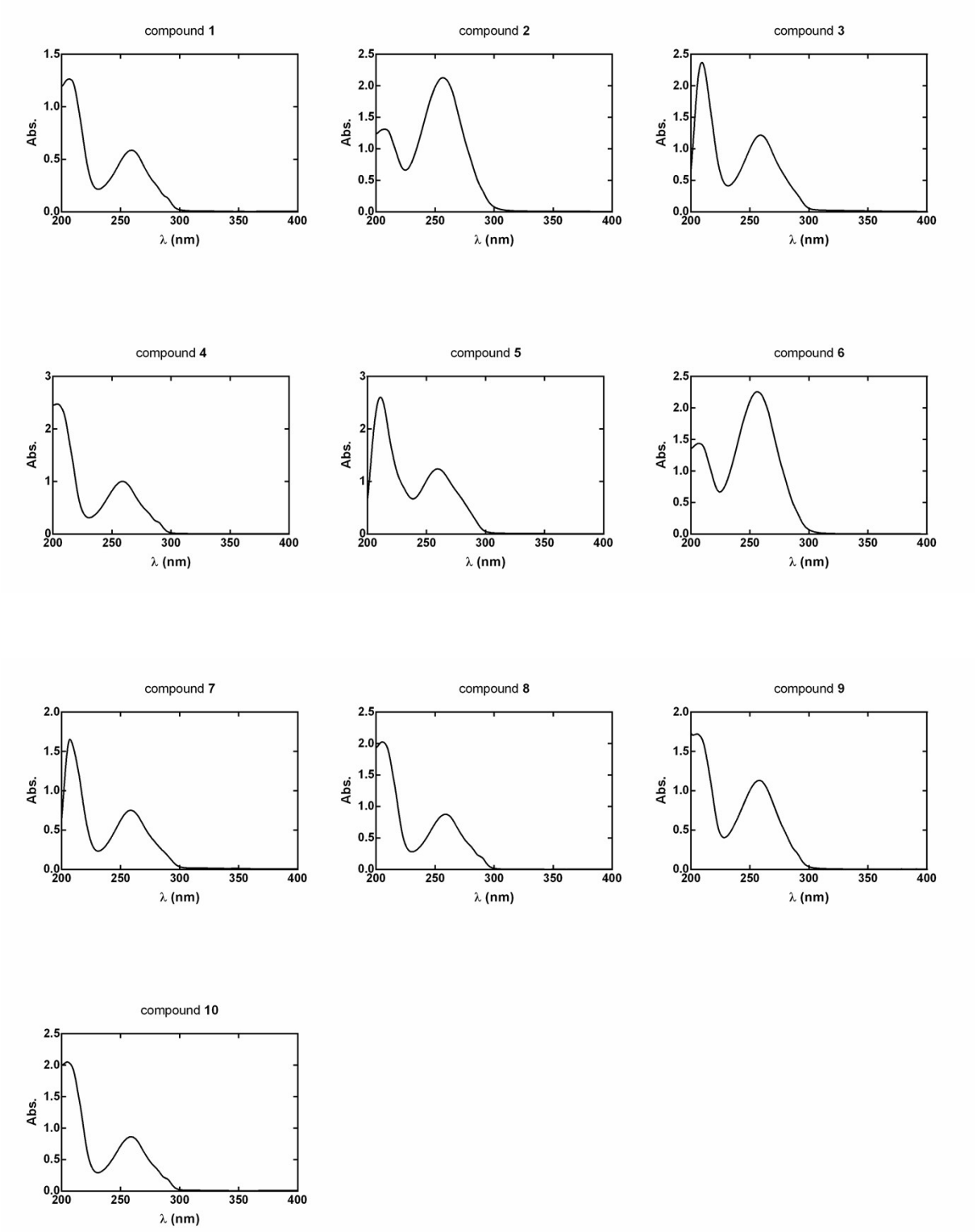

Figure S23. UV spectra of **1-10**.

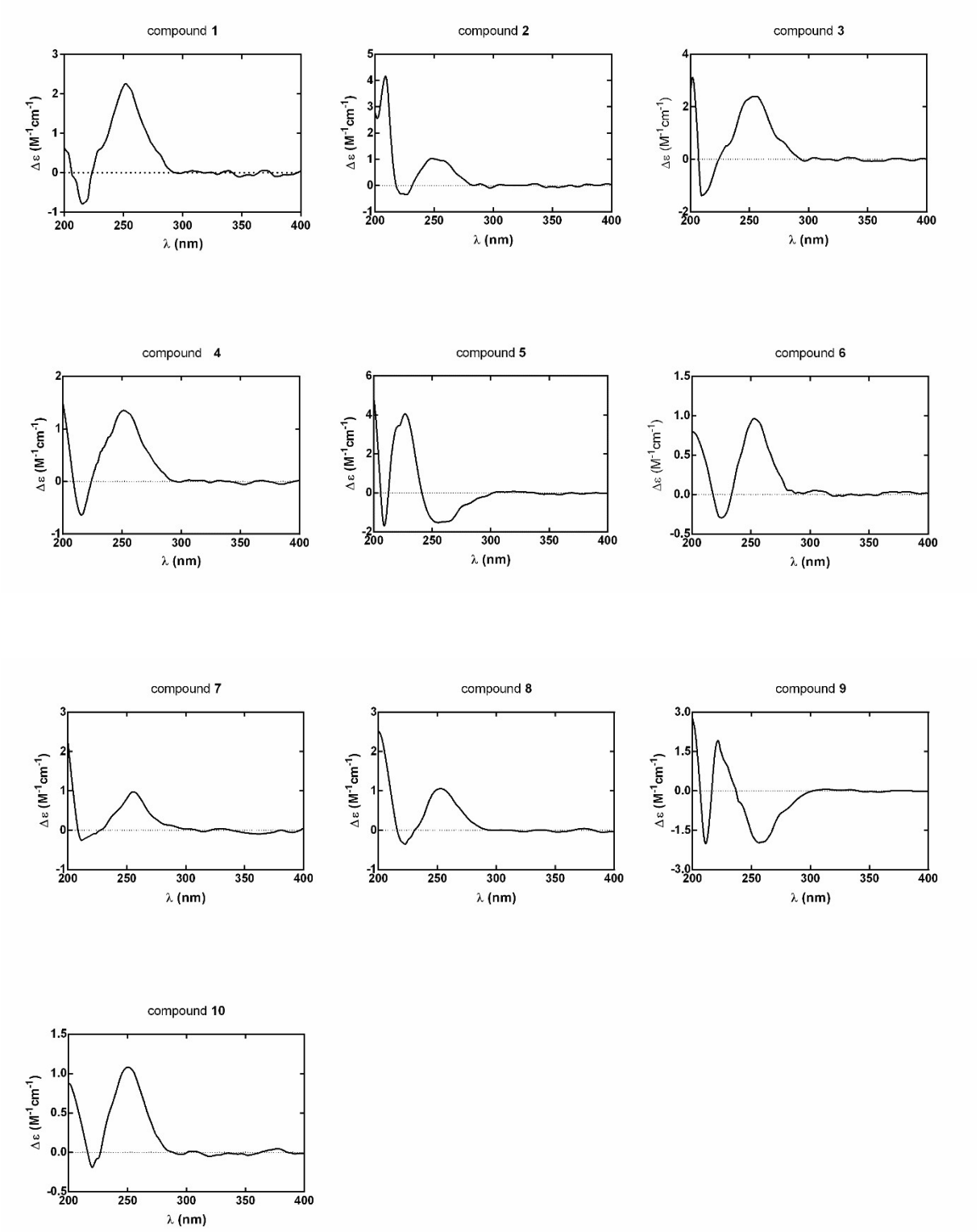

Figure S24. ECD spectra of **1-10**.

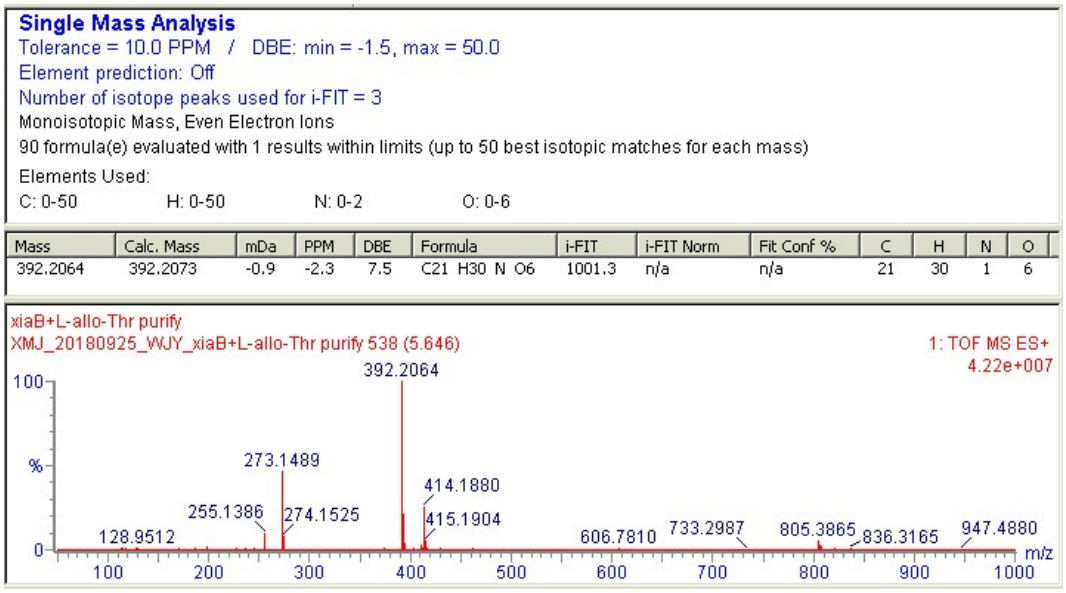

Figure S25. HR-ESI-MS of **1** (Positive mode).

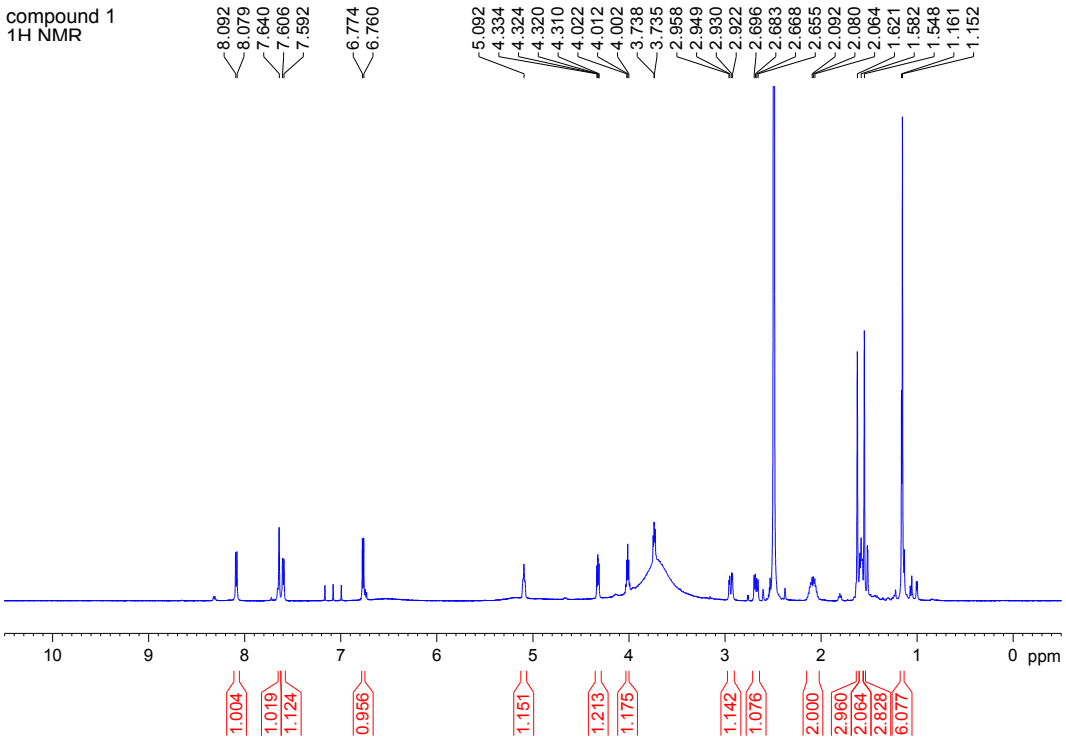

Figure S26. ^{1}H NMR (600 MHz, DMSO-d_6) spectrum of **1**.

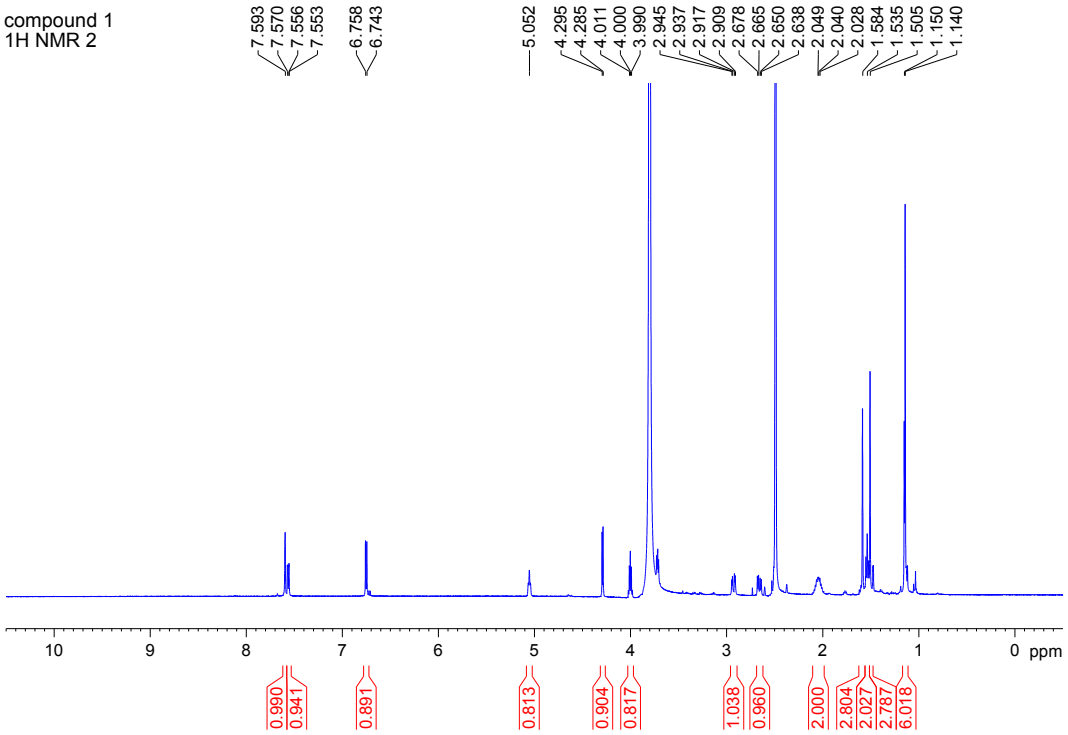

Figure S27. ^{1}H NMR (600 MHz, D_2O and DMSO-d_6) spectrum of **1**.

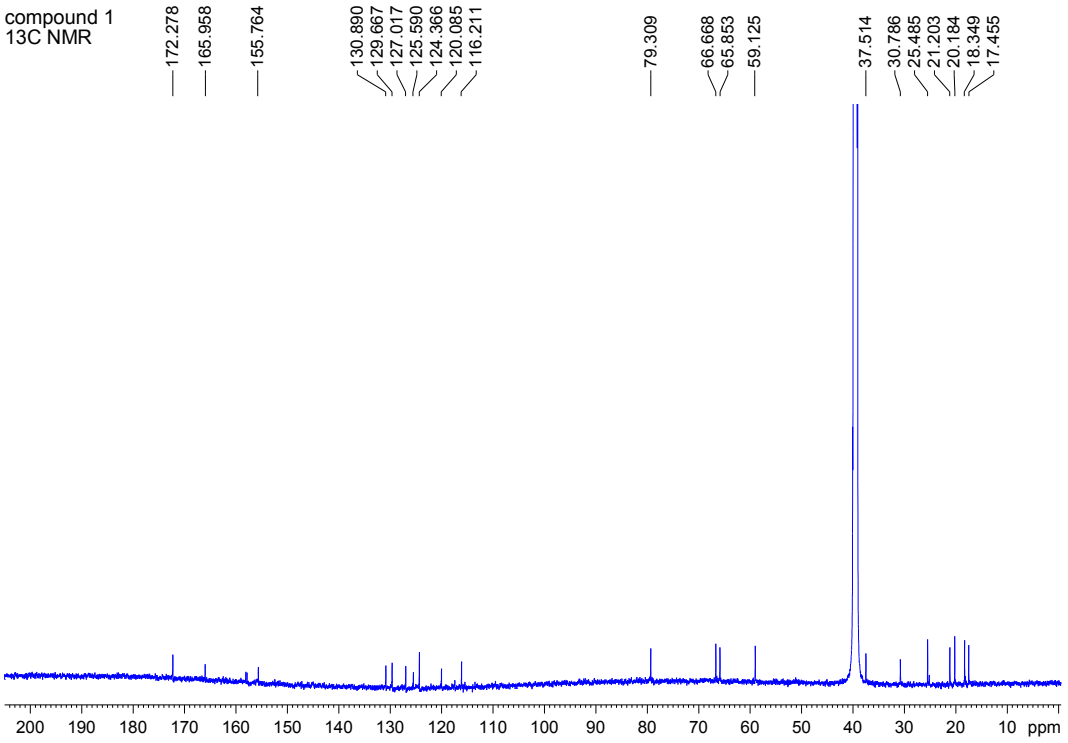

Figure S28. ^{13}C NMR (150 MHz, DMSO-d_6) spectrum of **1**.

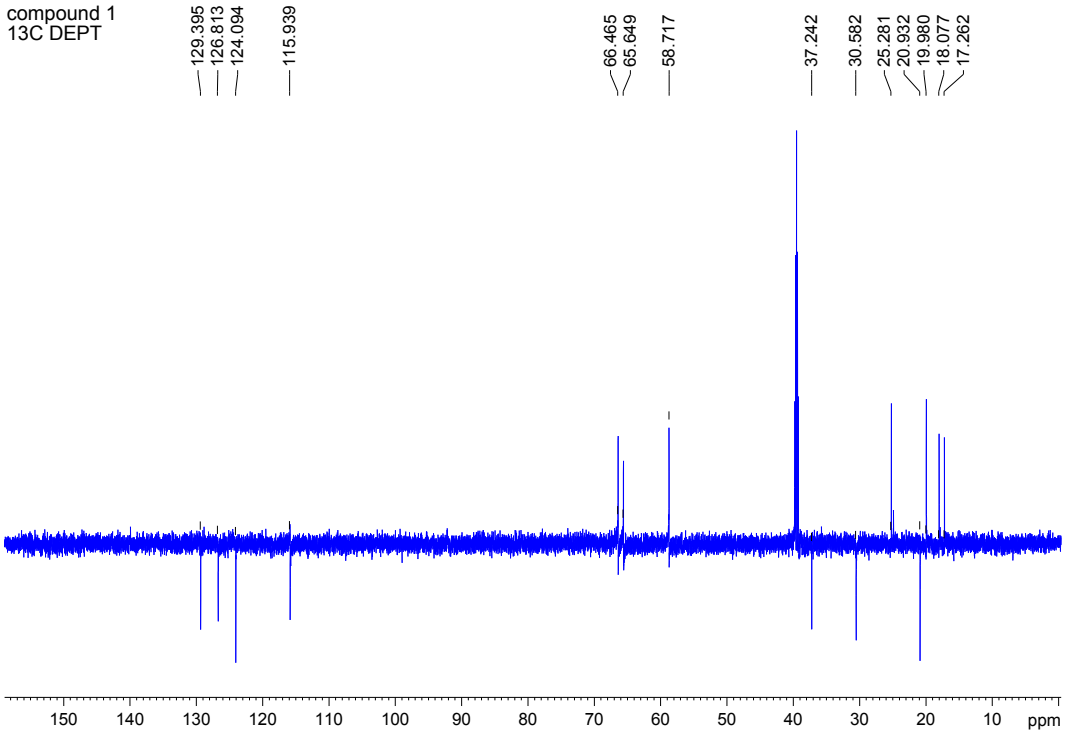

Figure S29. ^{13}C-DEPT (150 MHz, DMSO-d_6) spectrum of **1**.

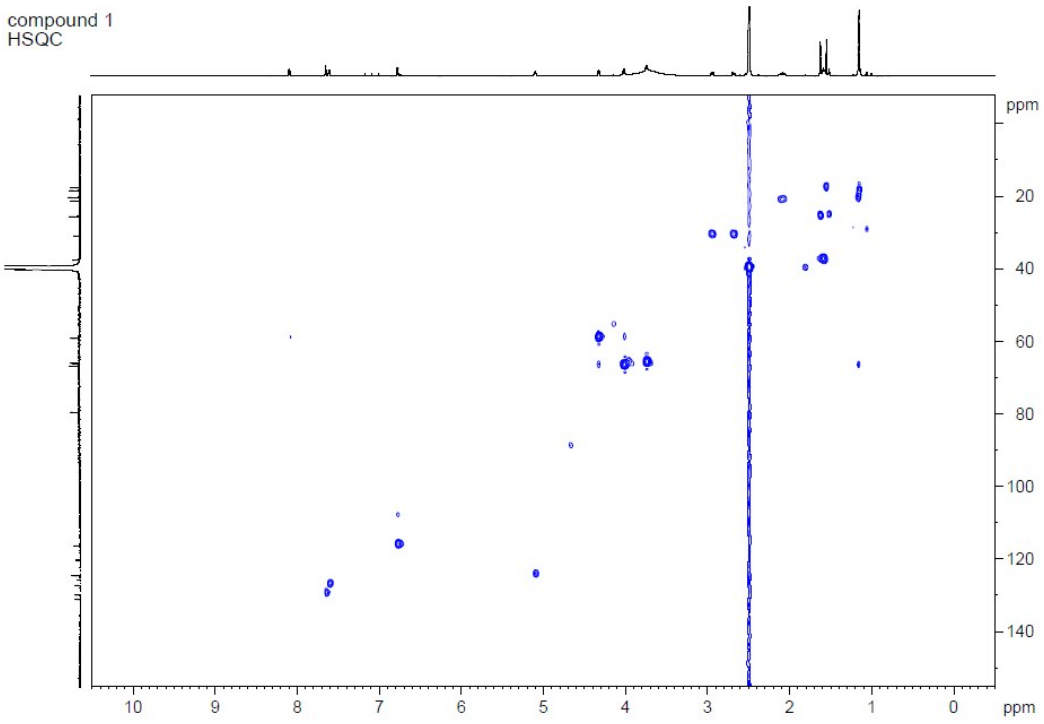

Figure S30. HSQC spectrum of **1**.

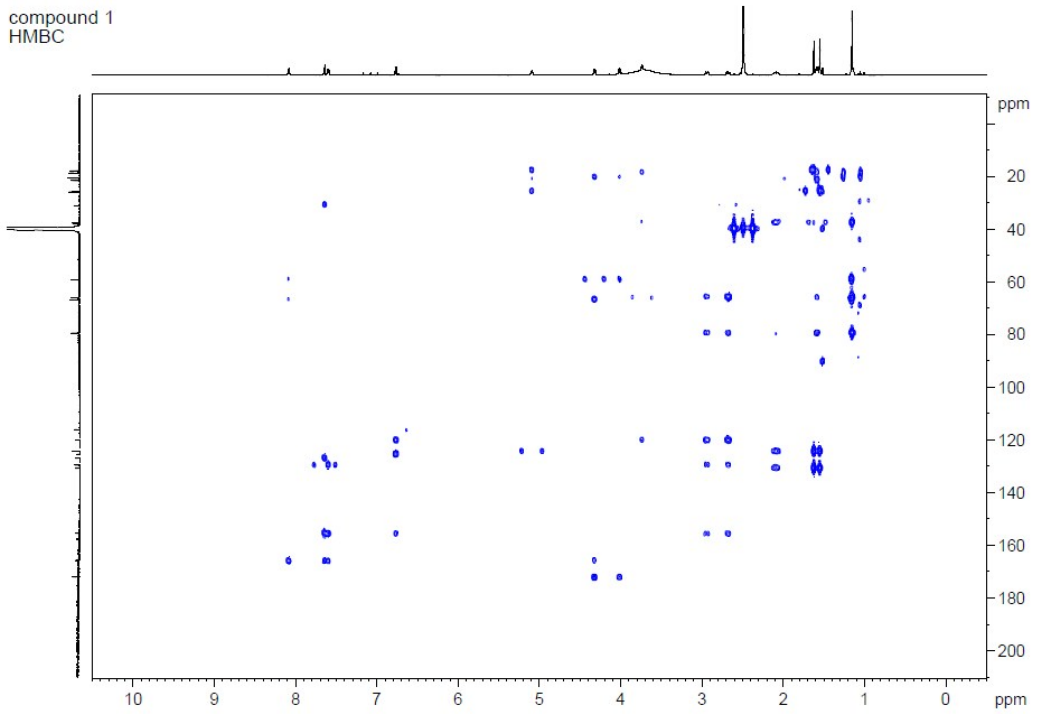

Figure S31. HMBC spectrum of **1**.

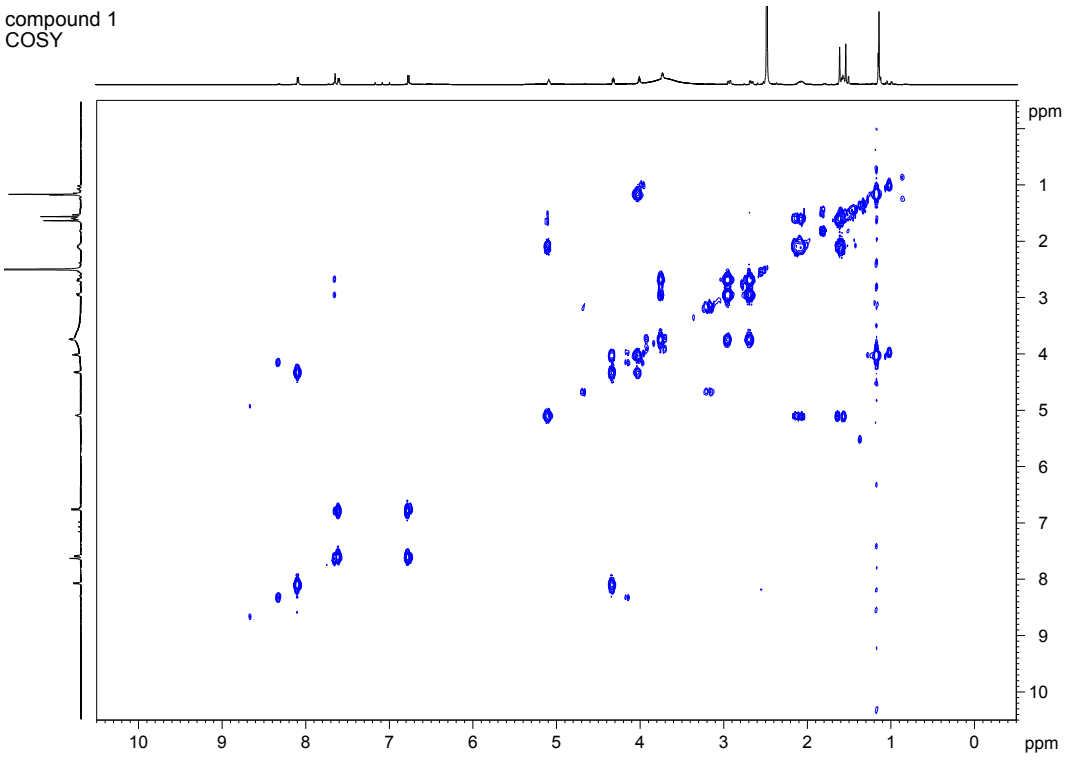

Figure S32. COSY spectrum of **1**.

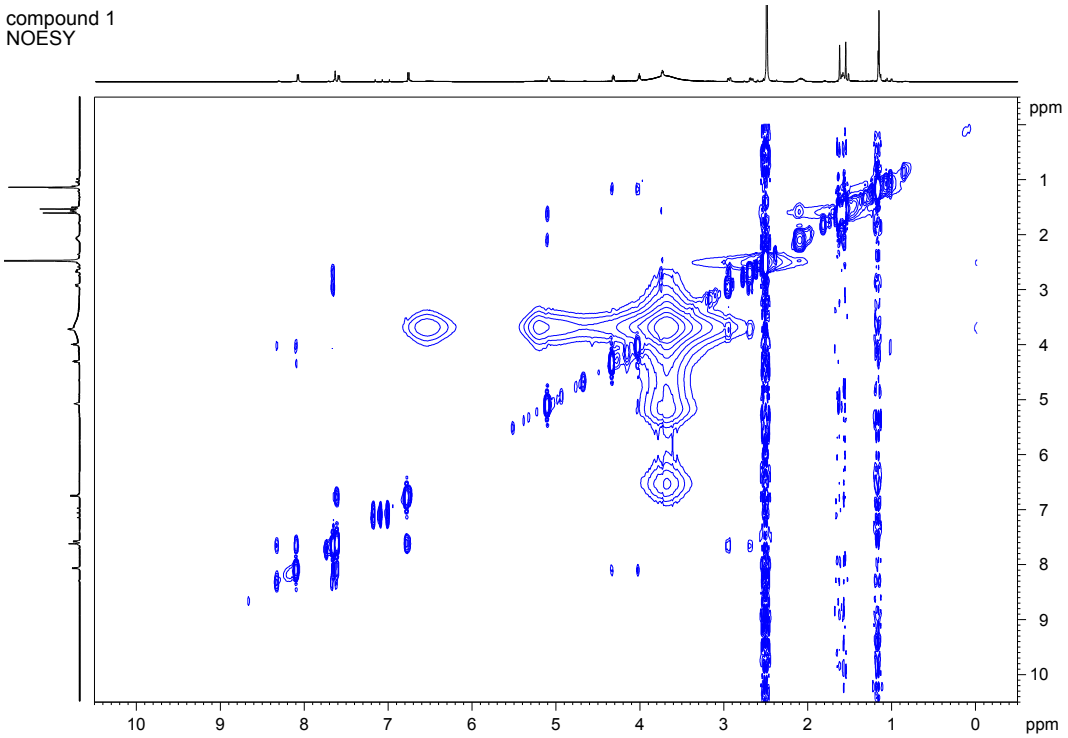

Figure S33. NOESY spectrum of **1**.

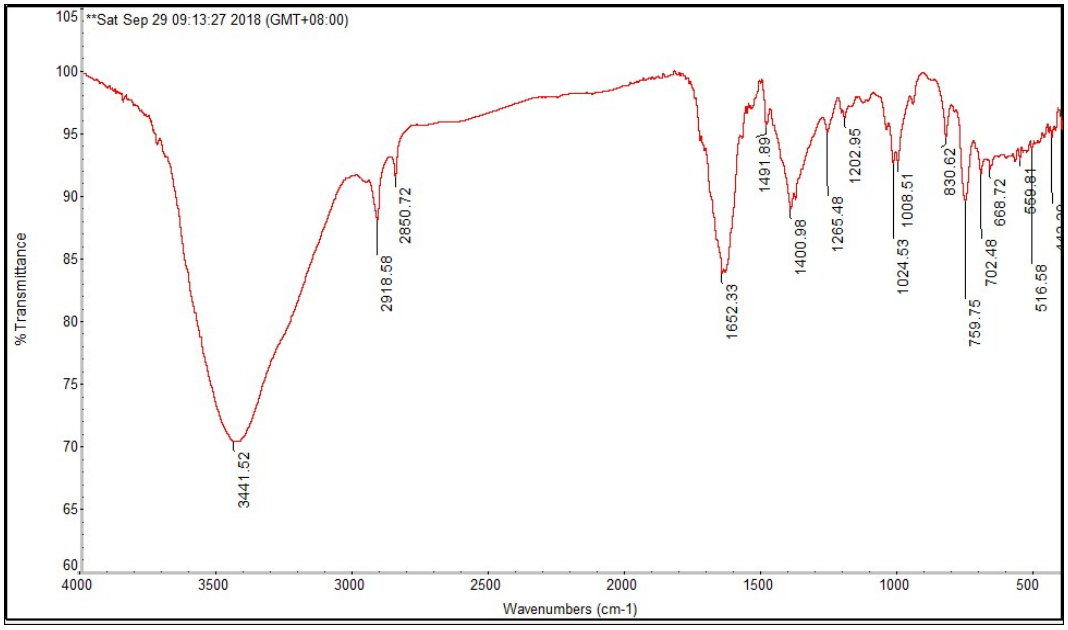

Figure S34. IR spectrum of **1**.

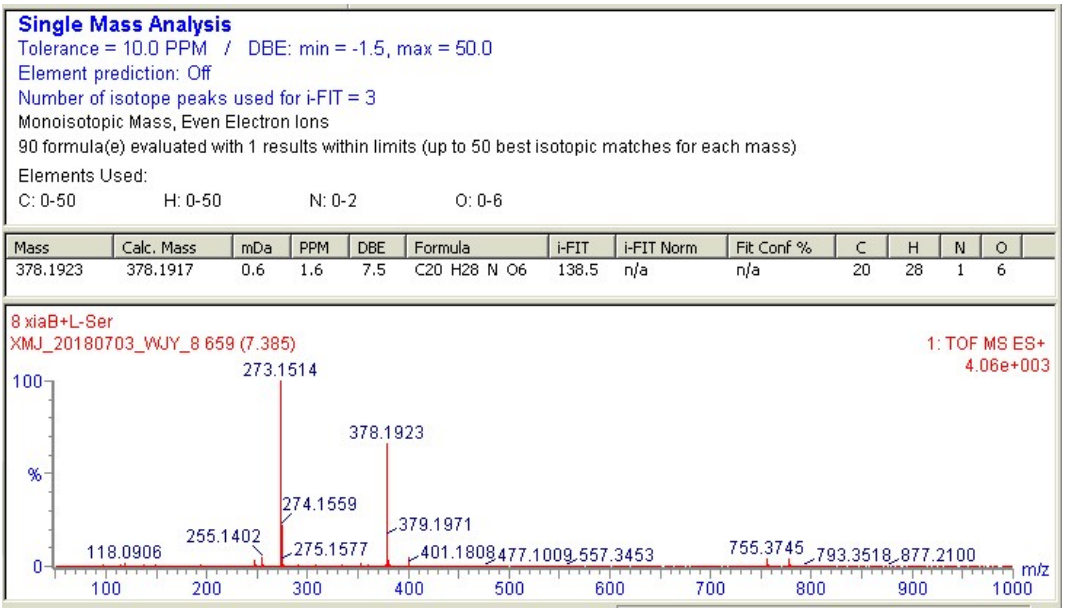

Figure S35. HR-ESI-MS analysis of **2** (Positive mode).

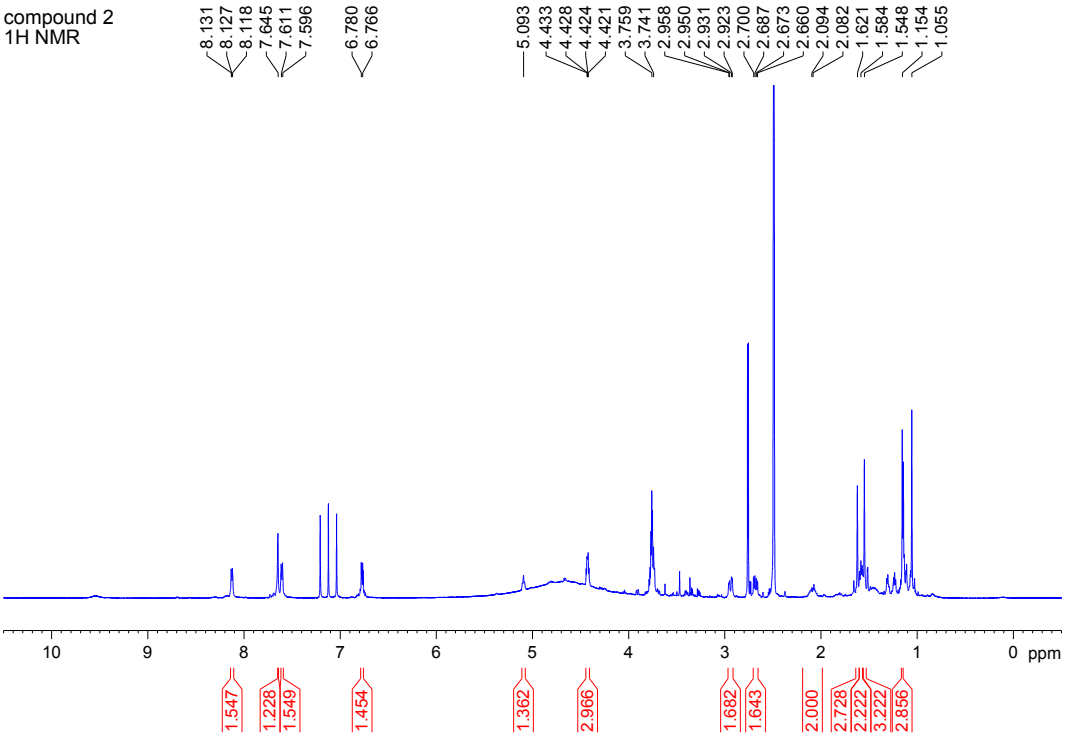

Figure S36. ^{1}H NMR (600 MHz, DMSO-d_6) spectrum of **2**.

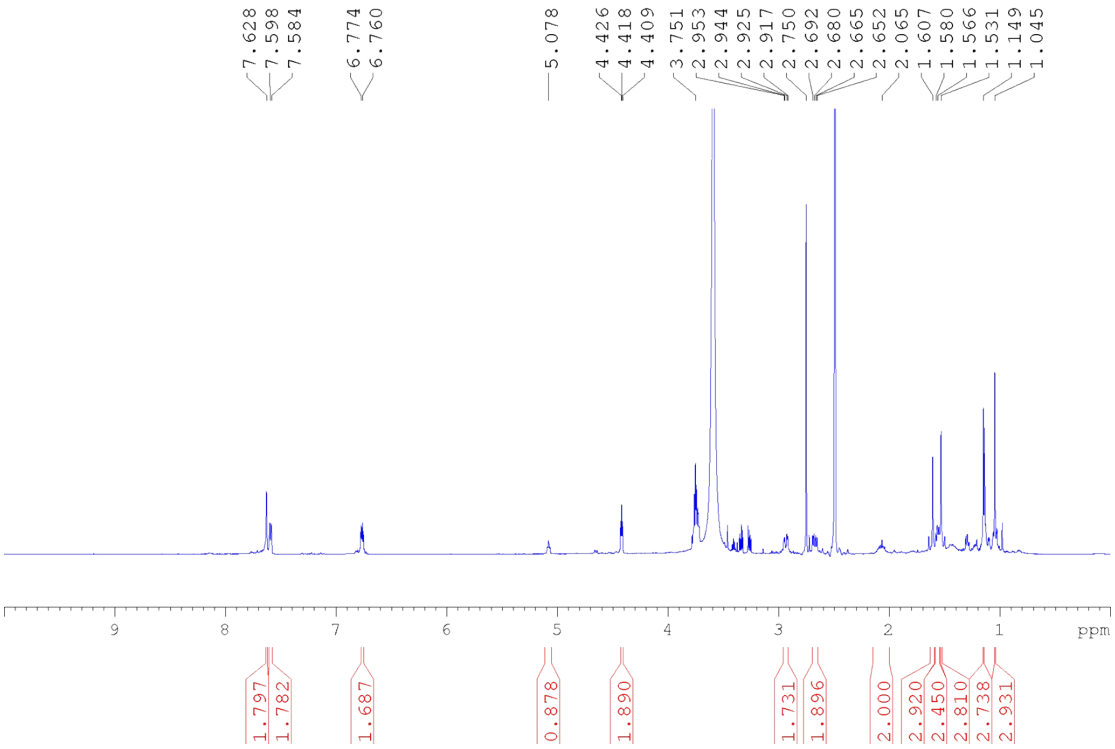

Figure S37. ^{1}H NMR (600 MHz, D_2O and DMSO-d_6) spectrum of **2**.

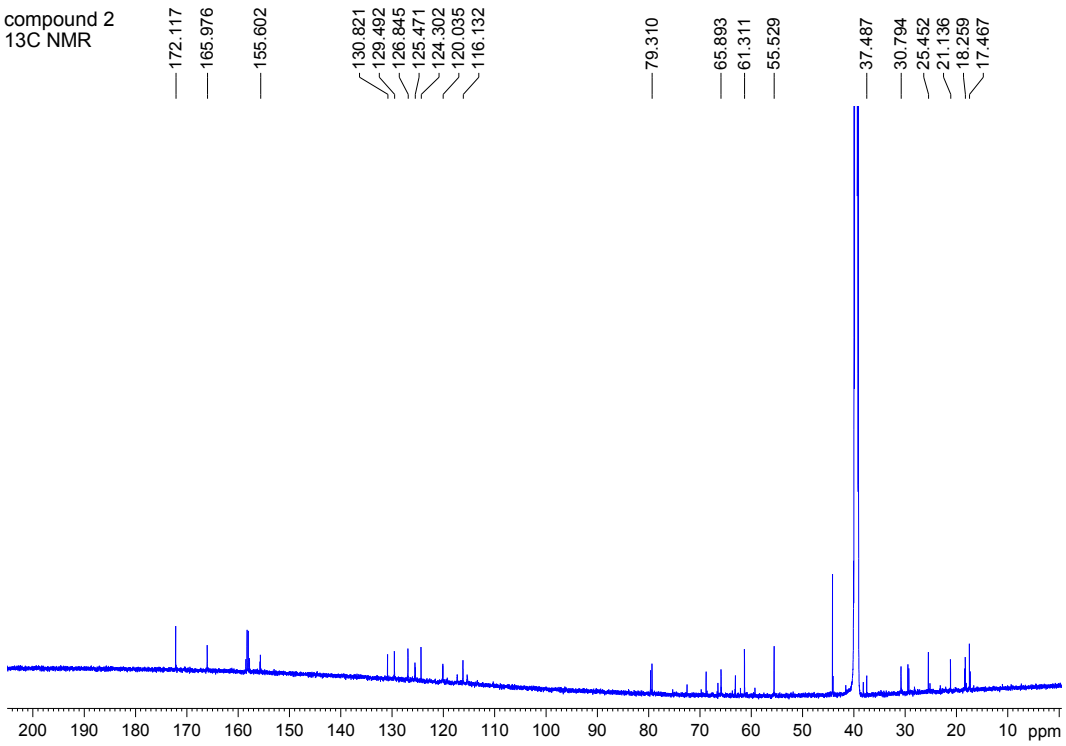

Figure S38. ^{13}C NMR (150 MHz, DMSO-d_6) spectrum of **2**.

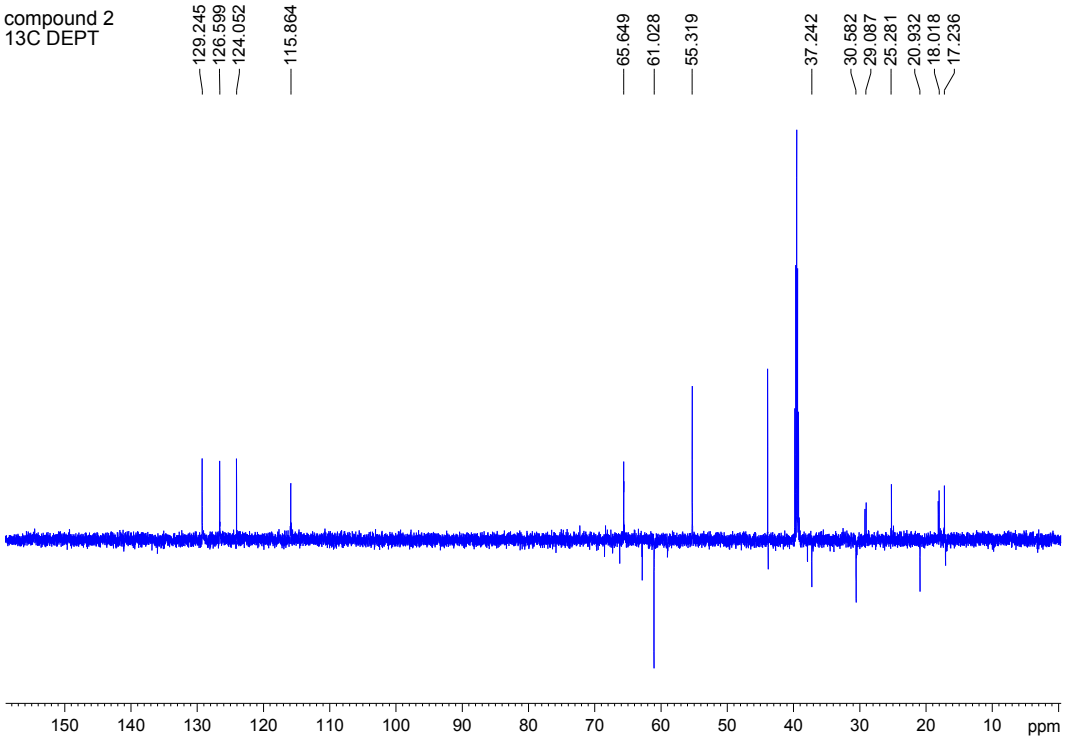

Figure S39. ^{13}C-DEPT (150 MHz, DMSO-d_6) spectrum of **2**.

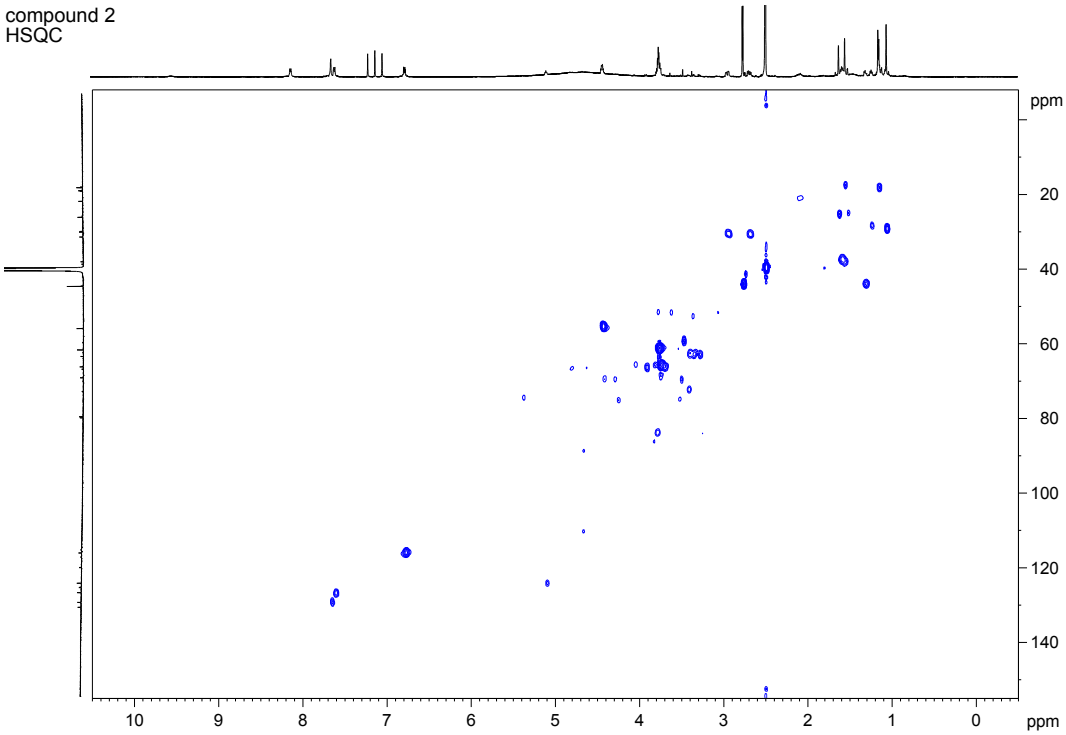

Figure S40. HSQC spectrum of **2**.

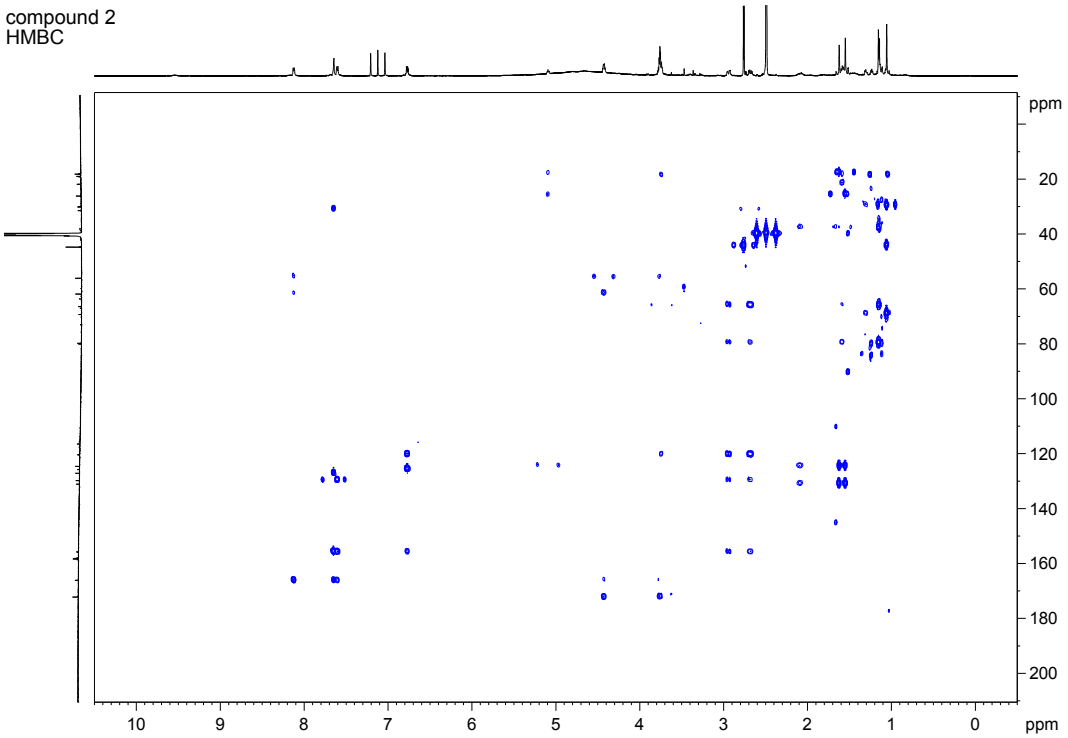

Figure S41. HMBC spectrum of **2**.

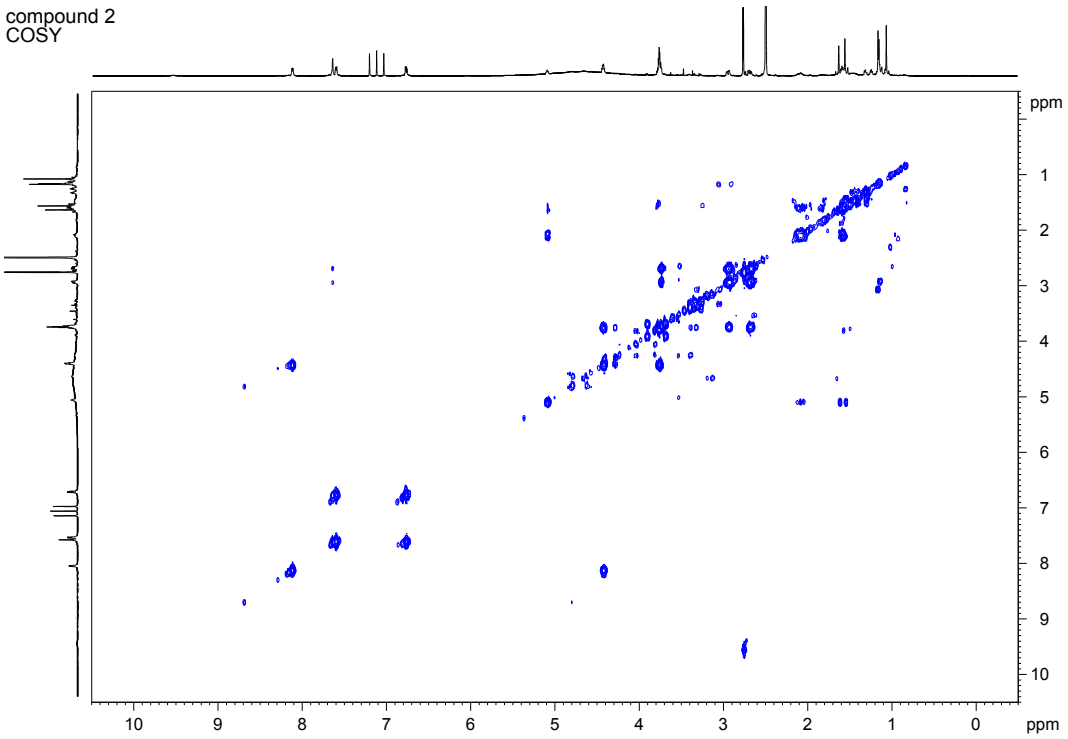

Figure S42. COSY spectrum of **2**.

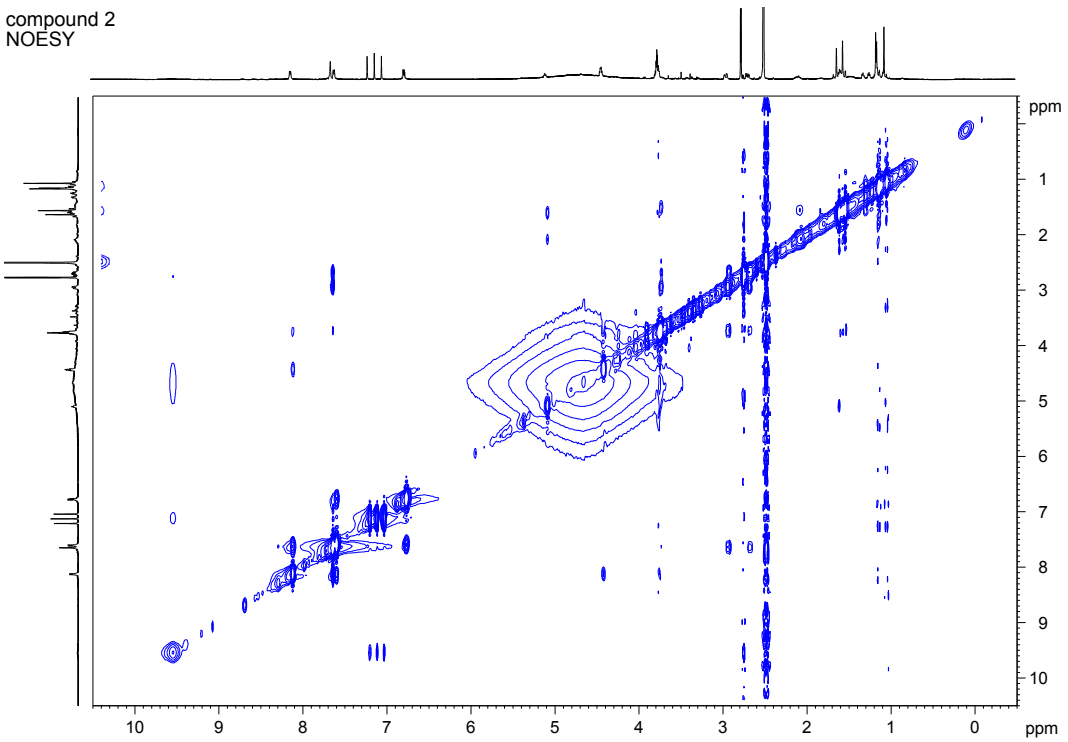

Figure S43. NOESY spectrum of **2**.

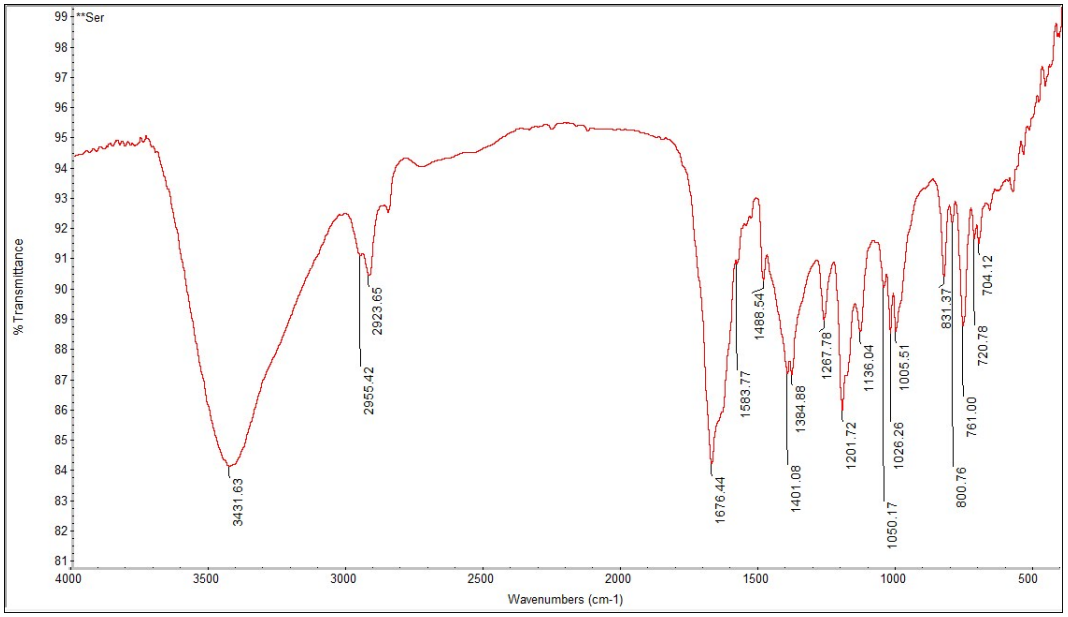

Figure S44. IR spectrum of **2**.

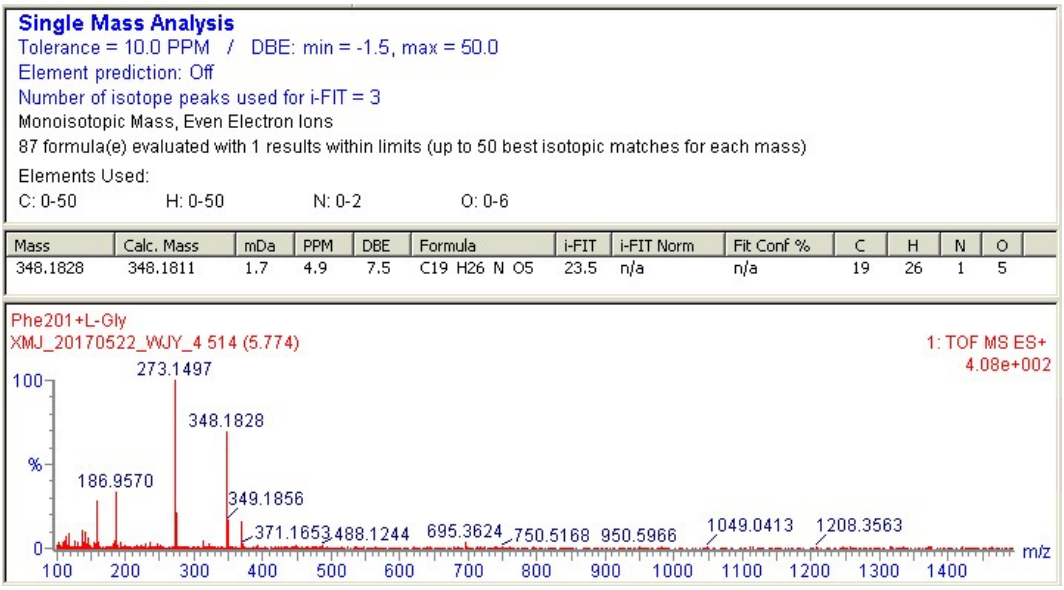

Figure S45. HR-ESI-MS analysis of **3** (Positive mode).

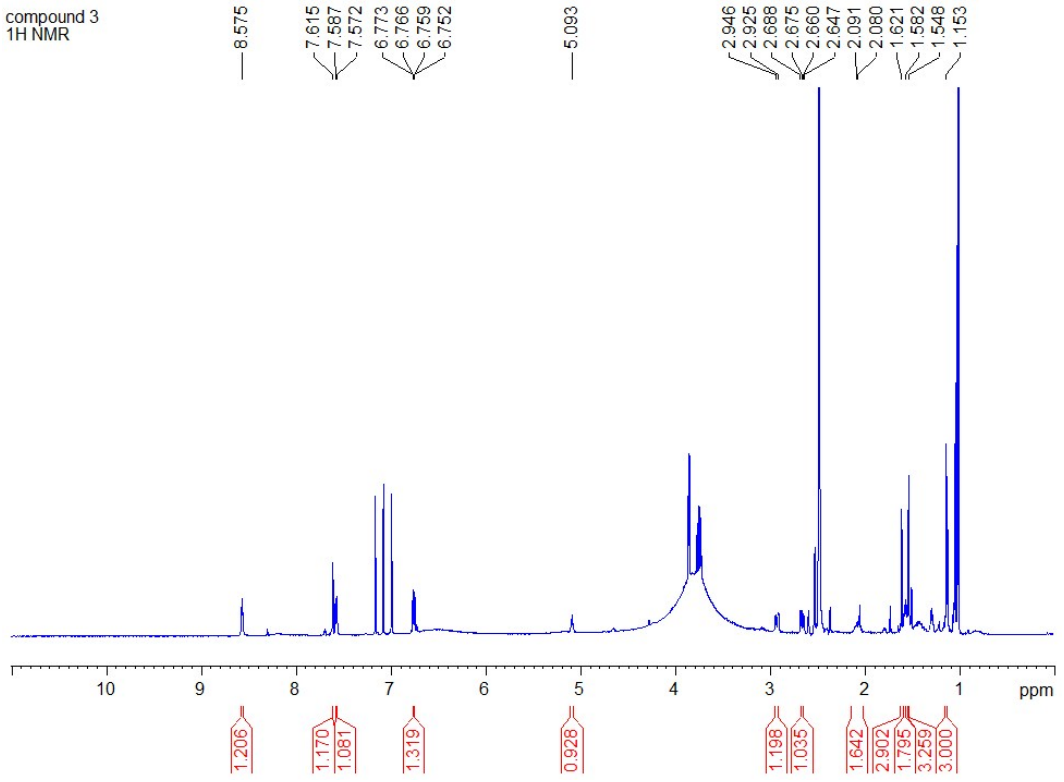

Figure S46. ^{1}H NMR (600 MHz, DMSO-d_6) spectrum of **3**.

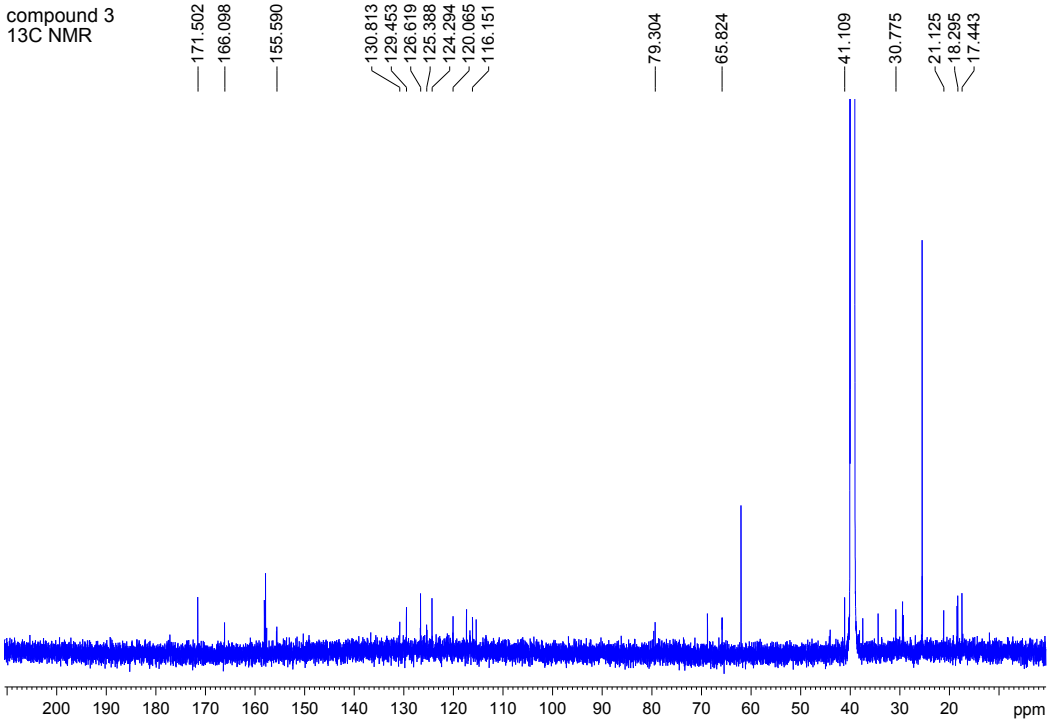

Figure S47. ^{13}C NMR (150 MHz, DMSO-d_6) spectrum of **3**.

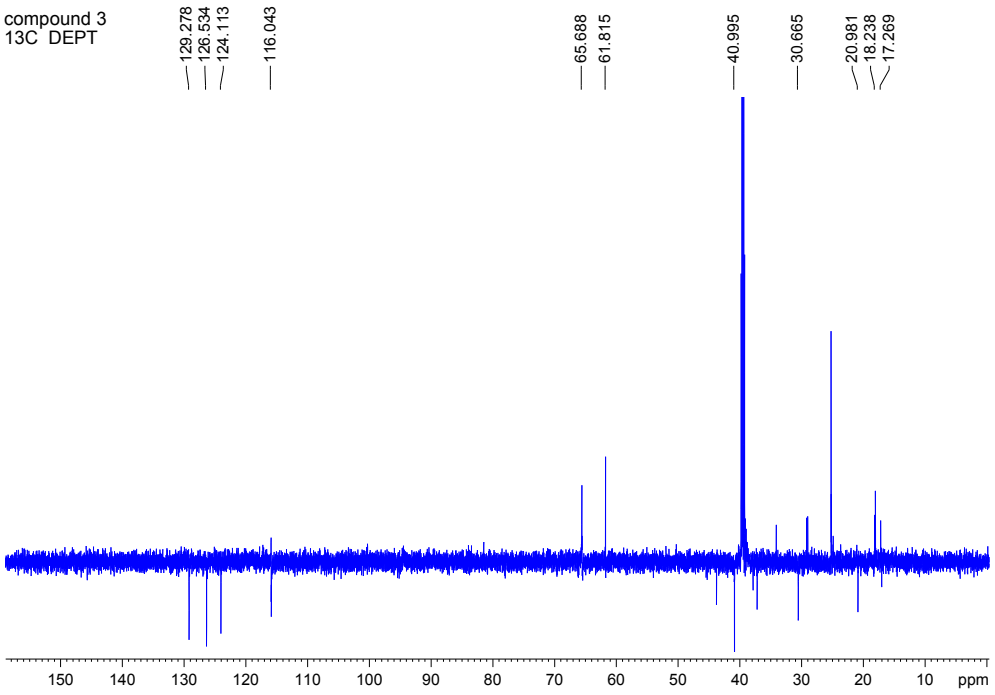

Figure S48. ^{13}C-DEPT (150 MHz, DMSO-d_6) spectrum of **3**.

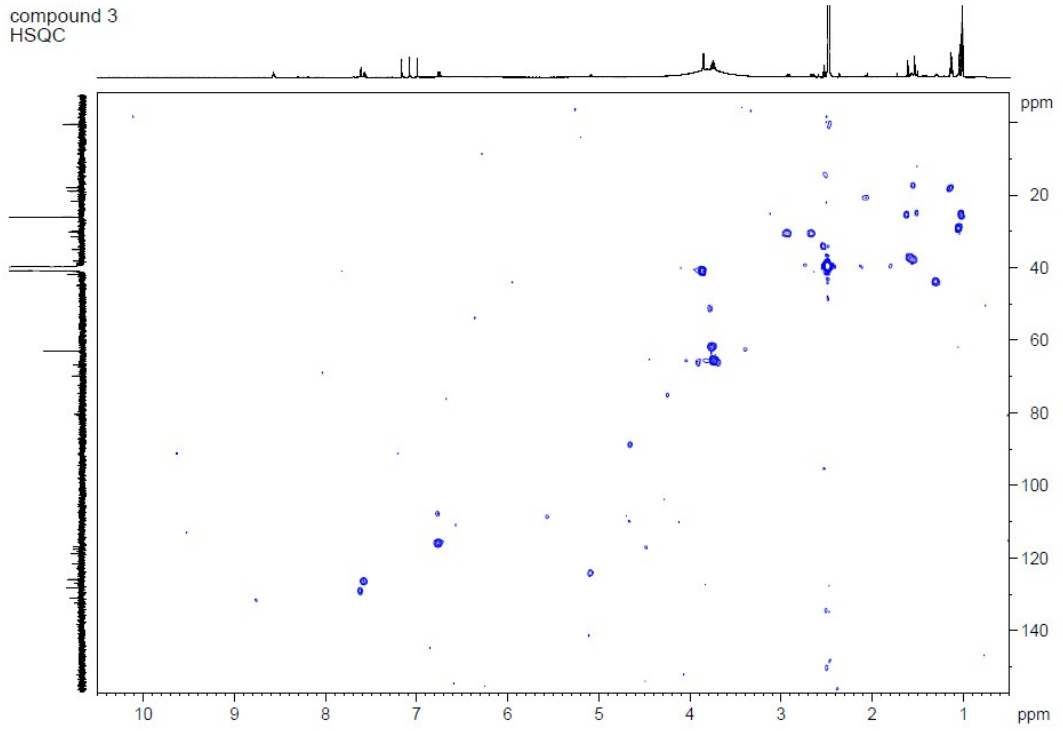

Figure S49. HSQC spectrum of **3**.

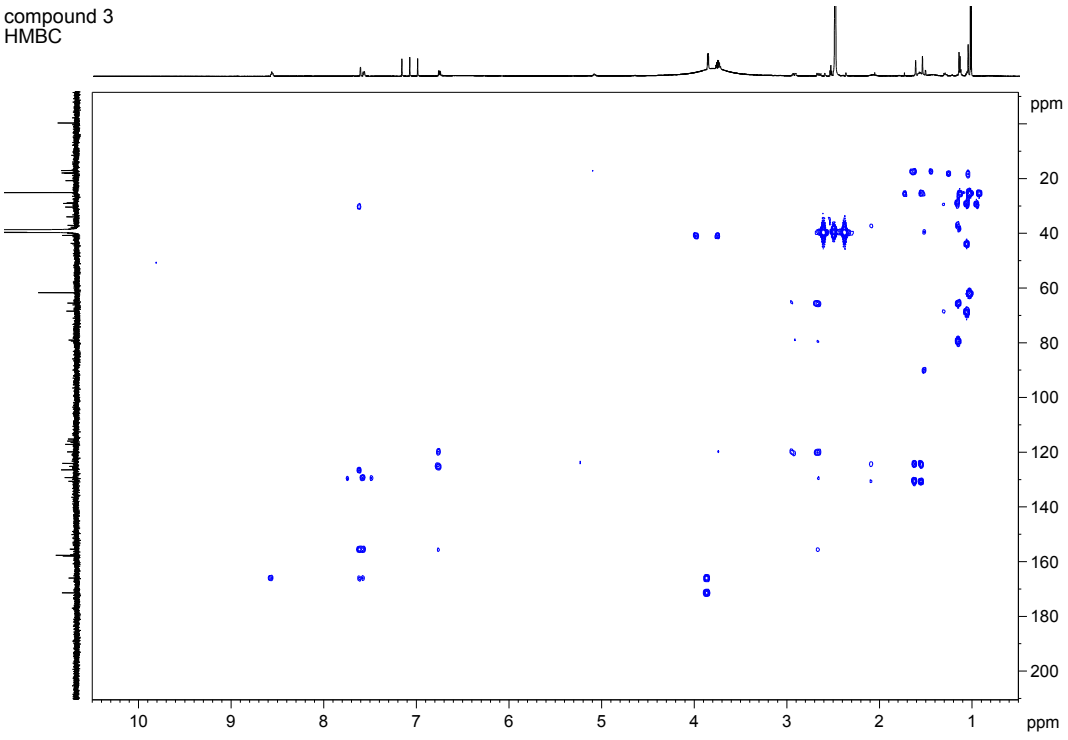

Figure S50. HMBC spectrum of **3**.

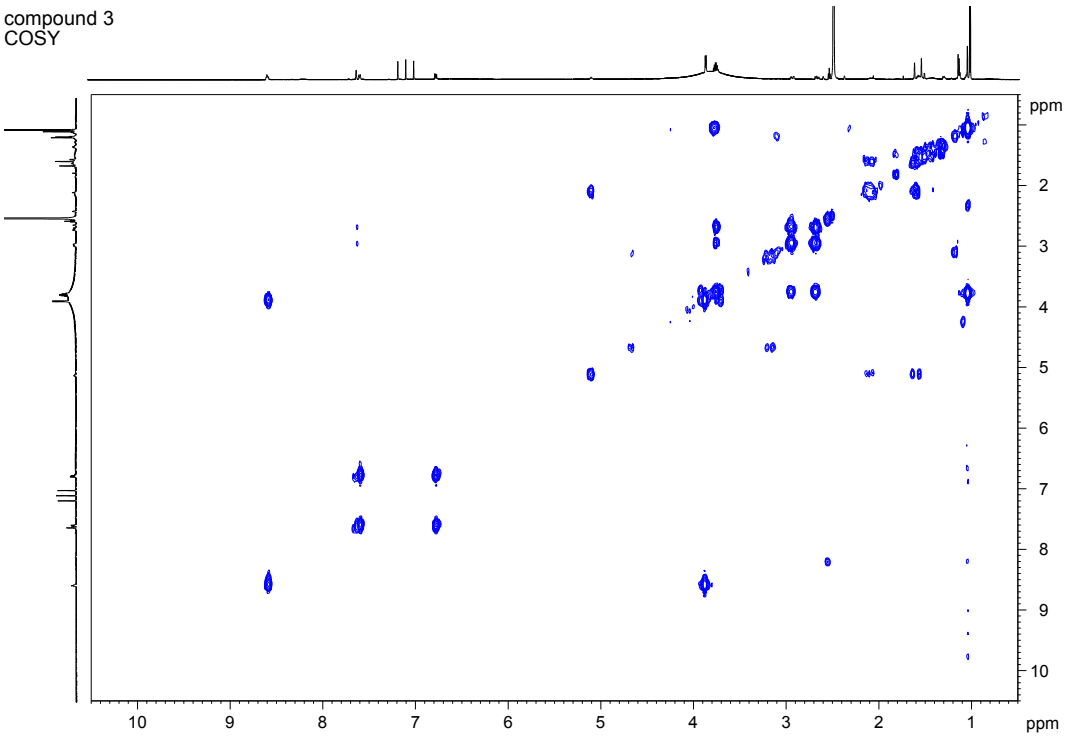

Figure S51. COSY spectrum of **3**.

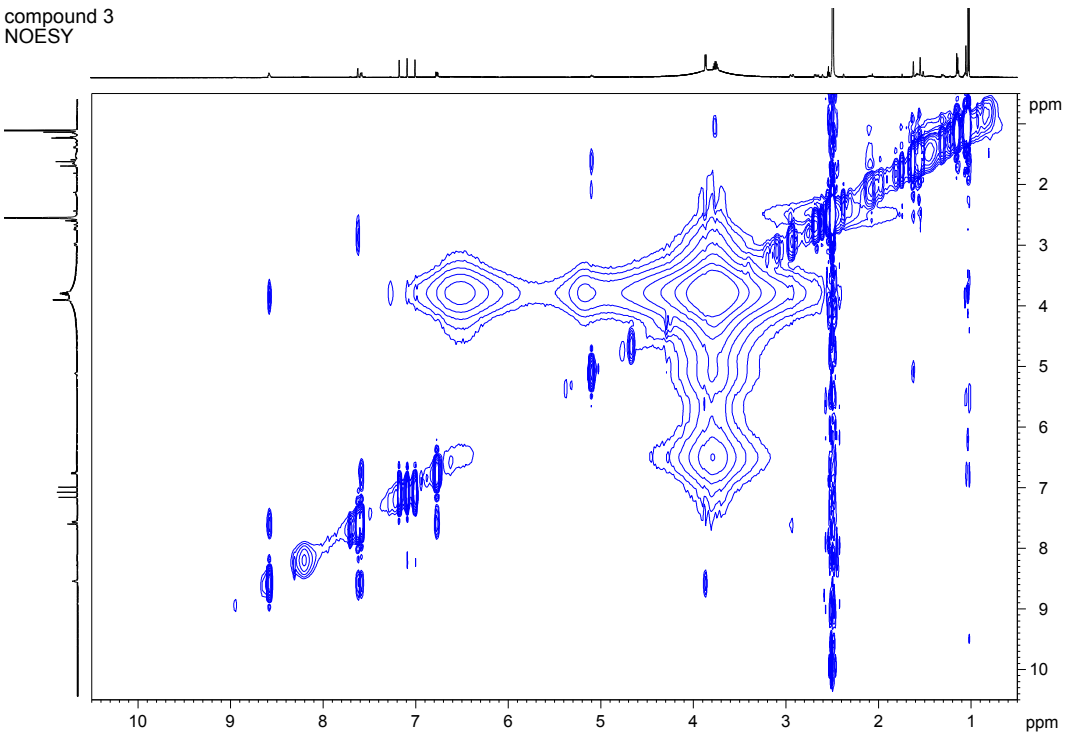

Figure S52. NOESY spectrum of **3**.

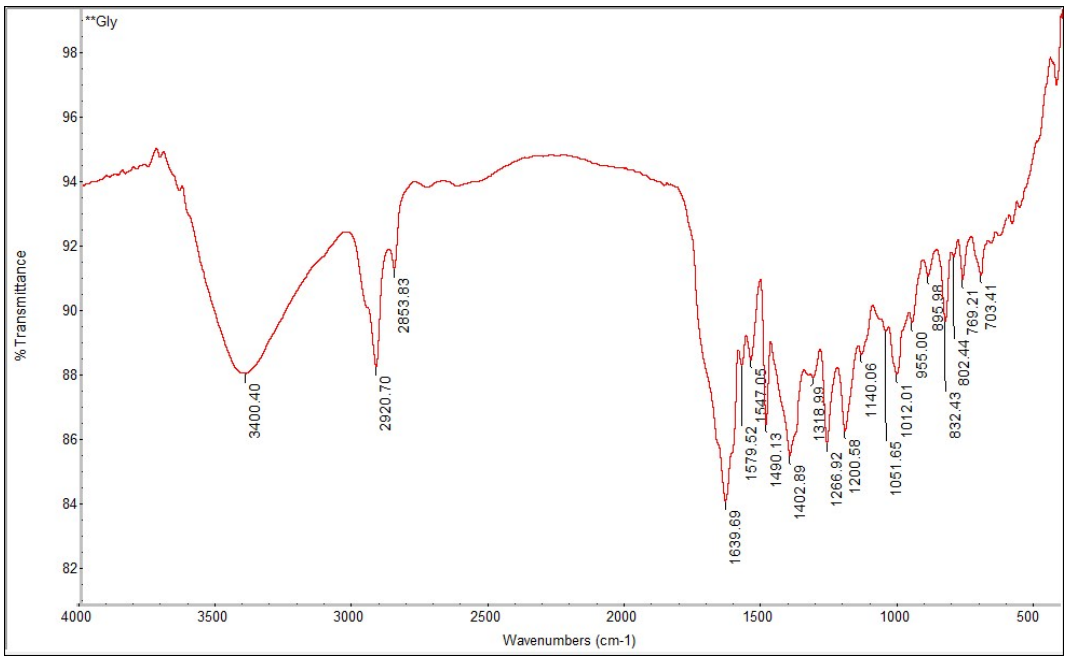

Figure S53. IR spectrum of **3**.

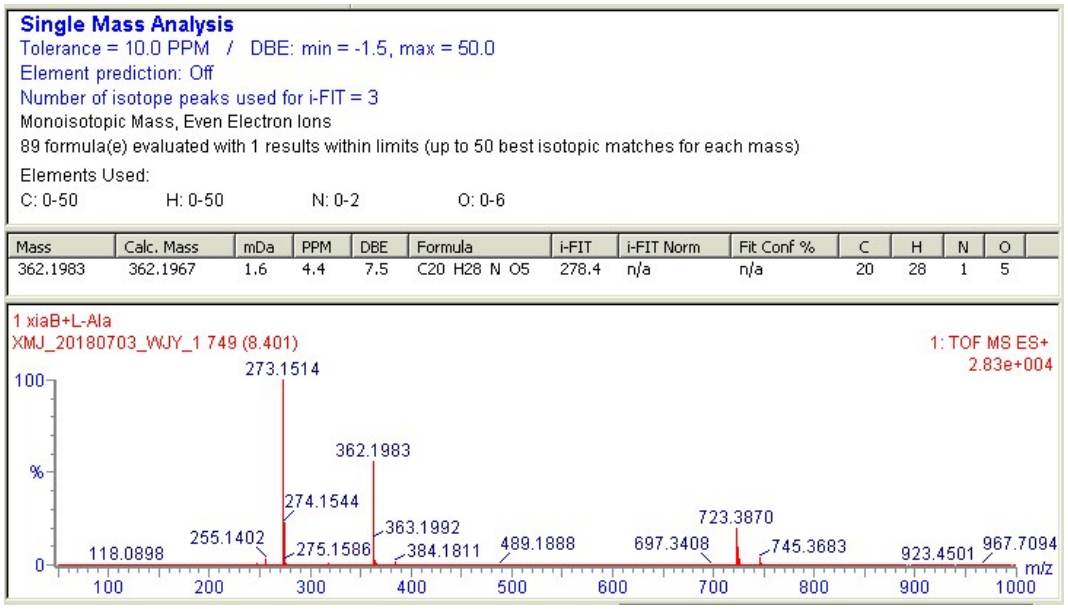

Figure S54. HR-ESI-MS analysis of **4** (Positive mode).

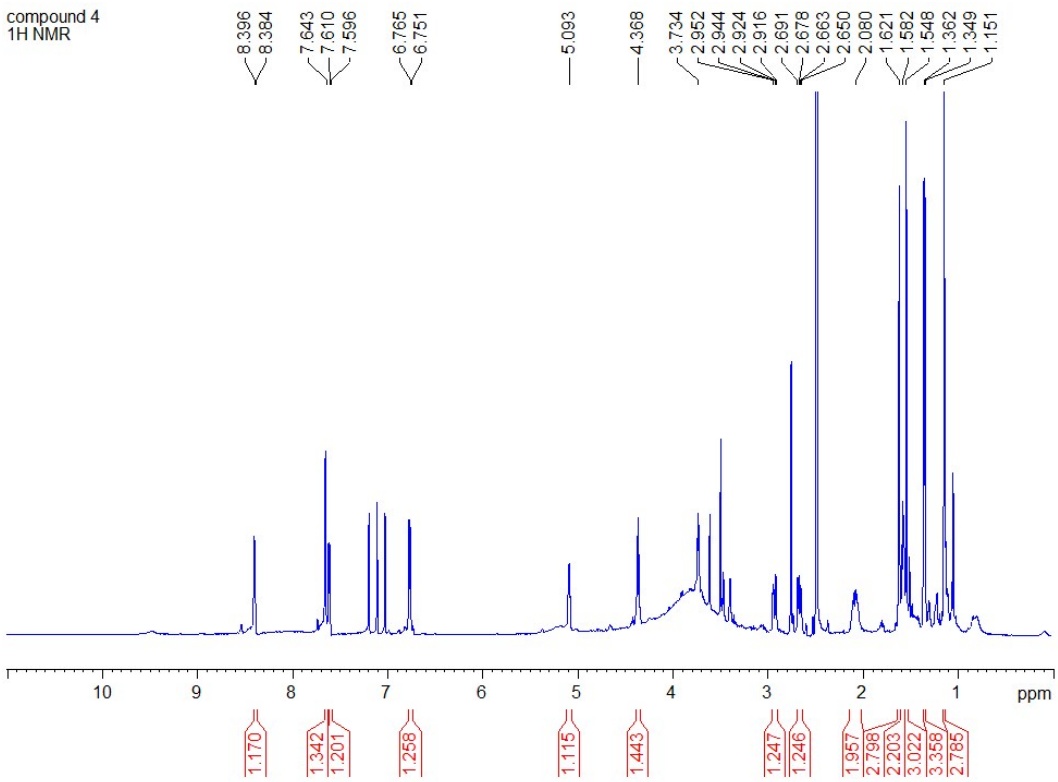

Figure S55. ^{1}H NMR (600 MHz, DMSO-d_6) spectrum of **4**.

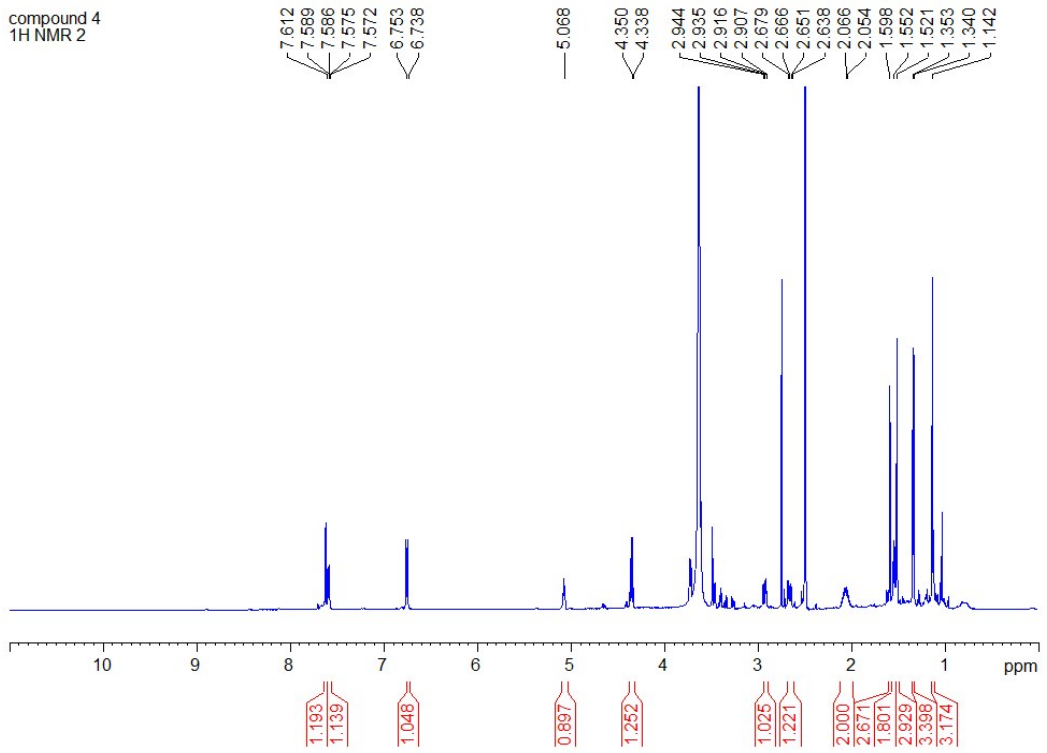

Figure S56. ^{1}H NMR (600 MHz, D_2O and DMSO-d_6) spectrum of **4**.

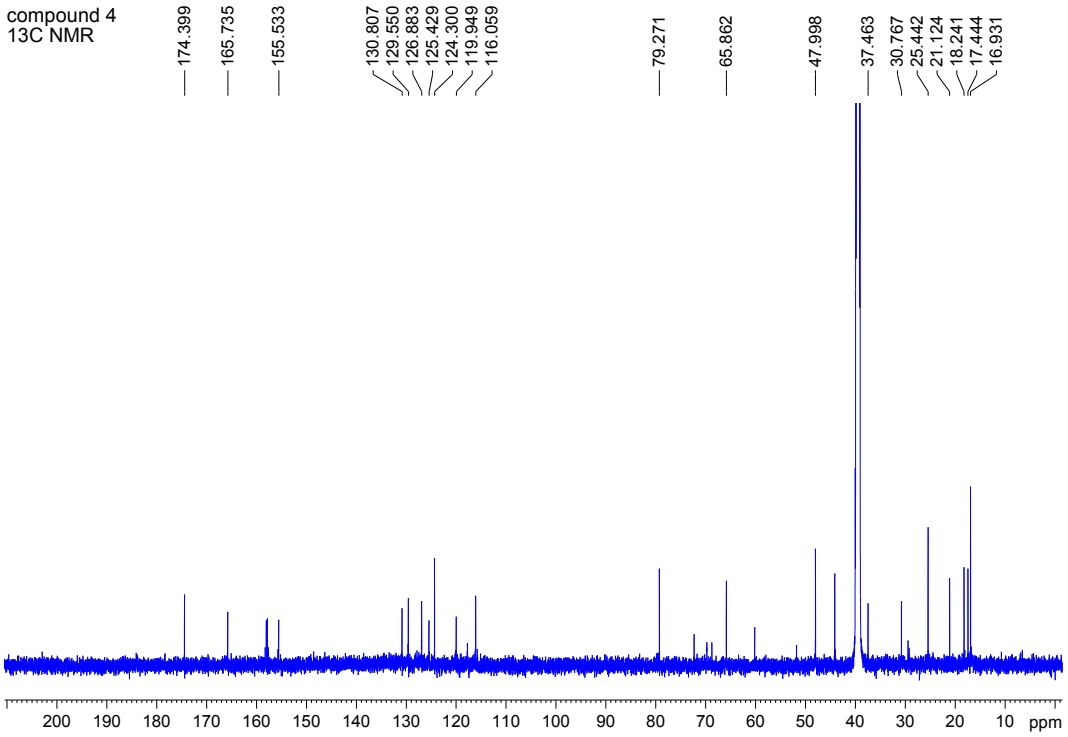

Figure S57. ^{13}C NMR (150 MHz, DMSO-d_6) spectrum of **4**.

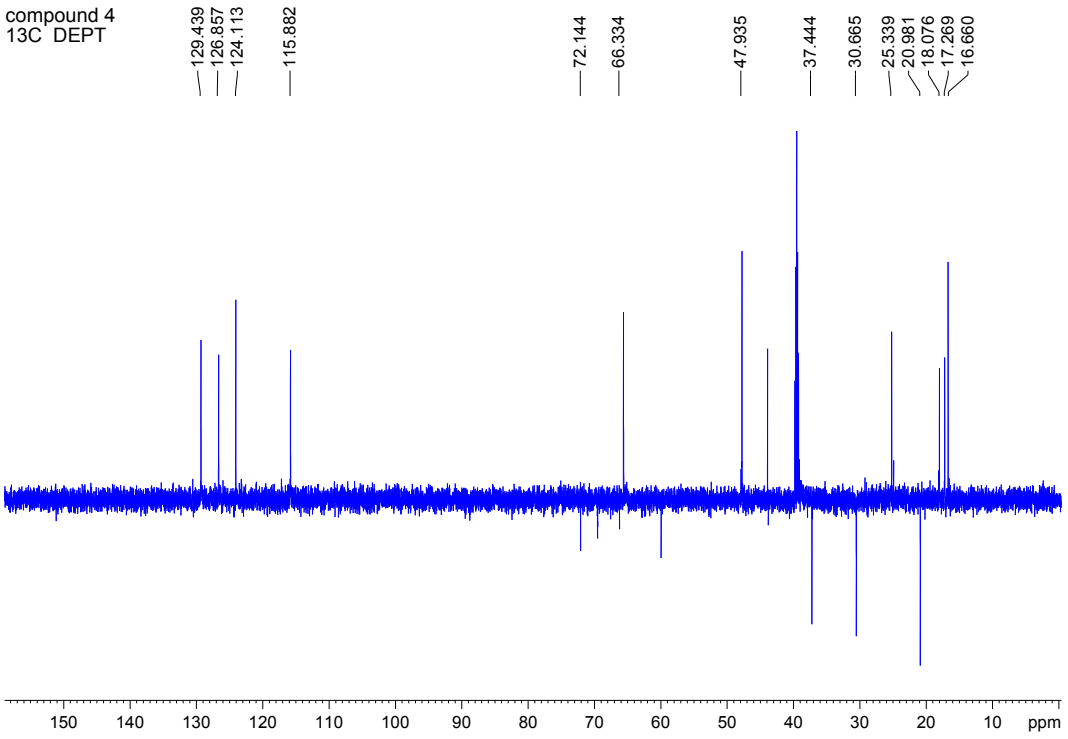

Figure S58. ^{13}C-DEPT NMR (150 MHz, DMSO-d_6) spectrum of **4**.

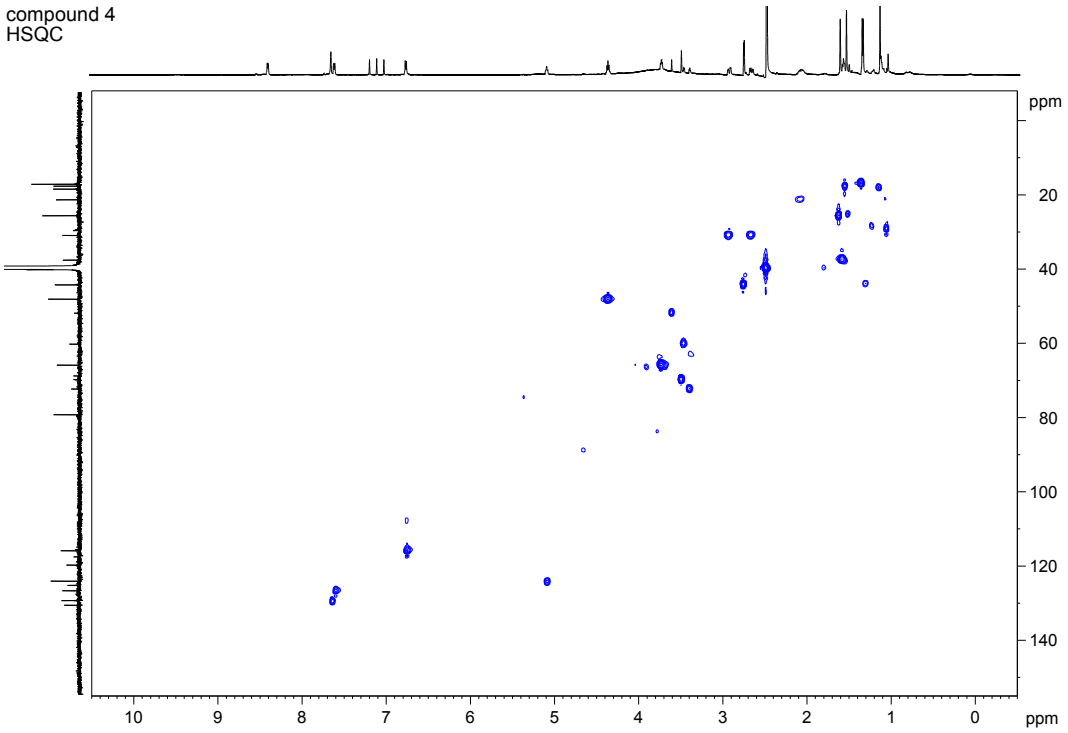

Figure S59. HSQC spectrum of **4**.

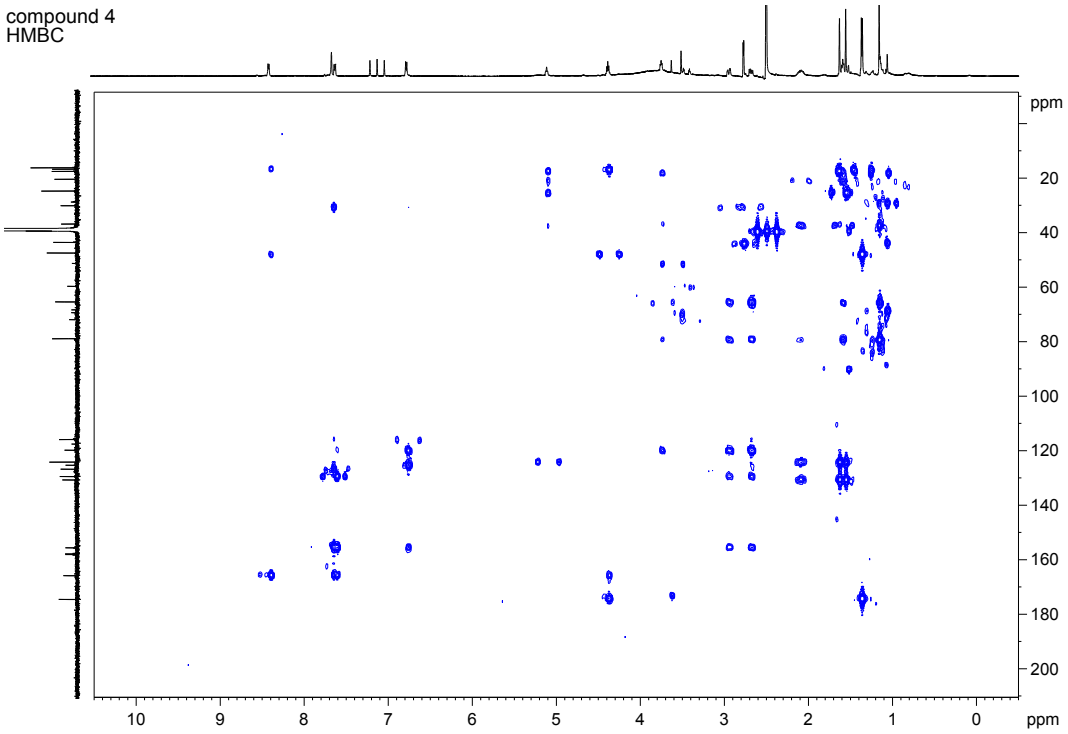

Figure S60. HMBC spectrum of **4**.

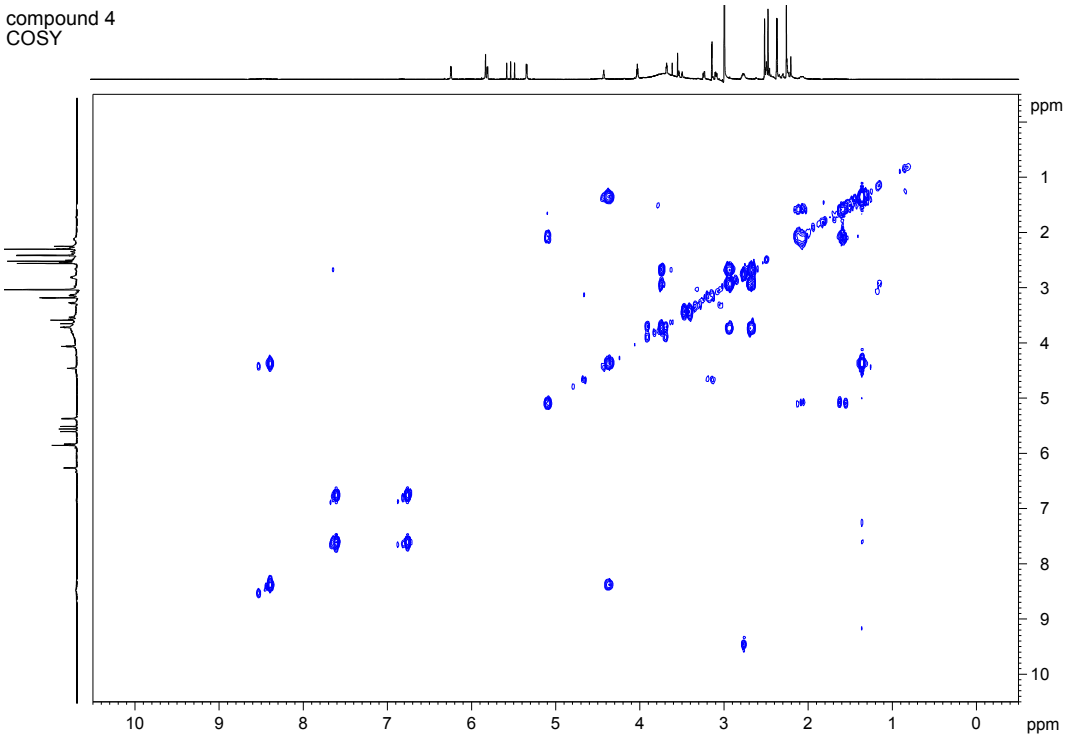

Figure S61. COSY spectrum of **4**.

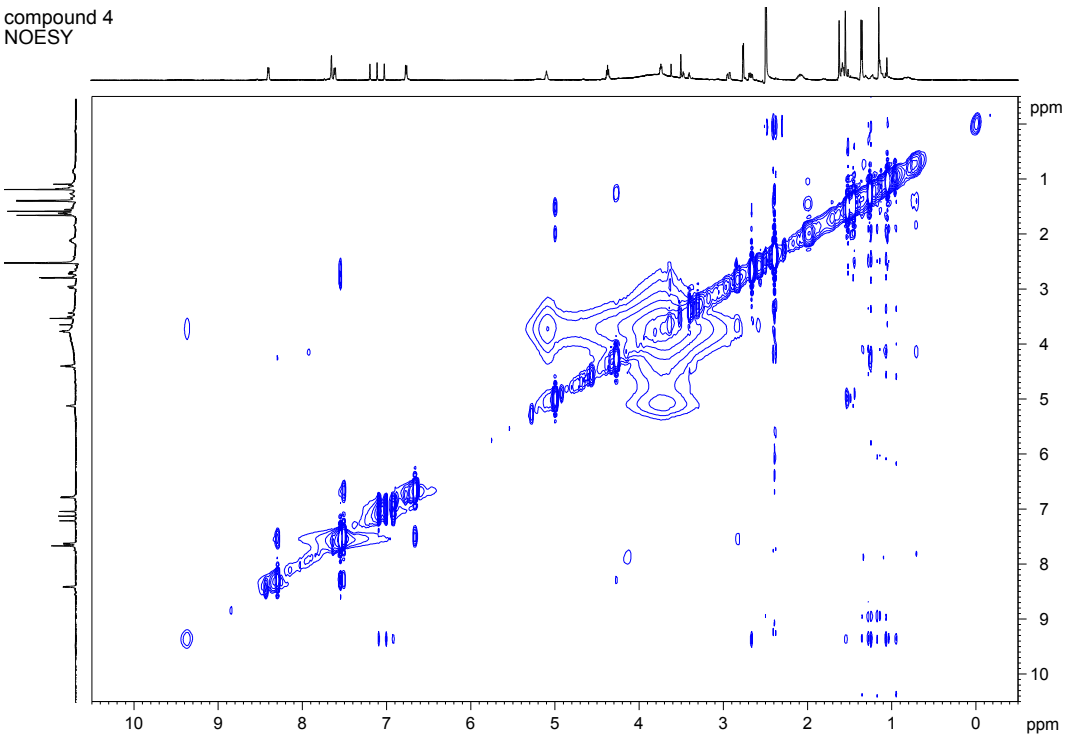

Figure S62. NOESY spectrum of **4**.

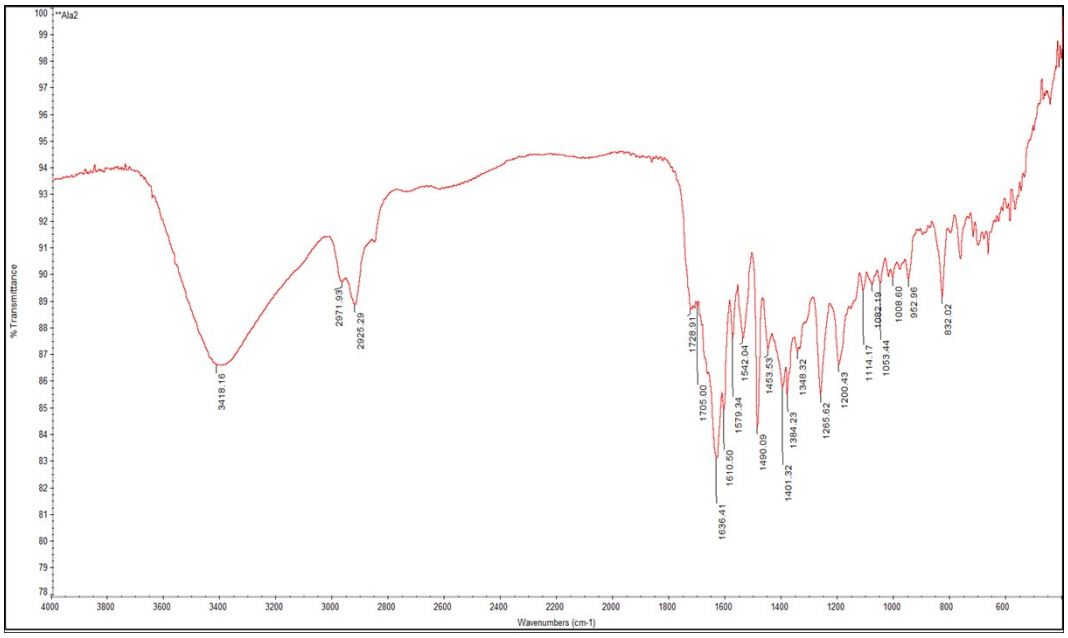

Figure S63. IR spectrum of **4**.

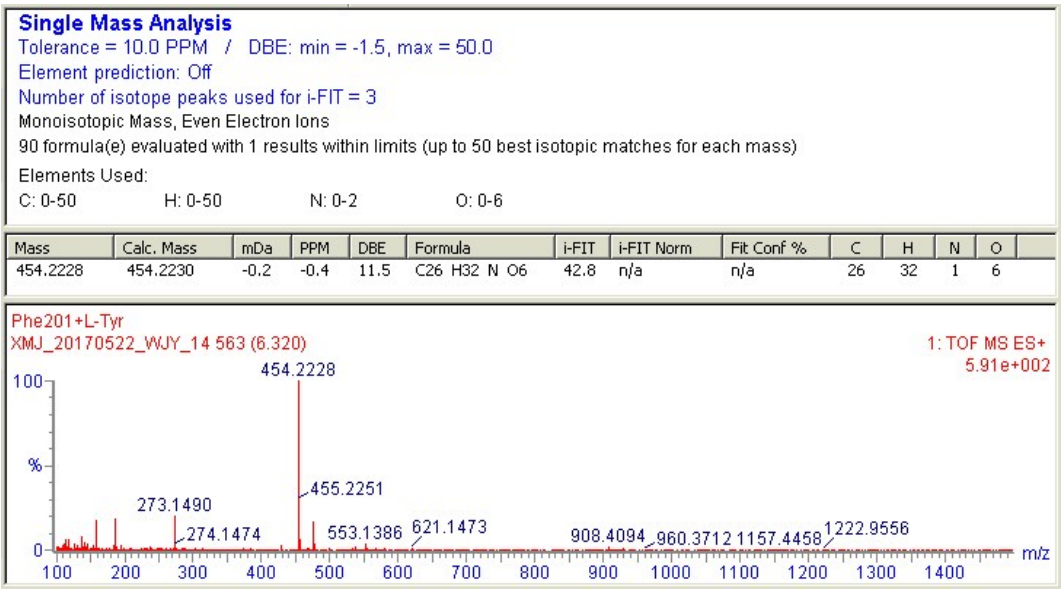

Figure S64. HR-ESI-MS analysis of **5** (Positive mode).

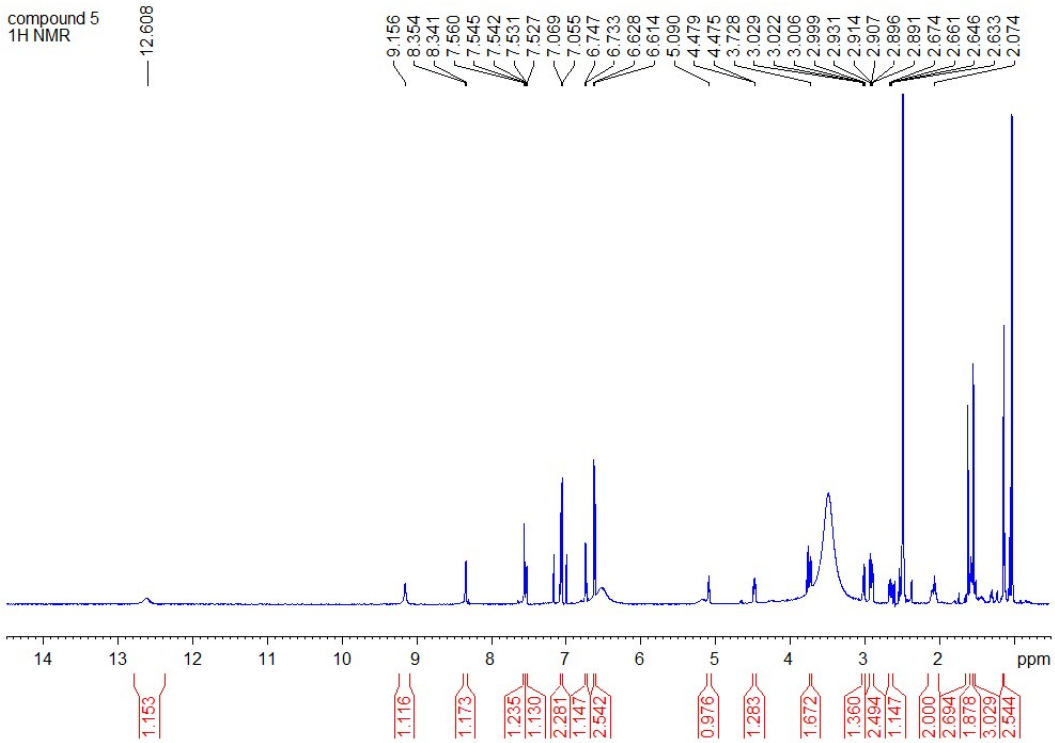

Figure S65. ^{1}H NMR (600 MHz, DMSO-d_6) spectrum of **5**.

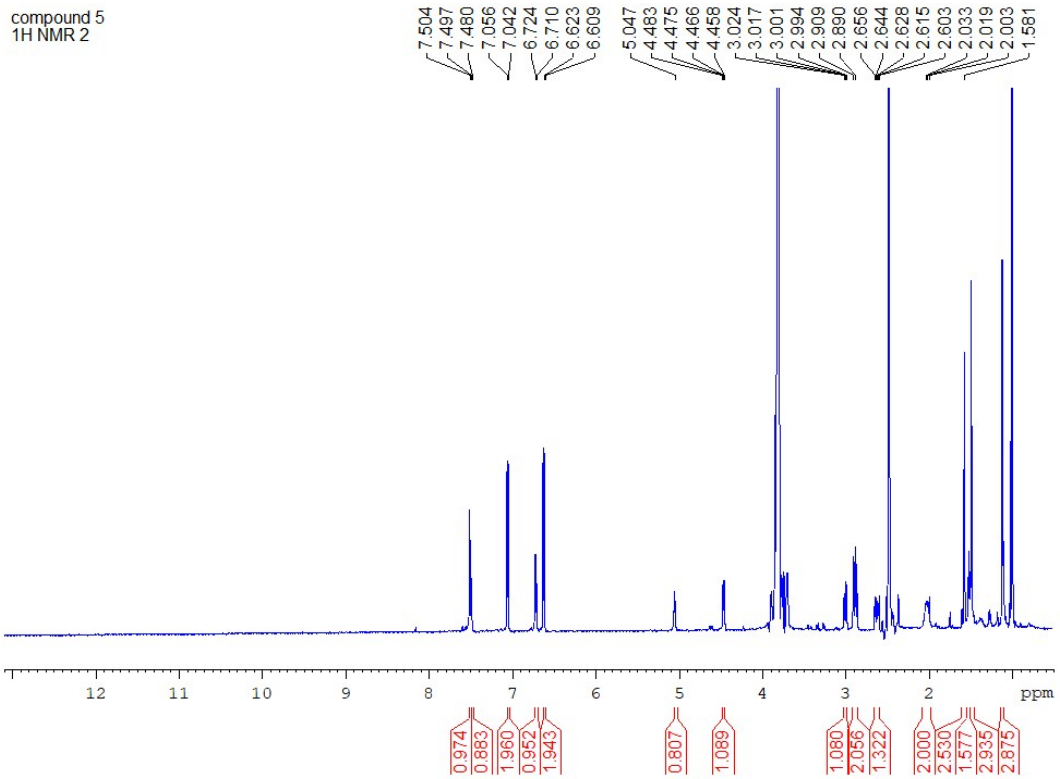

Figure S66. ^{1}H NMR (600 MHz, D_2O and DMSO-d_6) spectrum of **5**.

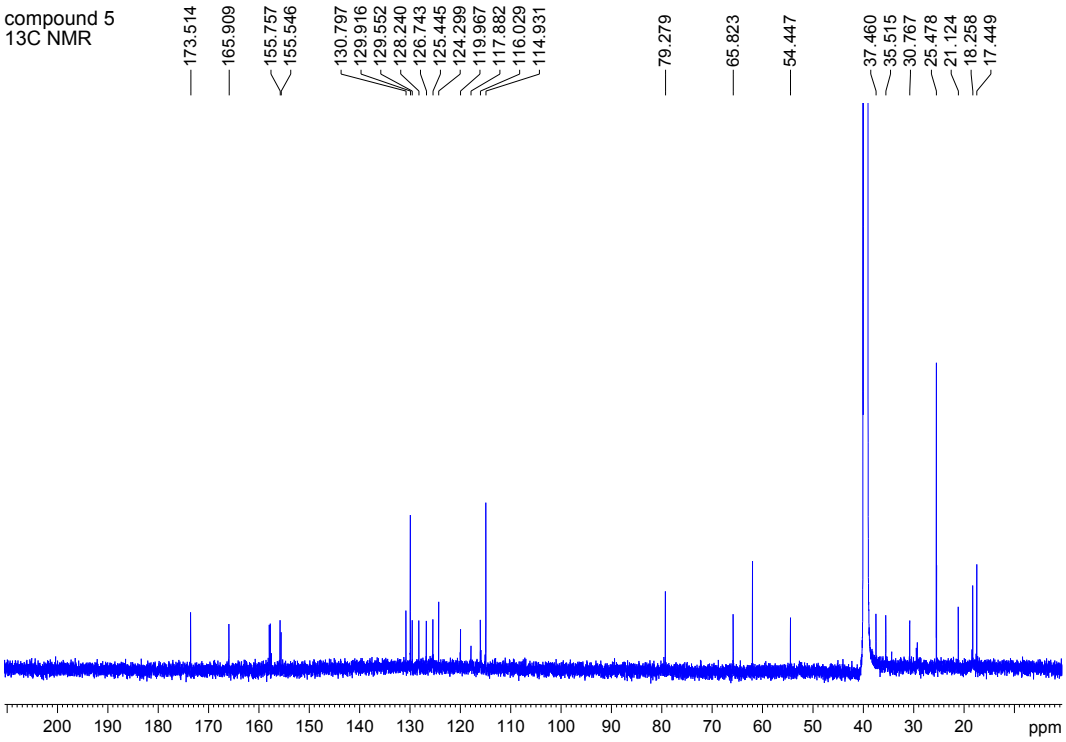

Figure S67. ^{13}C NMR (150 MHz, DMSO-d_6) spectrum of **5**.

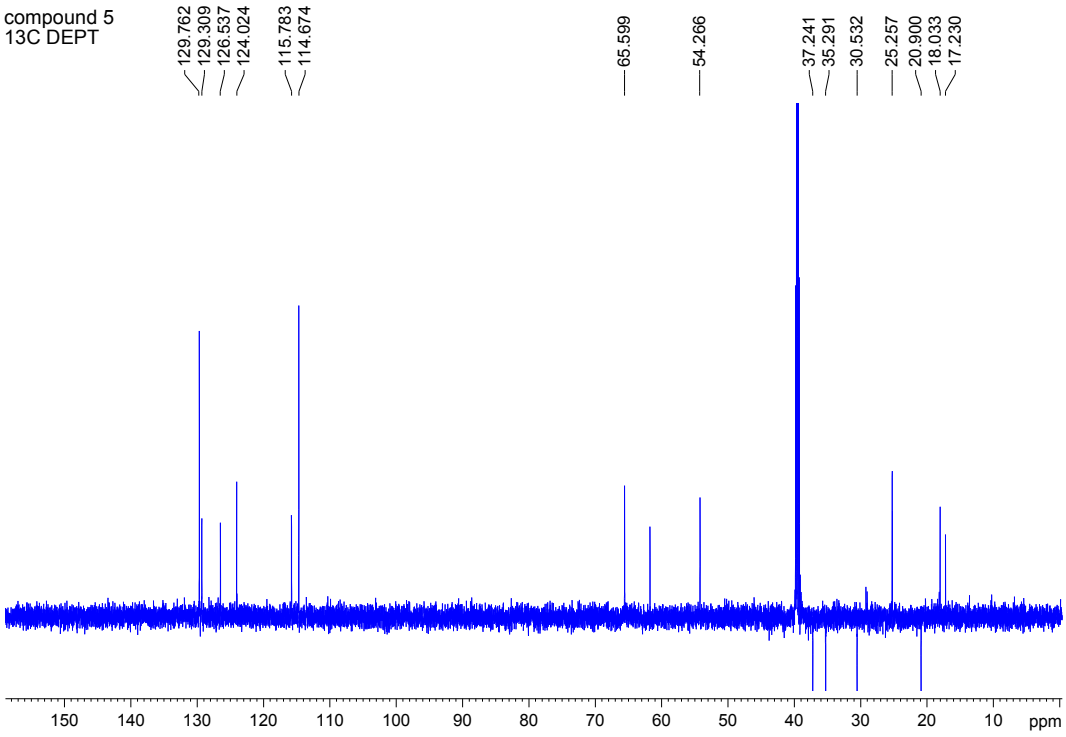

Figure S68. ^{13}C-DEPT NMR (150 MHz, DMSO-d_6) spectrum of **5**.

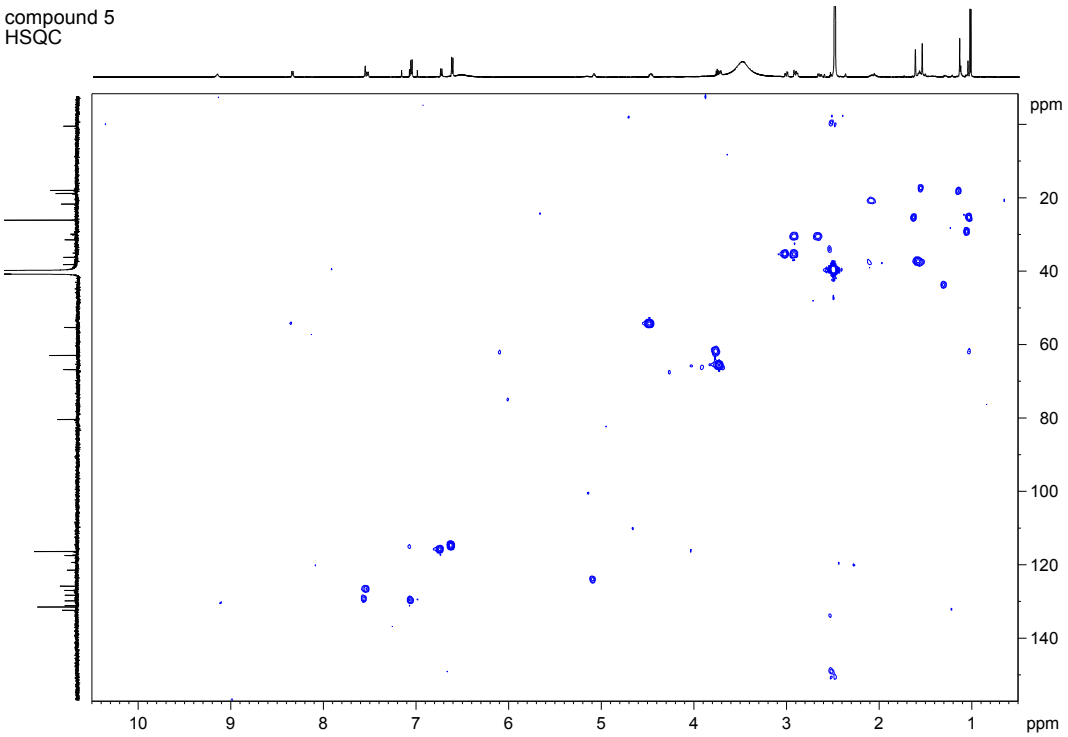

Figure S69. HSQC spectrum of **5**.

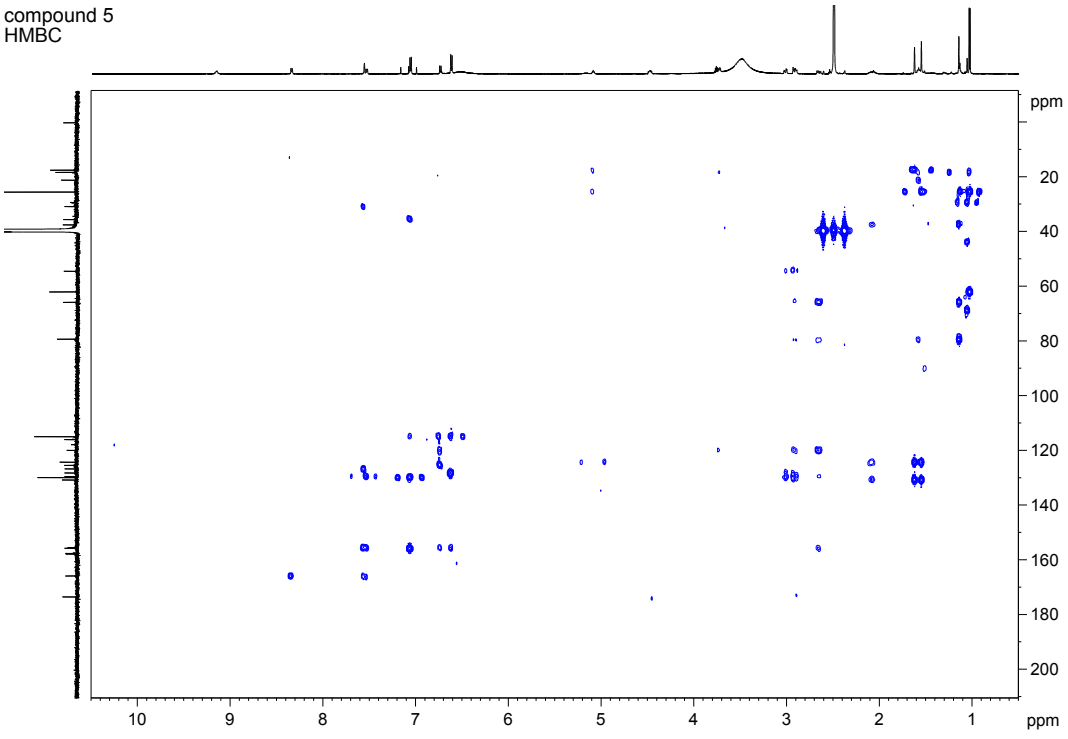

Figure S70. HMBC spectrum of **5**.

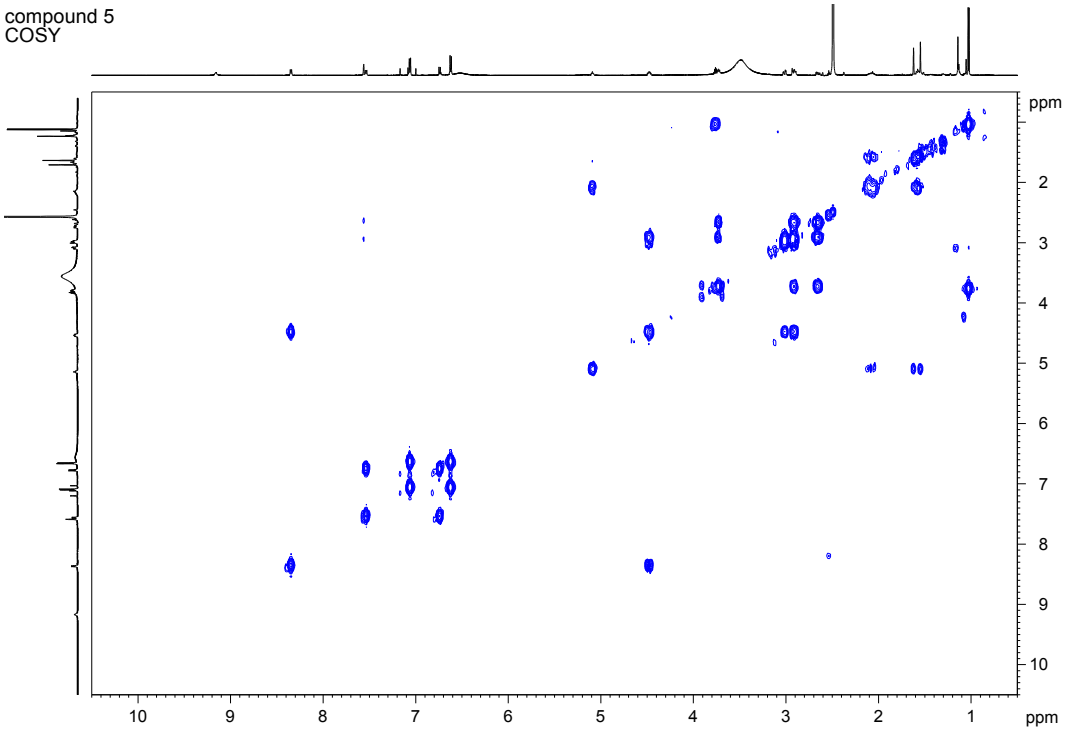

Figure S71. COSY spectrum of **5**.

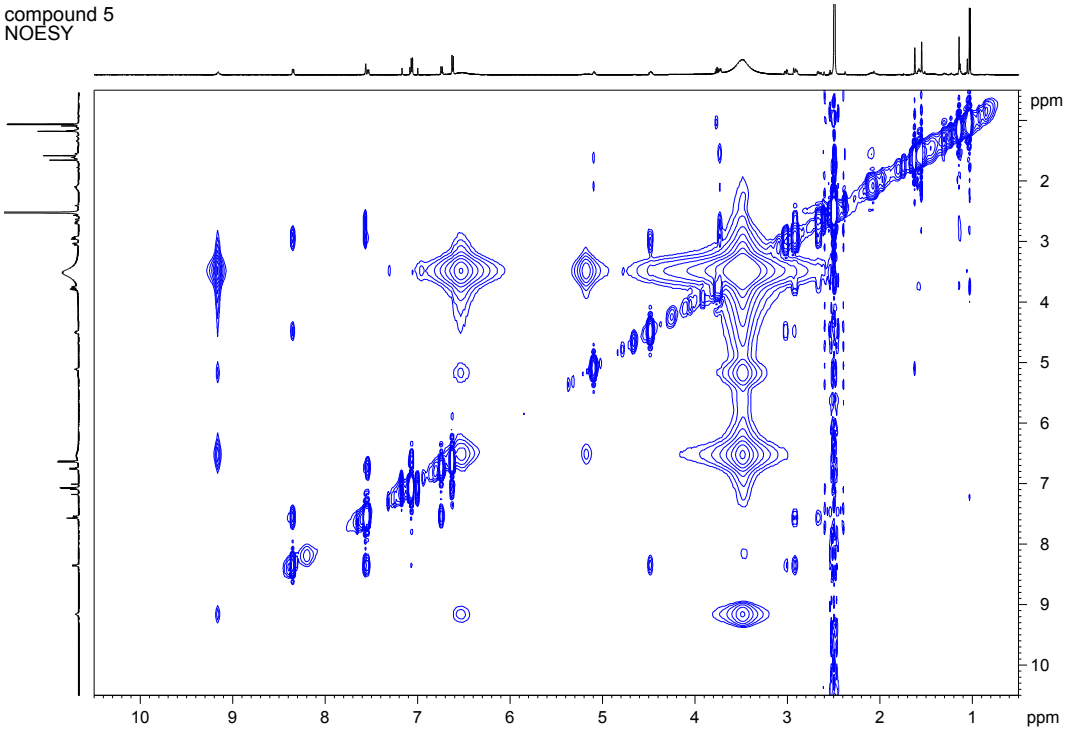

Figure S72. NOESY spectrum of **5**.

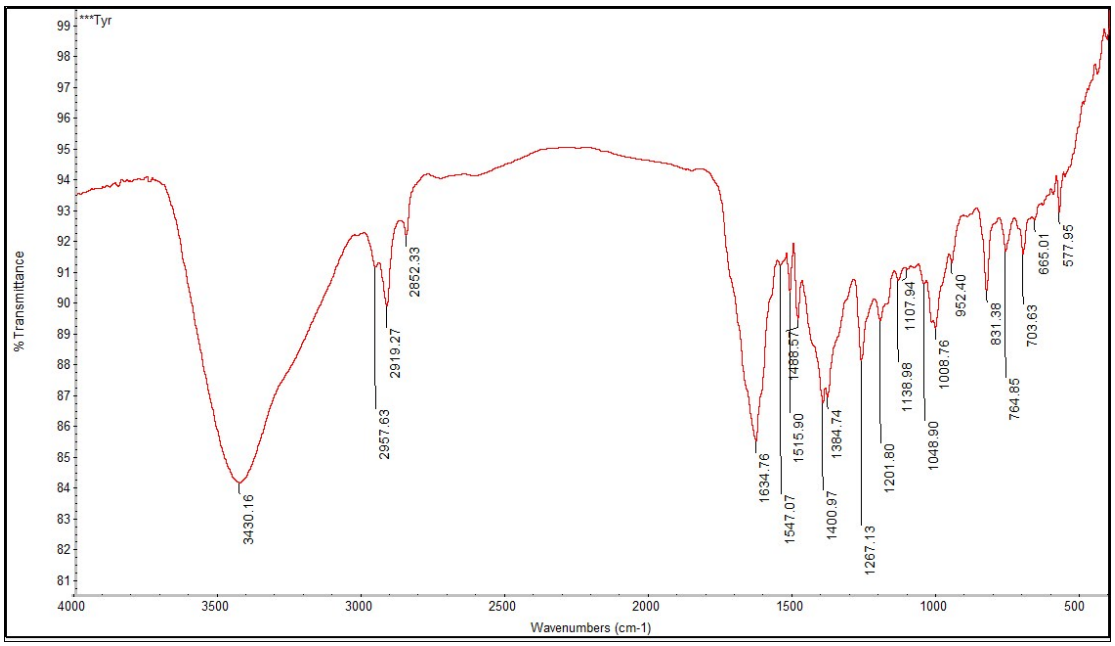

Figure S73. IR spectrum of **5**.

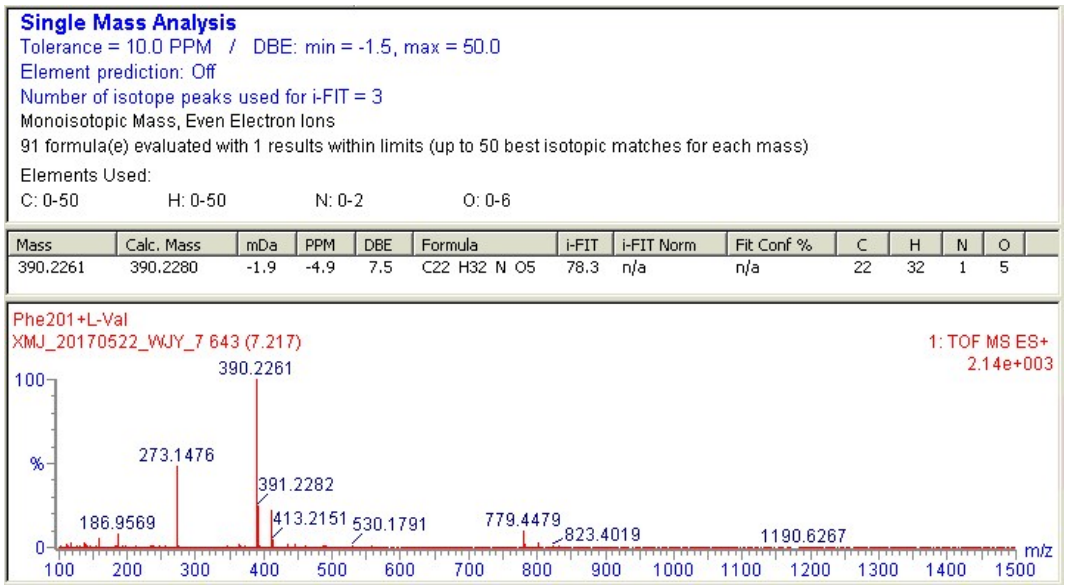

Figure S74. HR-ESI-MS analysis of **6** (Positive mode).

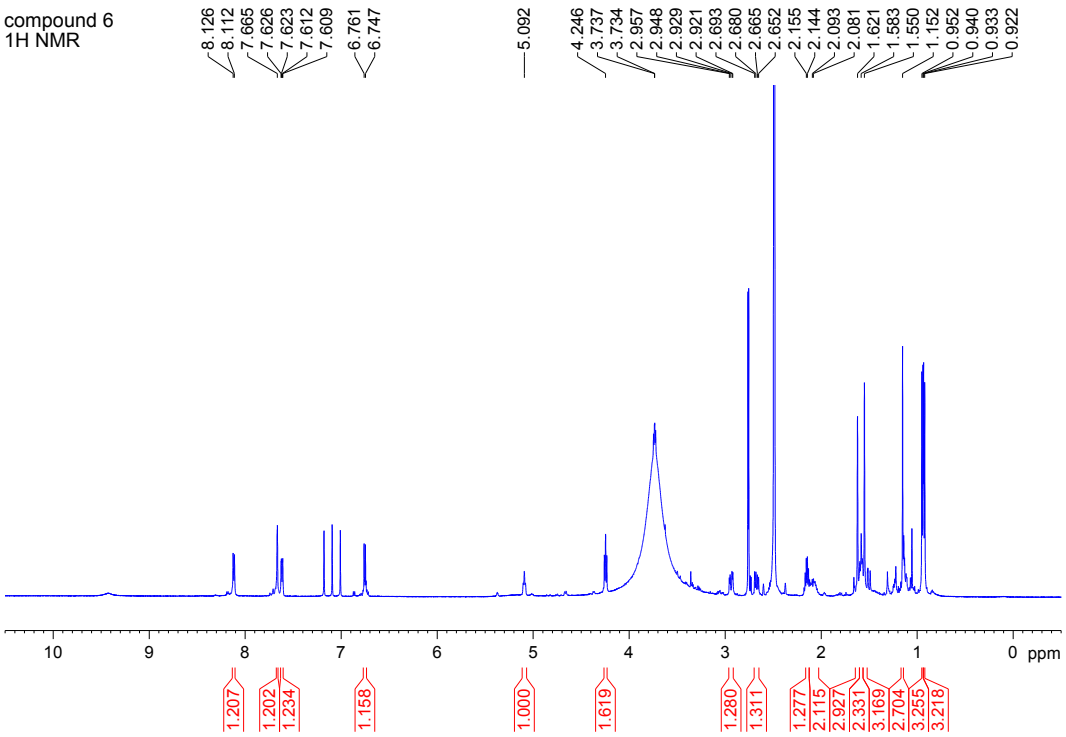

Figure S75. ^{1}H NMR (600 MHz, DMSO-d_6) spectrum of **6**.

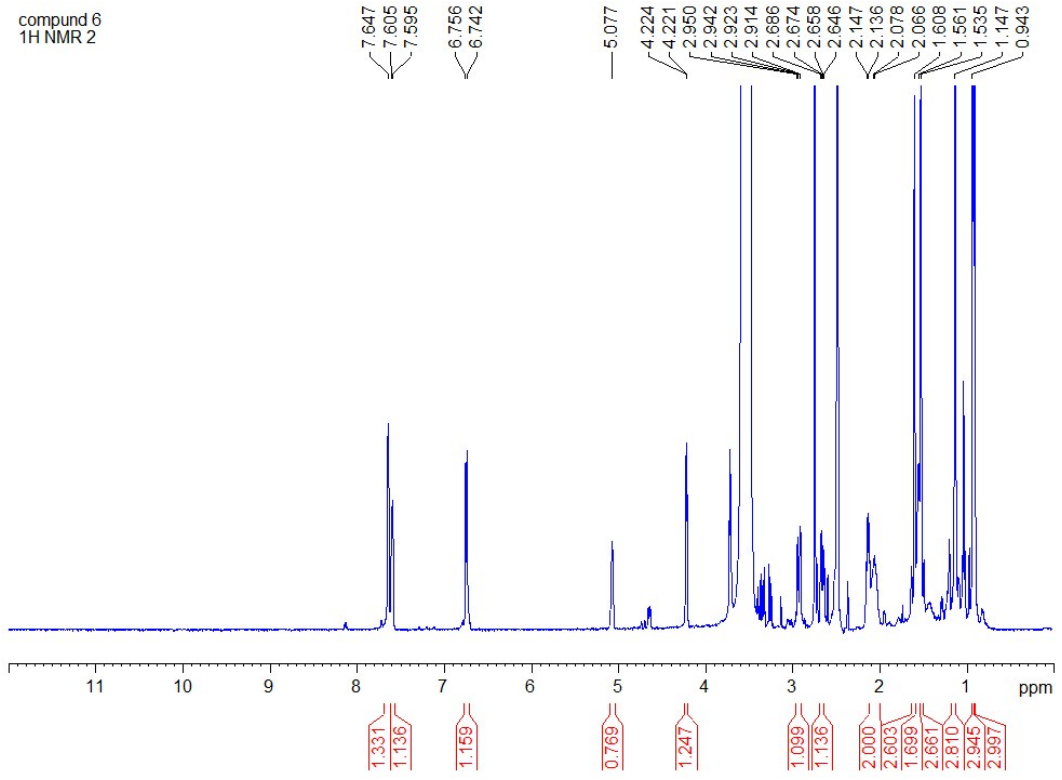

Figure S76. ^{1}H NMR (600 MHz, D_2O and DMSO-d_6) spectrum of **6**.

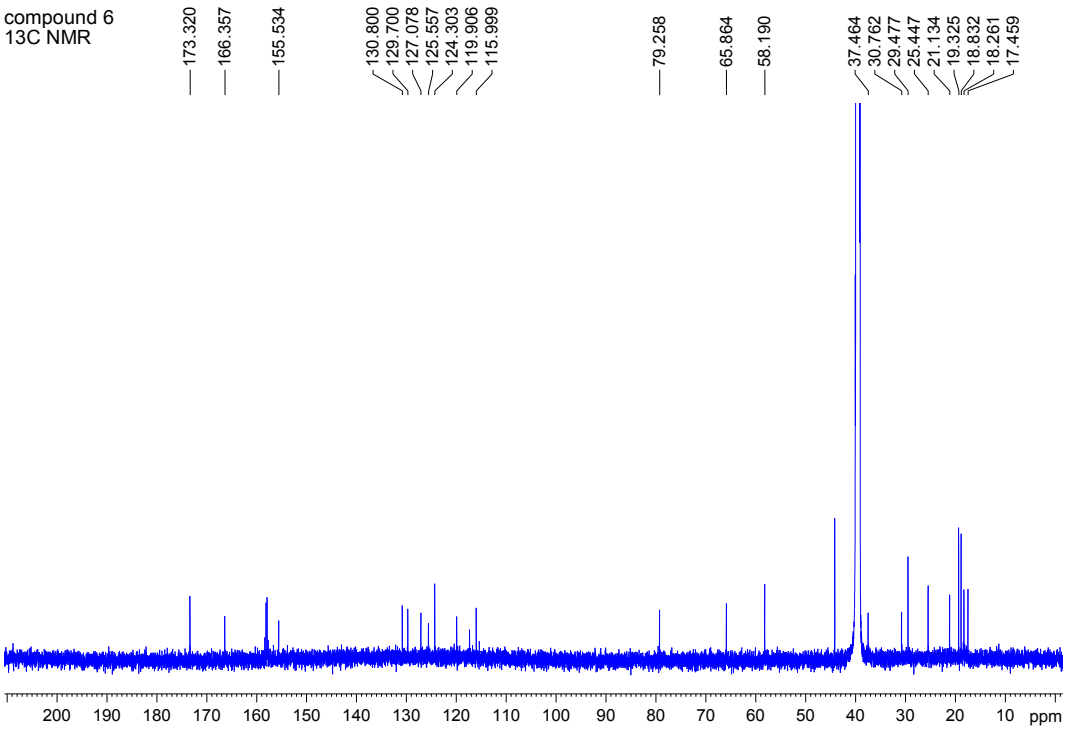

Figure S77. ^{13}C NMR (150 MHz, DMSO-d_6) spectrum of **6**.

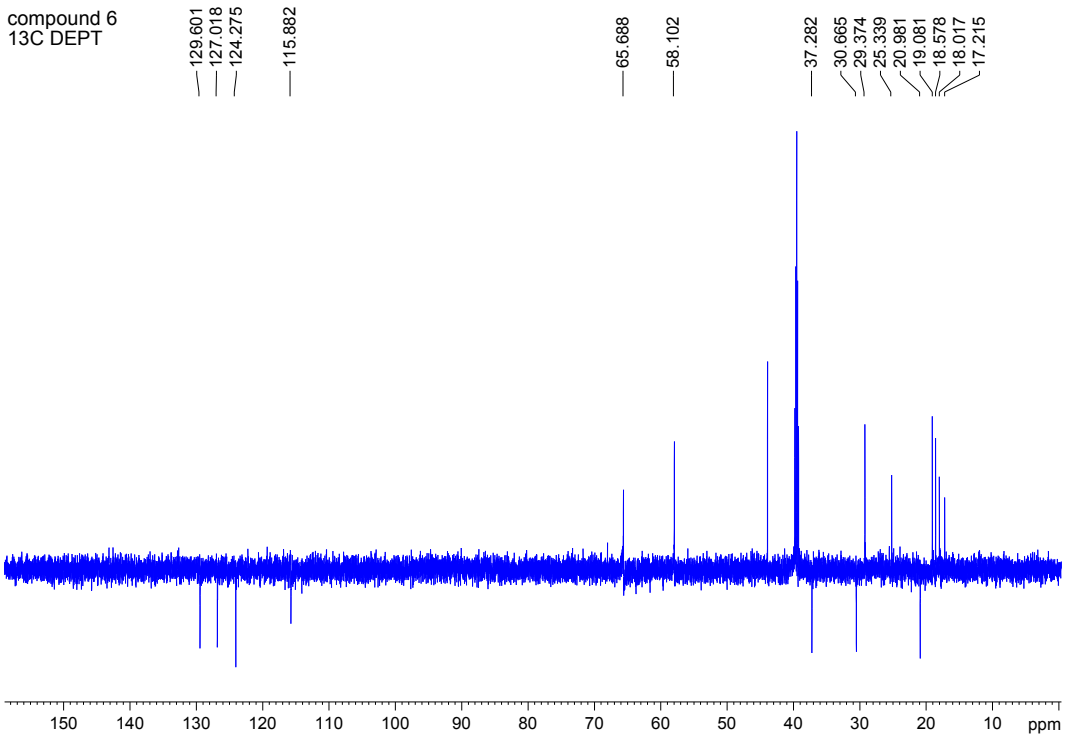

Figure S78. ^{13}C-DEPT NMR (150 MHz, DMSO-d_6) spectrum of **6**.

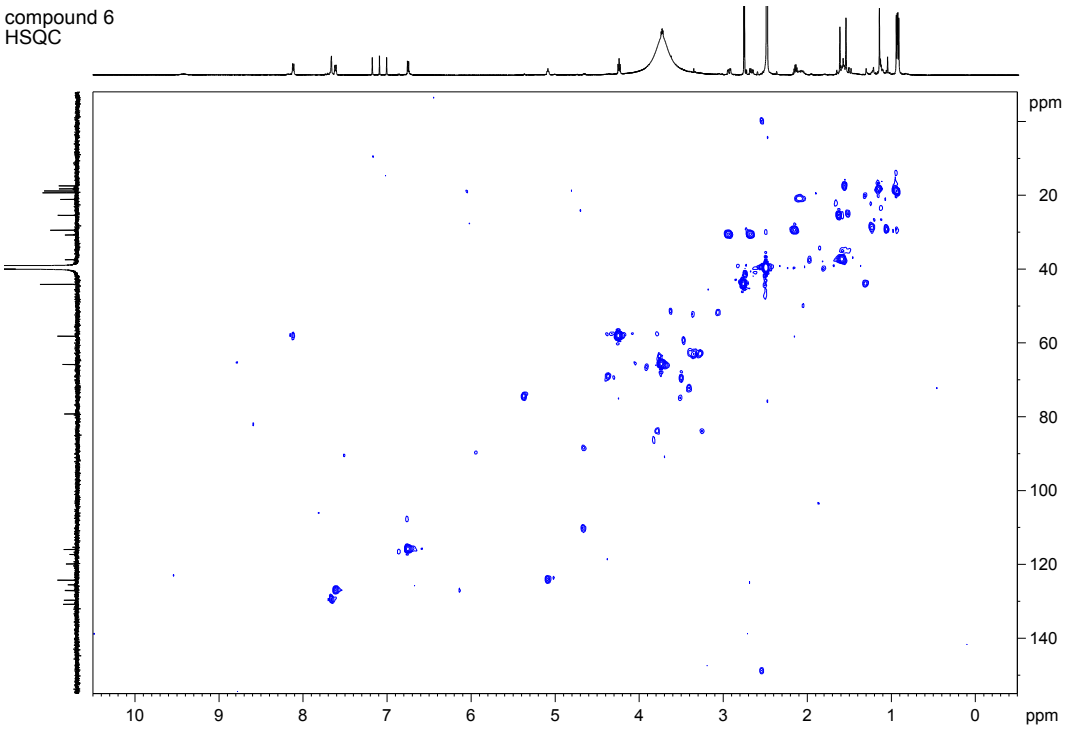

Figure S79. HSQC spectrum of **6**.

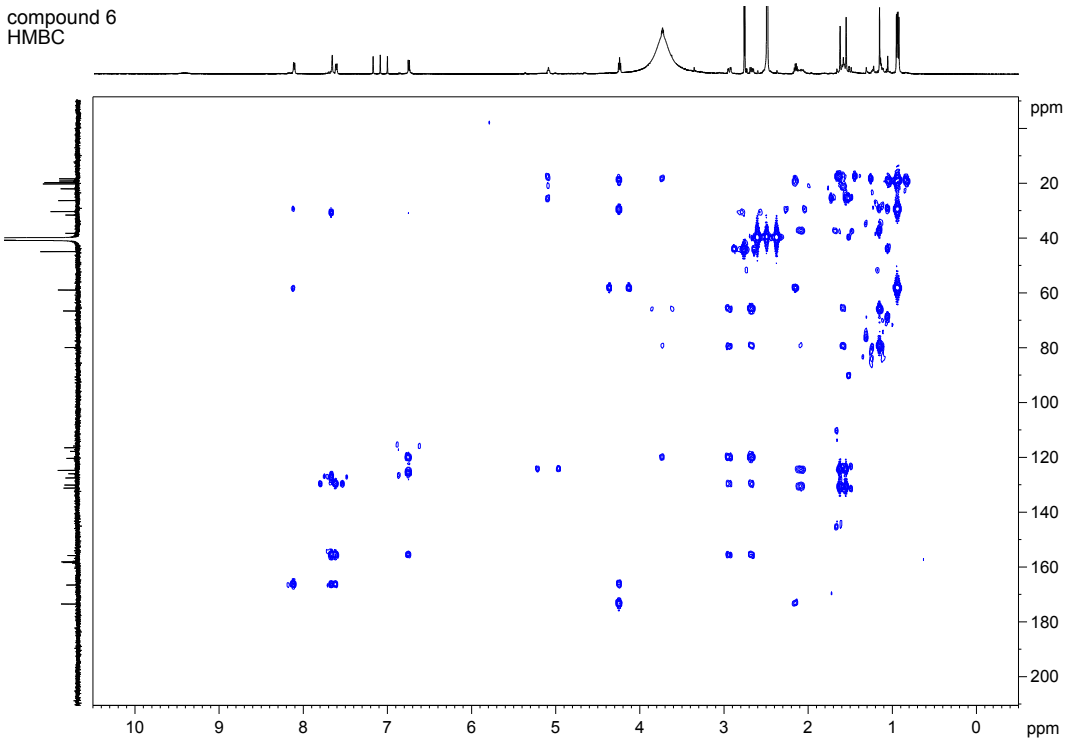

Figure S80. HMBC spectrum of **6**.

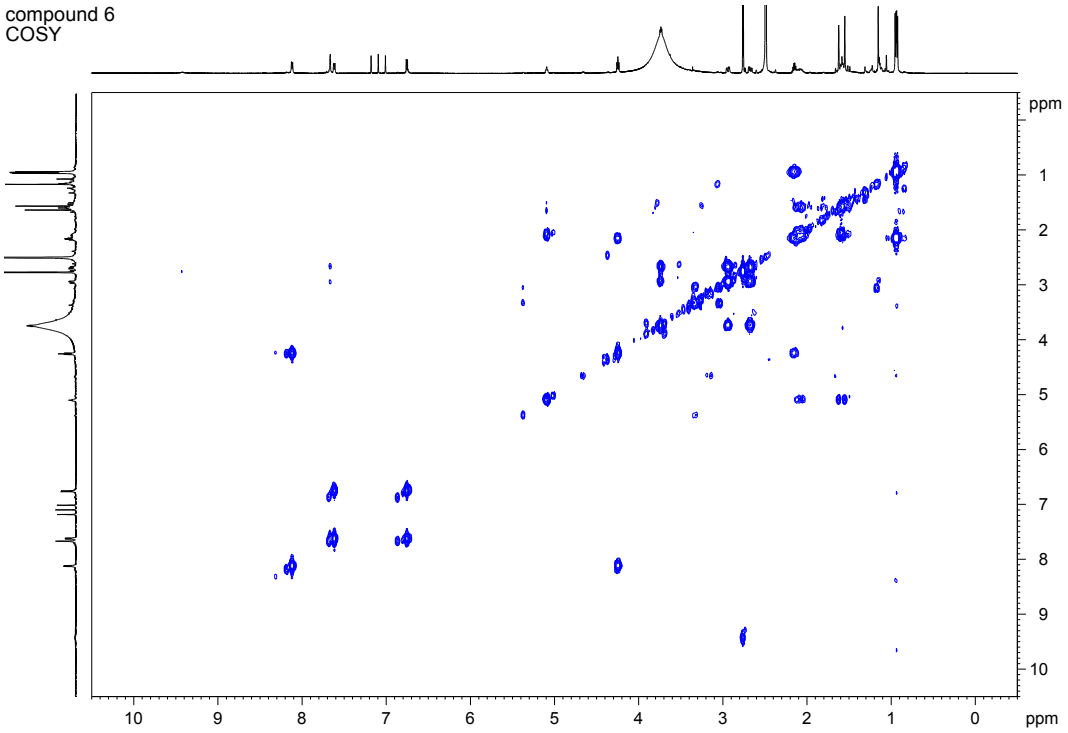

Figure S81. COSY spectrum of **6**.

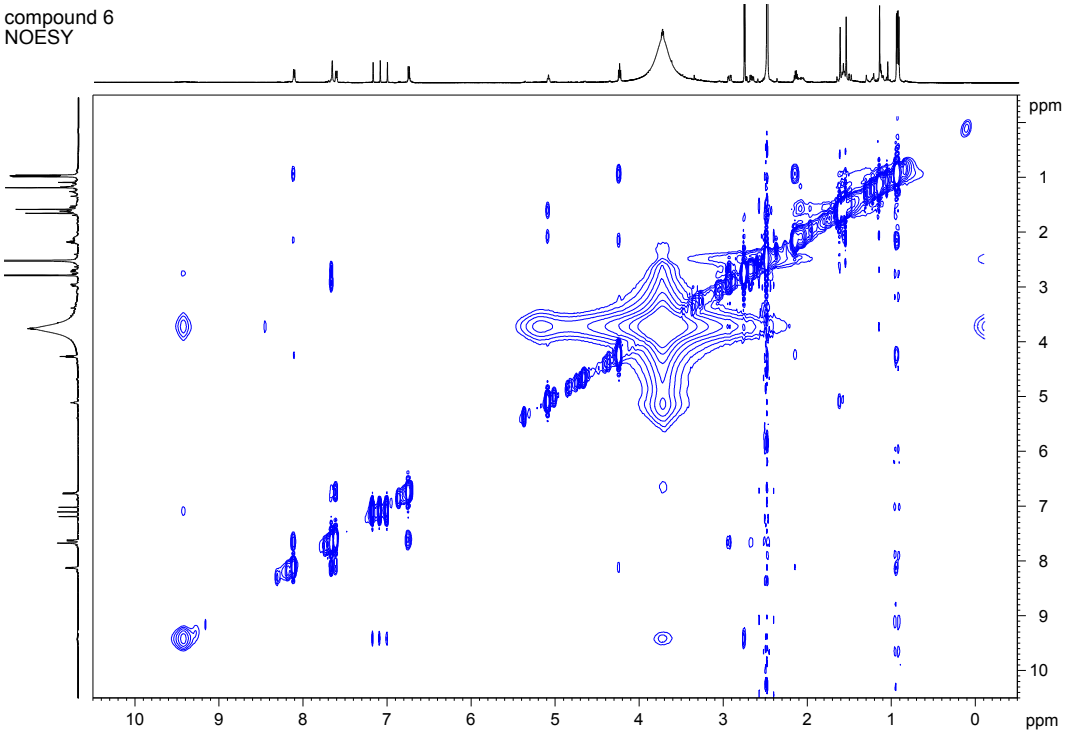

Figure S82. NOESY spectrum of **6**.

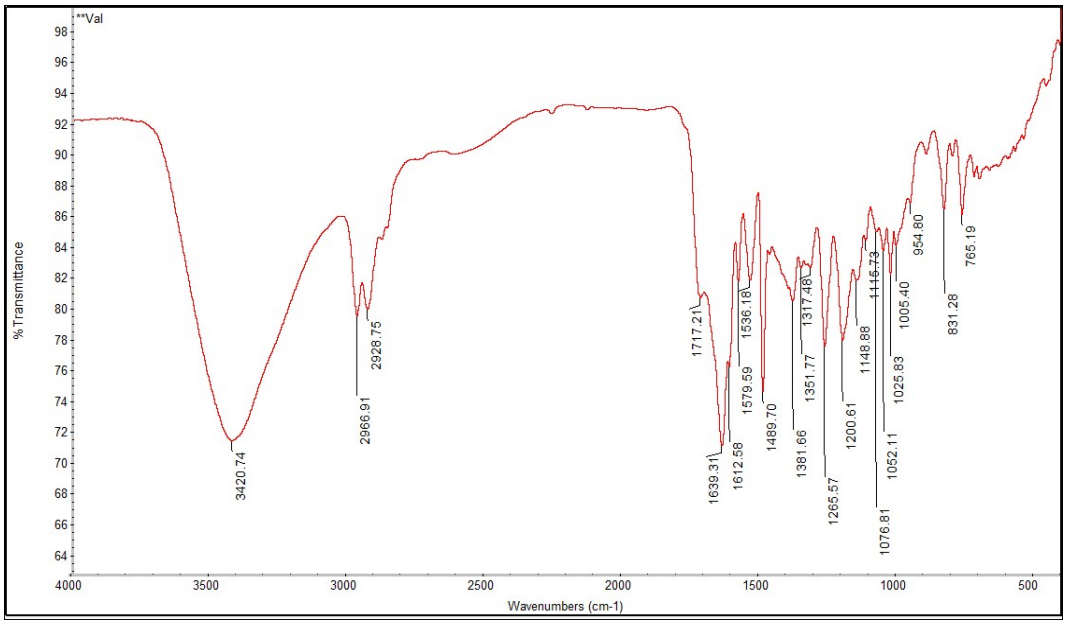

Figure S83. IR spectrum of **6**.

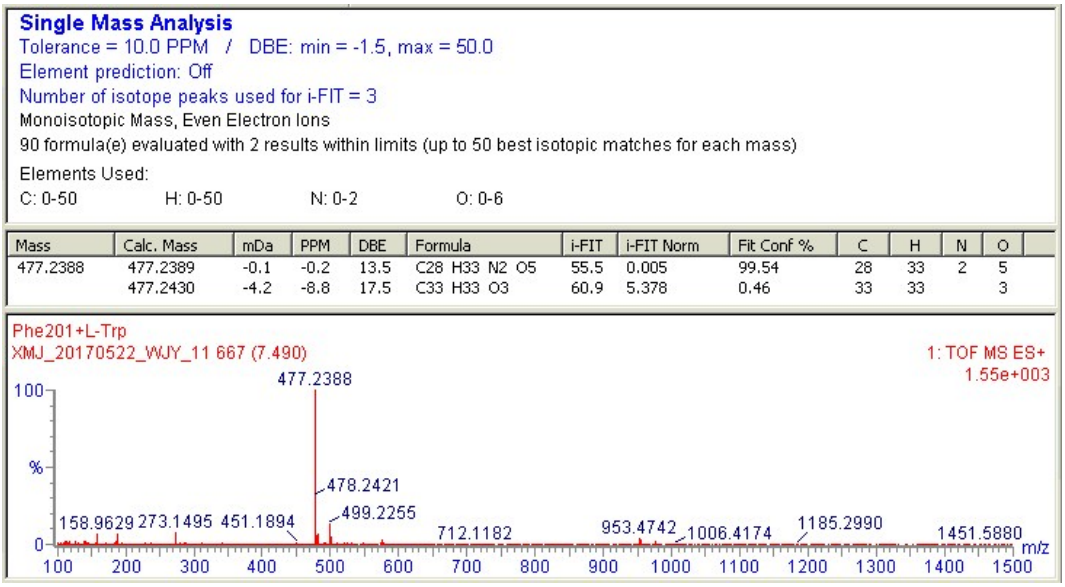

Figure S84. HR-ESI-MS analysis of **7** (Positive mode).

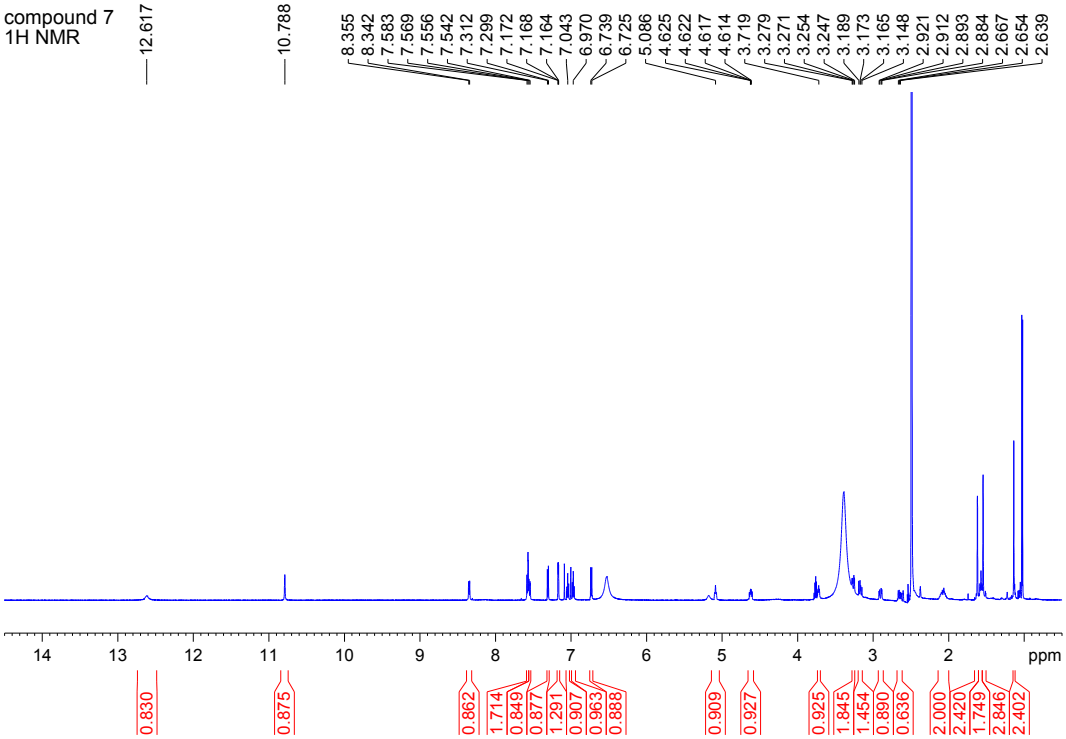

Figure S85. ^{1}H NMR (600 MHz, DMSO-d_6) spectrum of **7**.

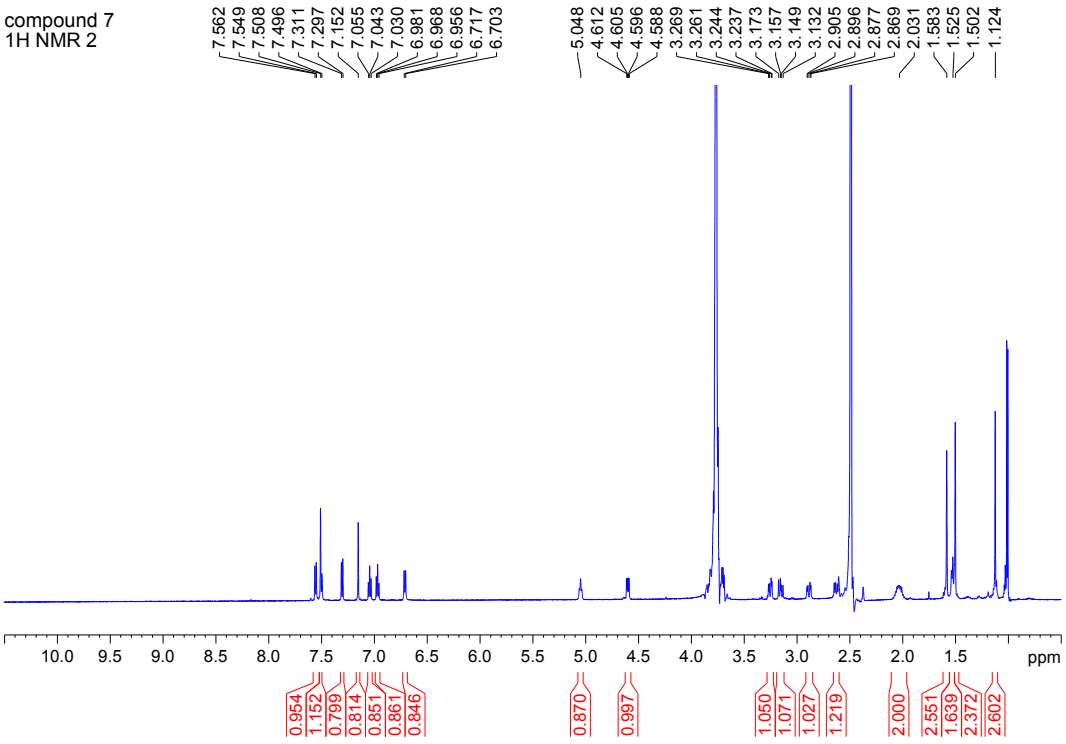

Figure S86. ^{1}H NMR (600 MHz, D_2O and DMSO-d_6) spectrum of **7**.

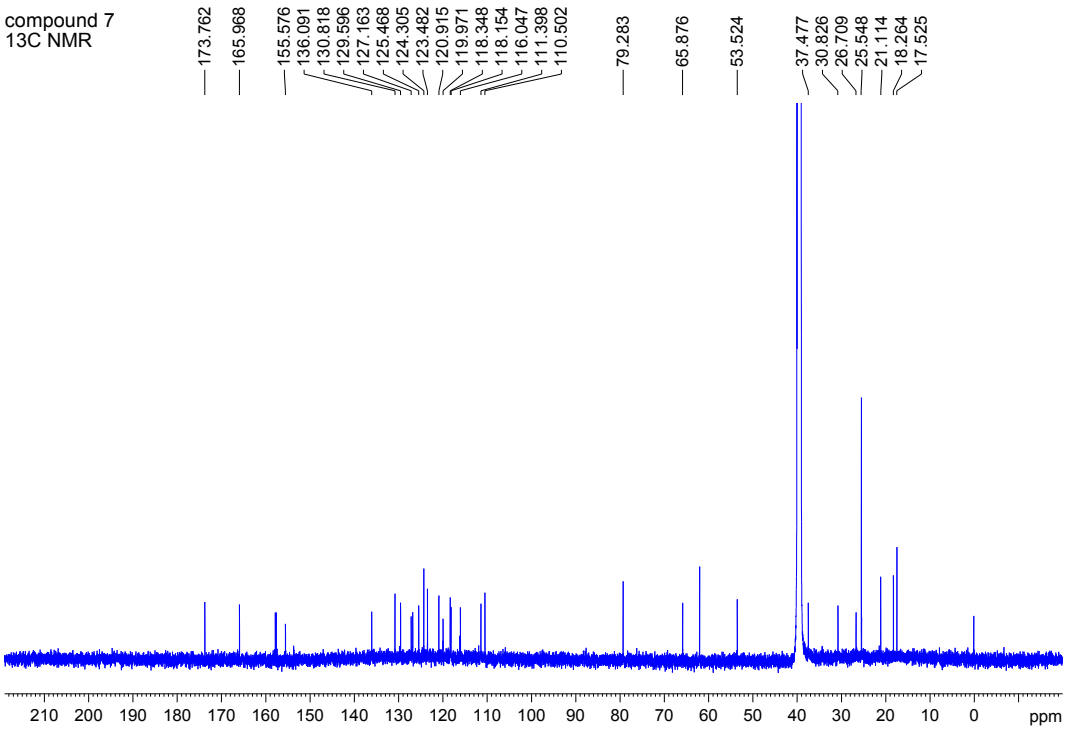

Figure S87. ^{13}C NMR (150 MHz, DMSO-d_6) spectrum of **7**.

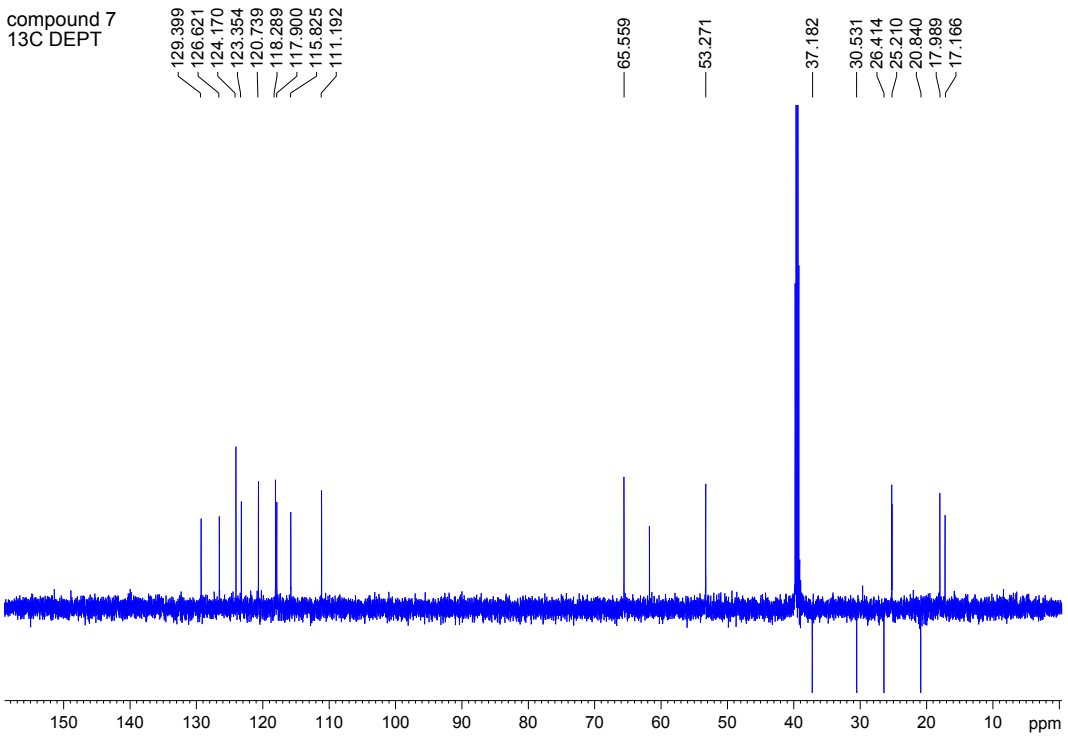

Figure S88. ^{13}C-DEPT (150 MHz, DMSO-d_6) spectrum of **7**.

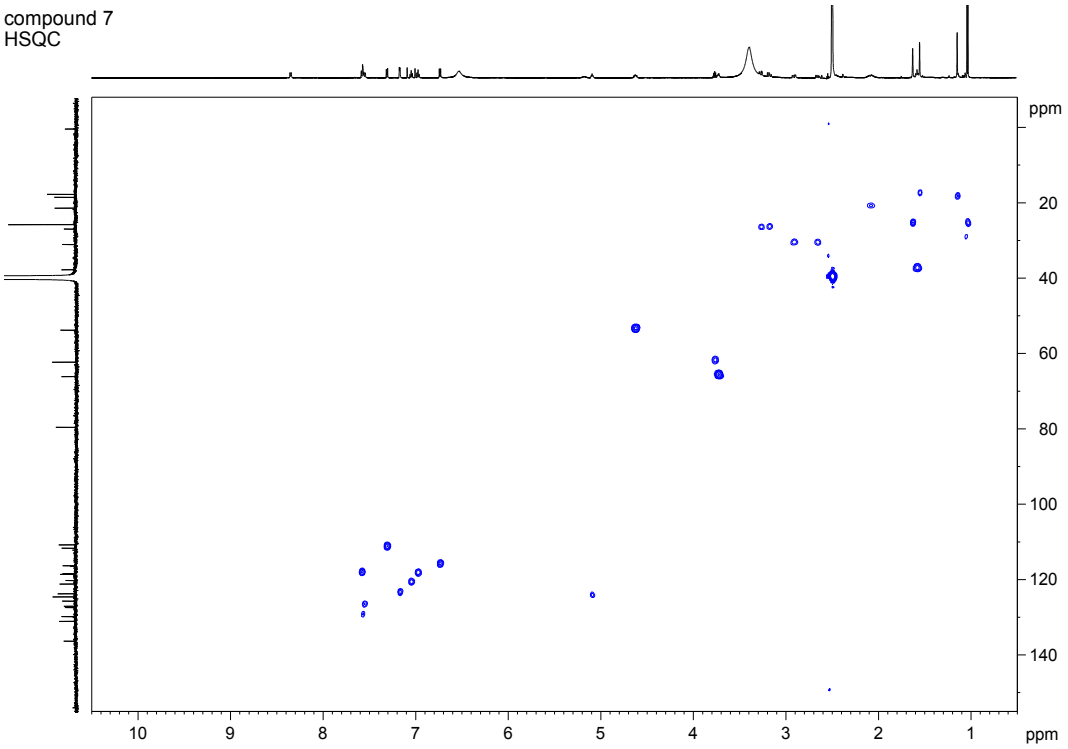

Figure S89. HSQC spectrum of **7**.

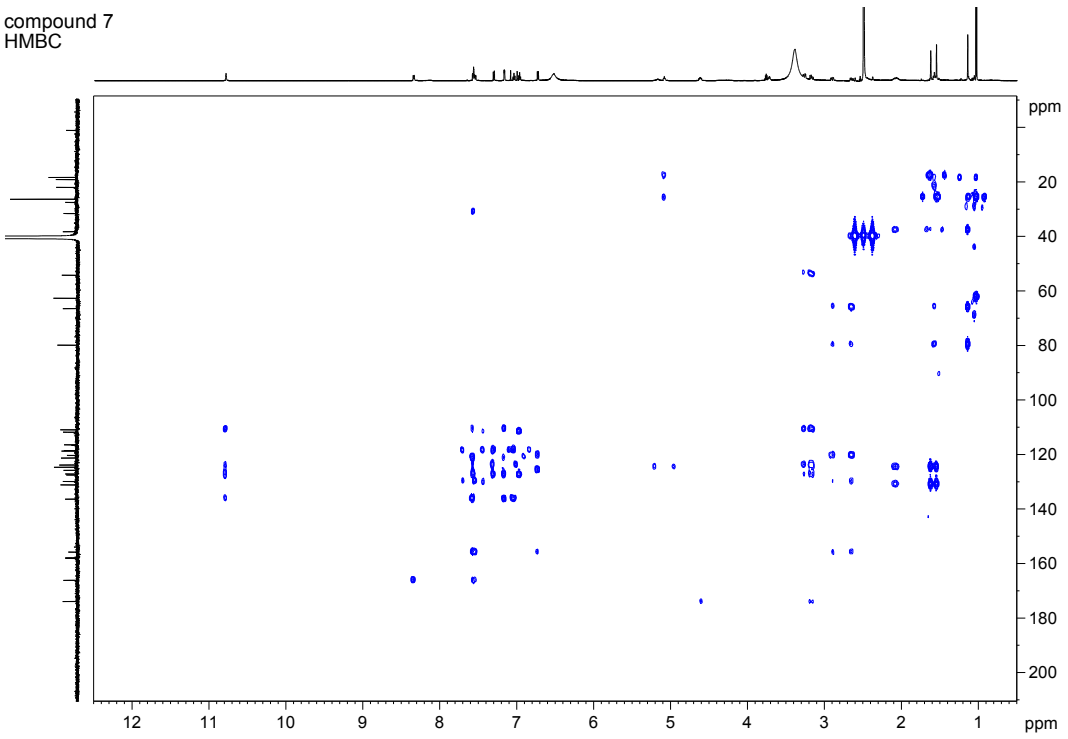

Figure S90. HMBC spectrum of **7**.

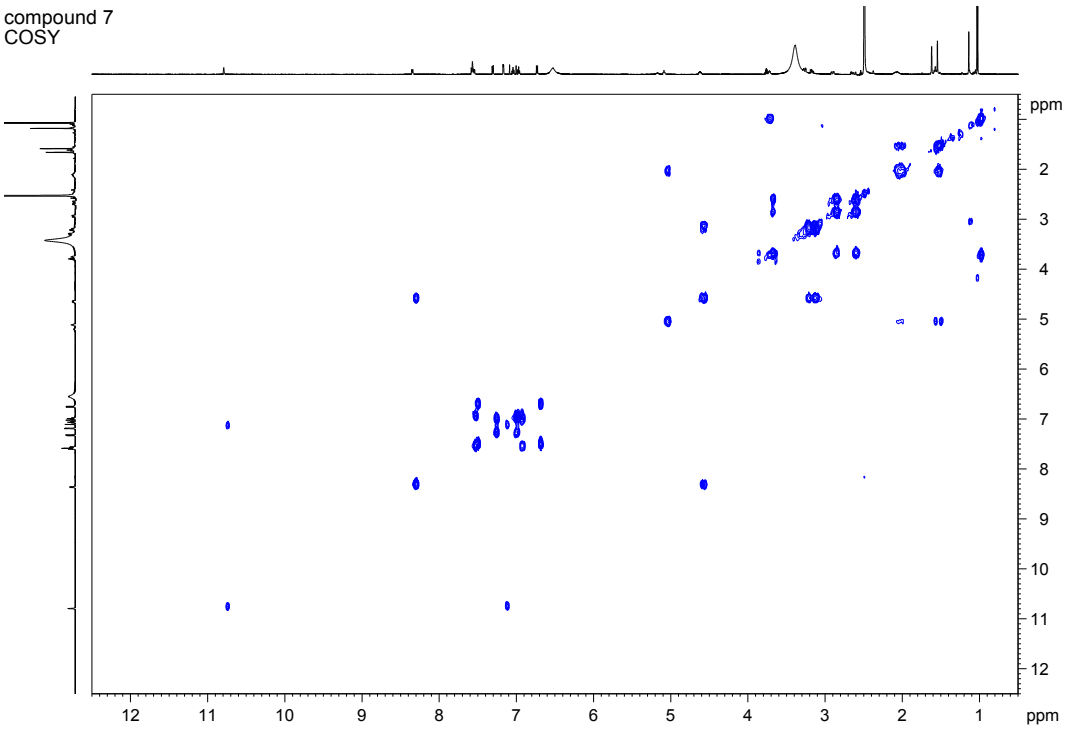

Figure S91. COSY spectrum of **7**.

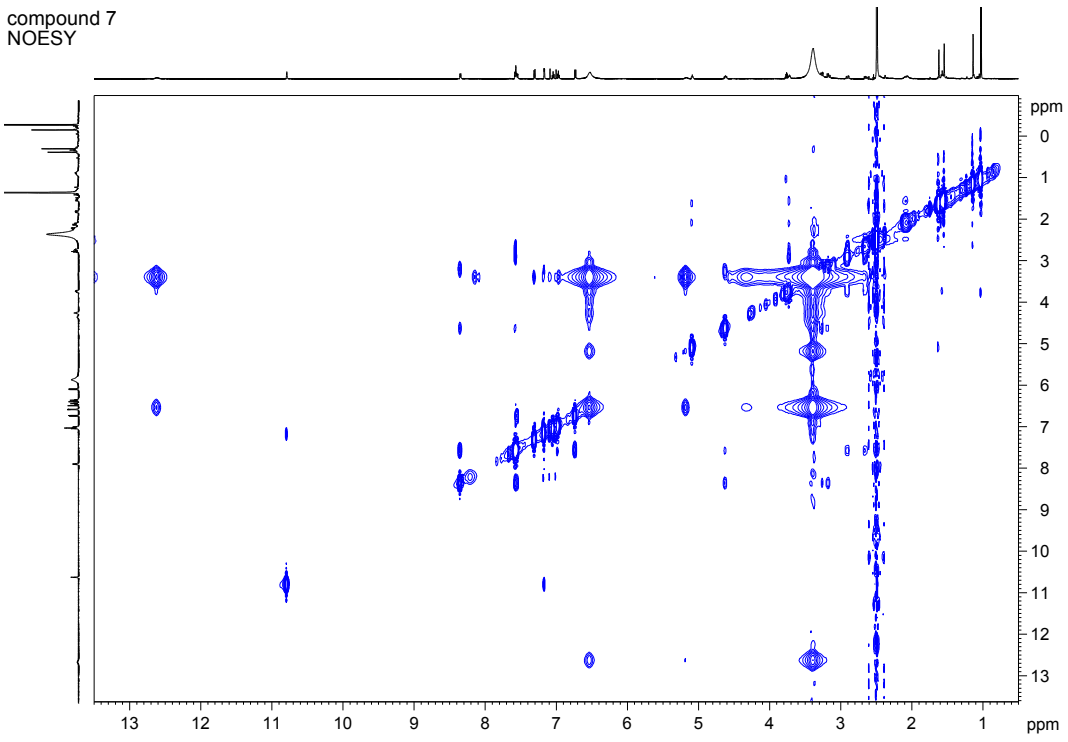

Figure S92. NOESY spectrum of **7**.

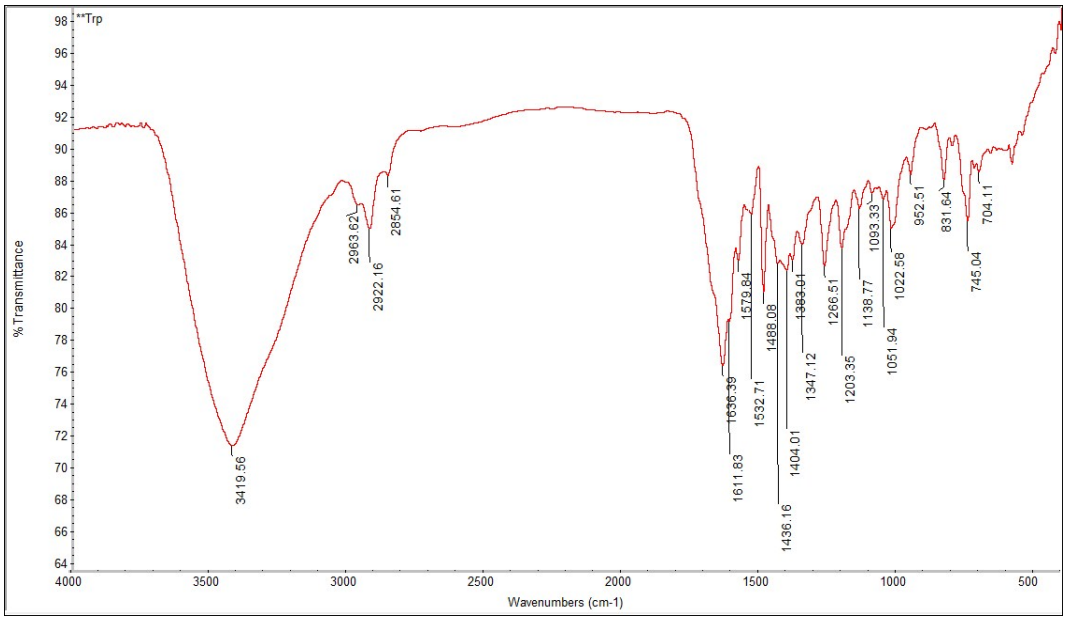

Figure S93. IR spectrum of **7**.

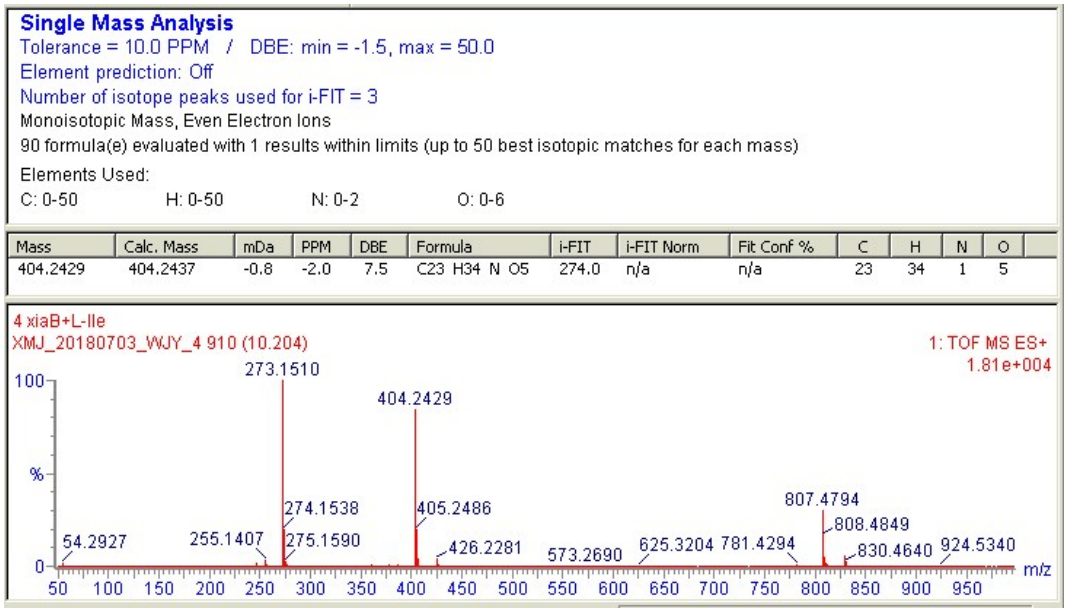

Figure S94. HR-ESI-MS analysis of **8** (Positive mode).

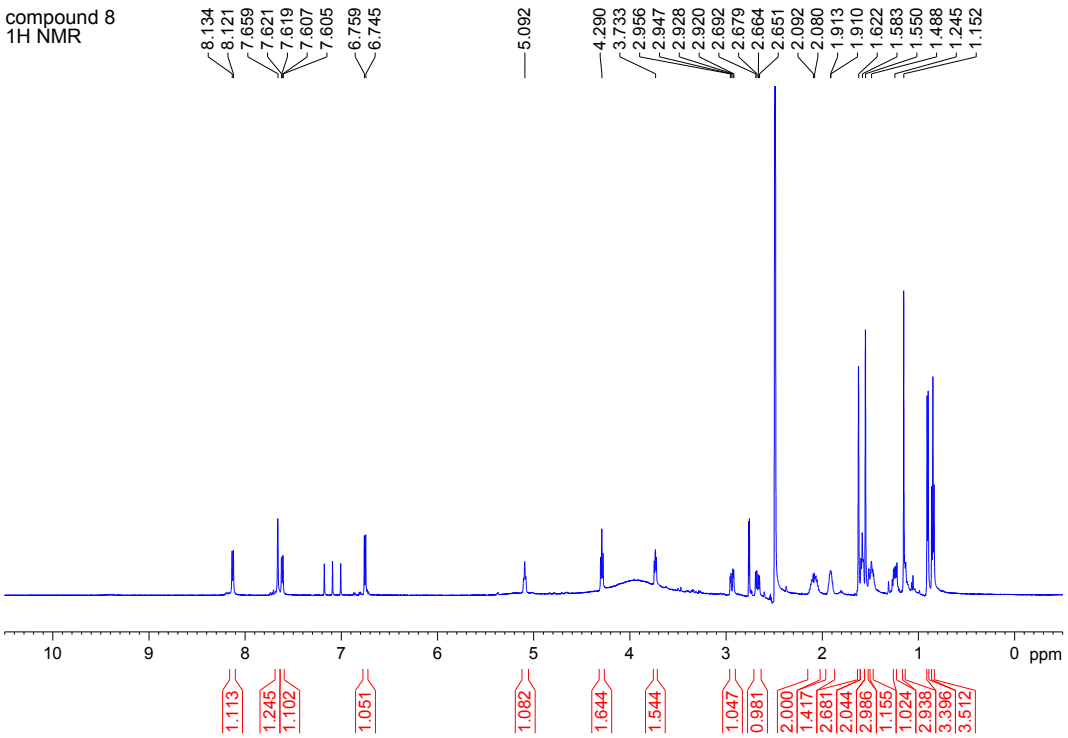

Figure S95. ^{1}H NMR (600 MHz, DMSO-d_6) spectrum of **8**.

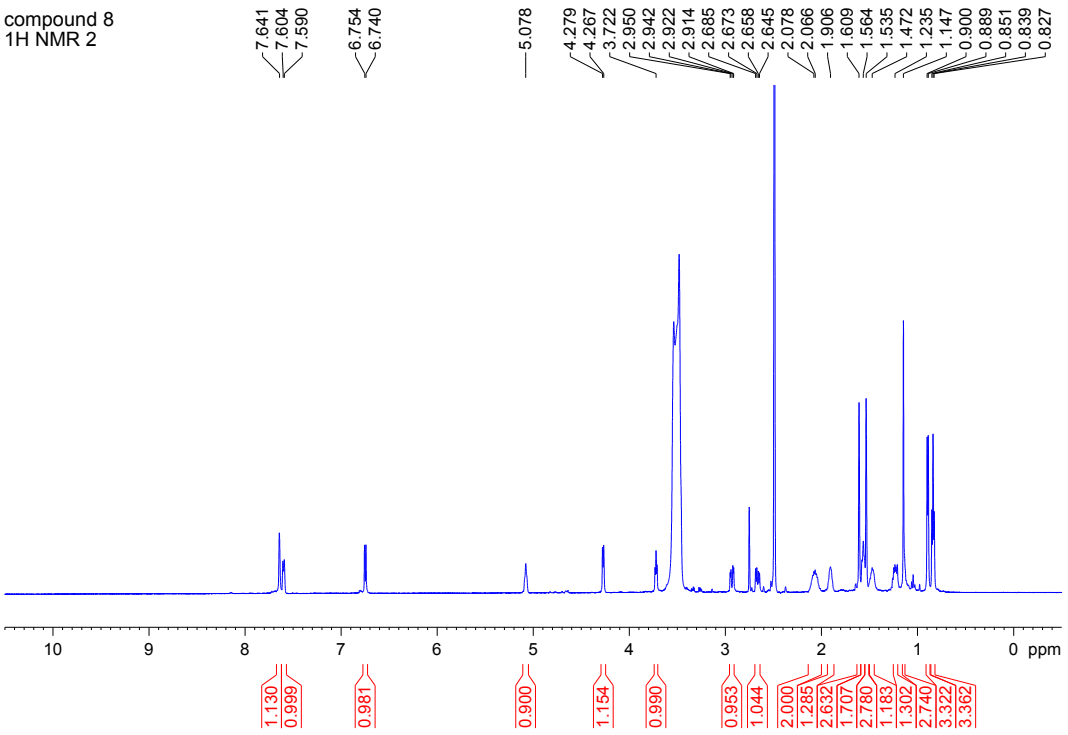

Figure S96. ^{1}H NMR (600 MHz, D_2O and DMSO-d_6) spectrum of **8**.

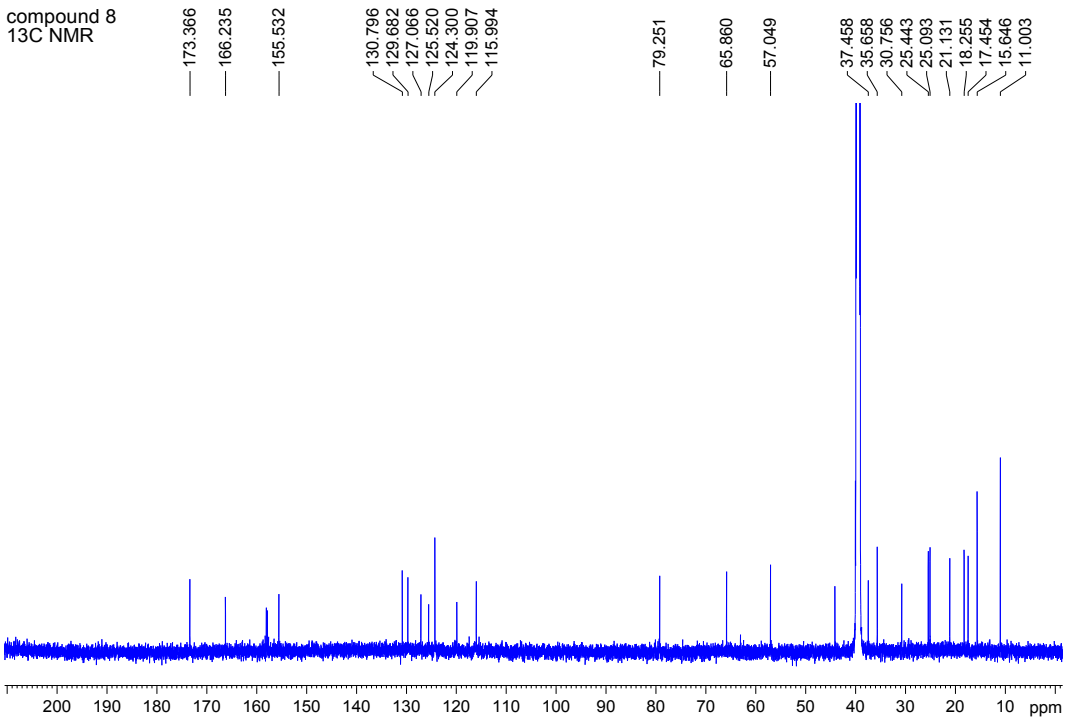

Figure S97. ^{13}C NMR (150 MHz, DMSO-d_6) spectrum of **8**.

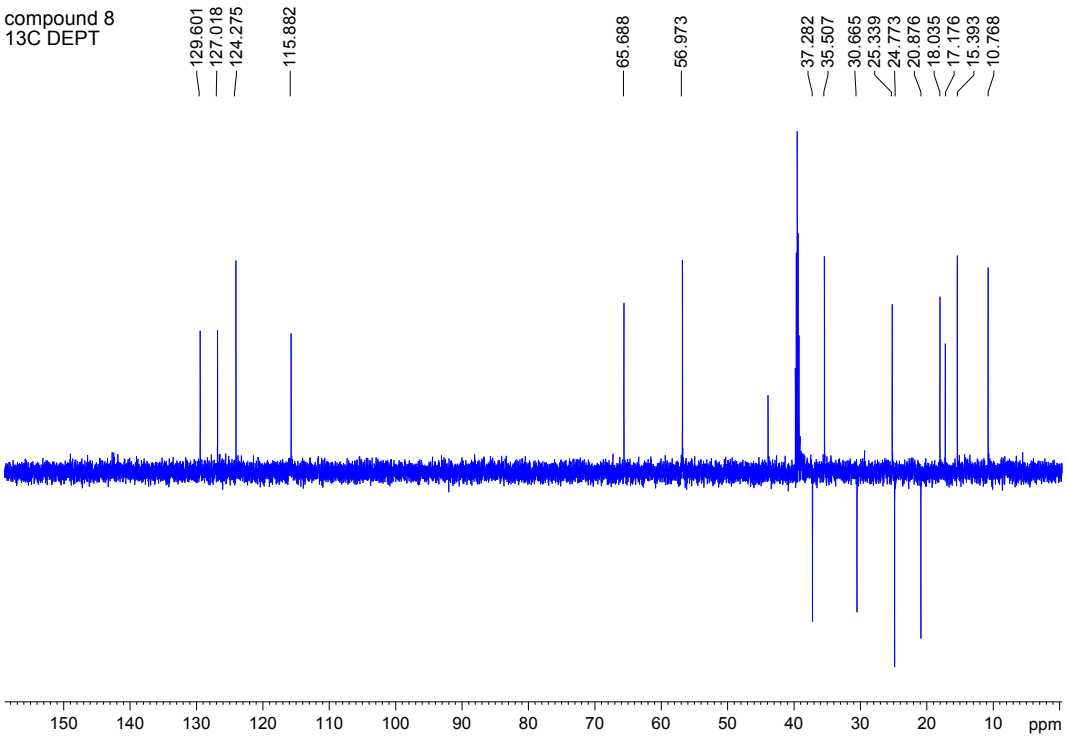

Figure S98. ^{13}C-DEPT (150 MHz, DMSO-d_6) spectrum of **8**.

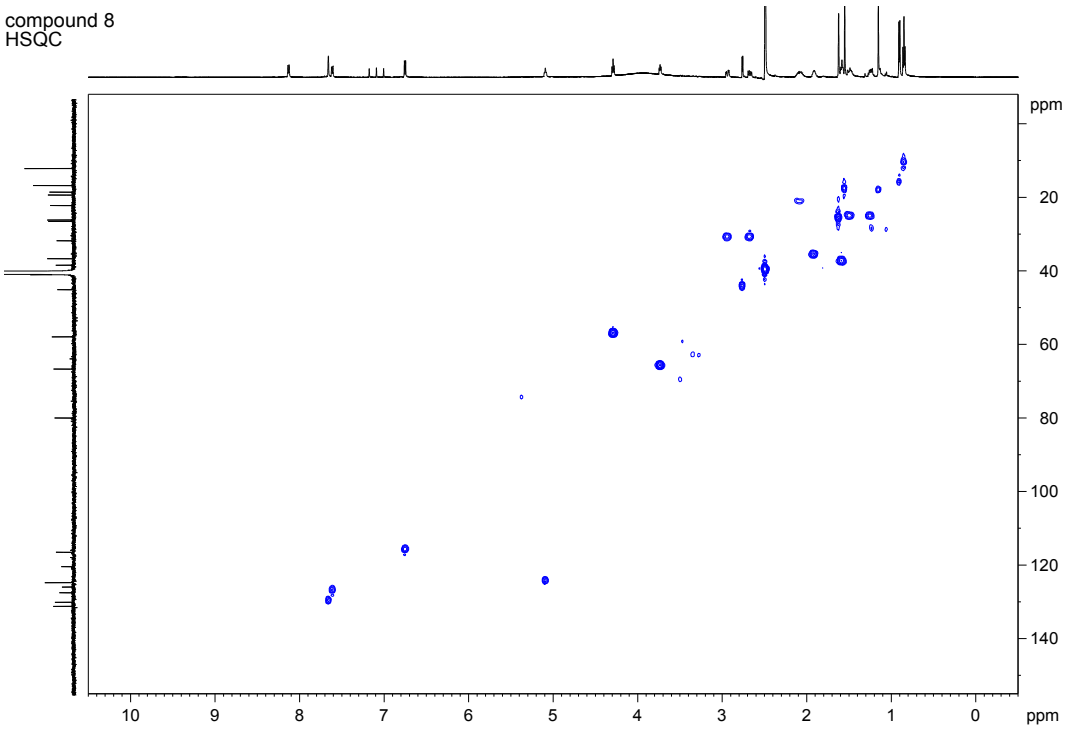

Figure S99. HSQC spectrum of **8**.

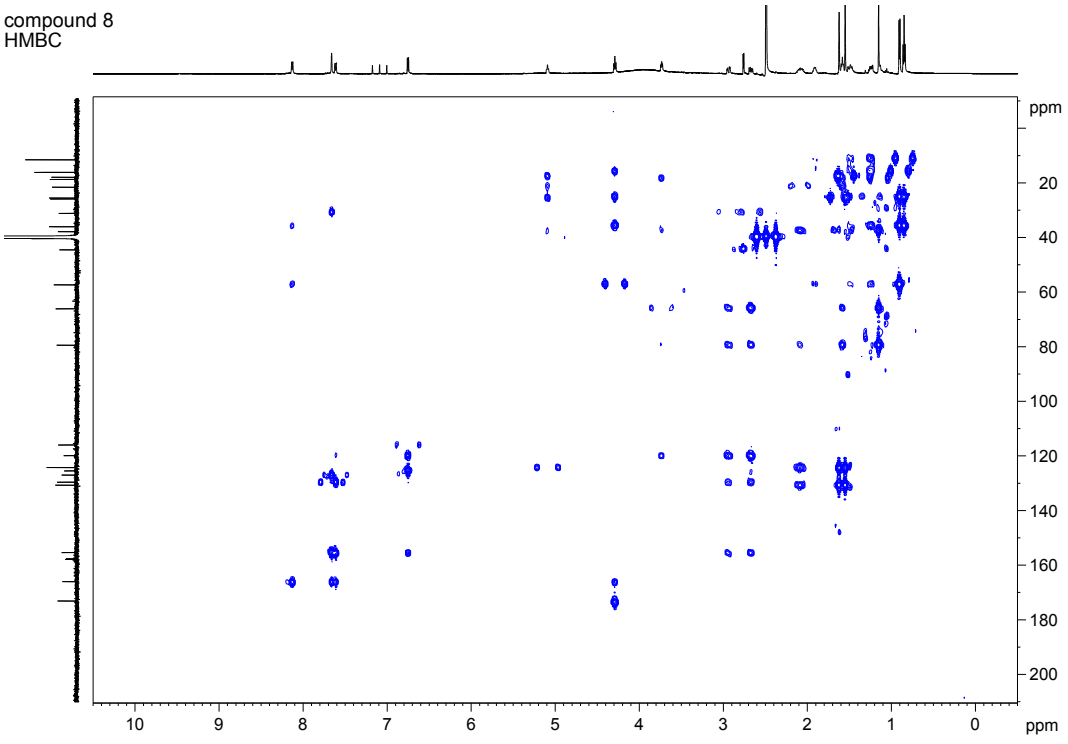

Figure S100. HMBC spectrum of **8**.

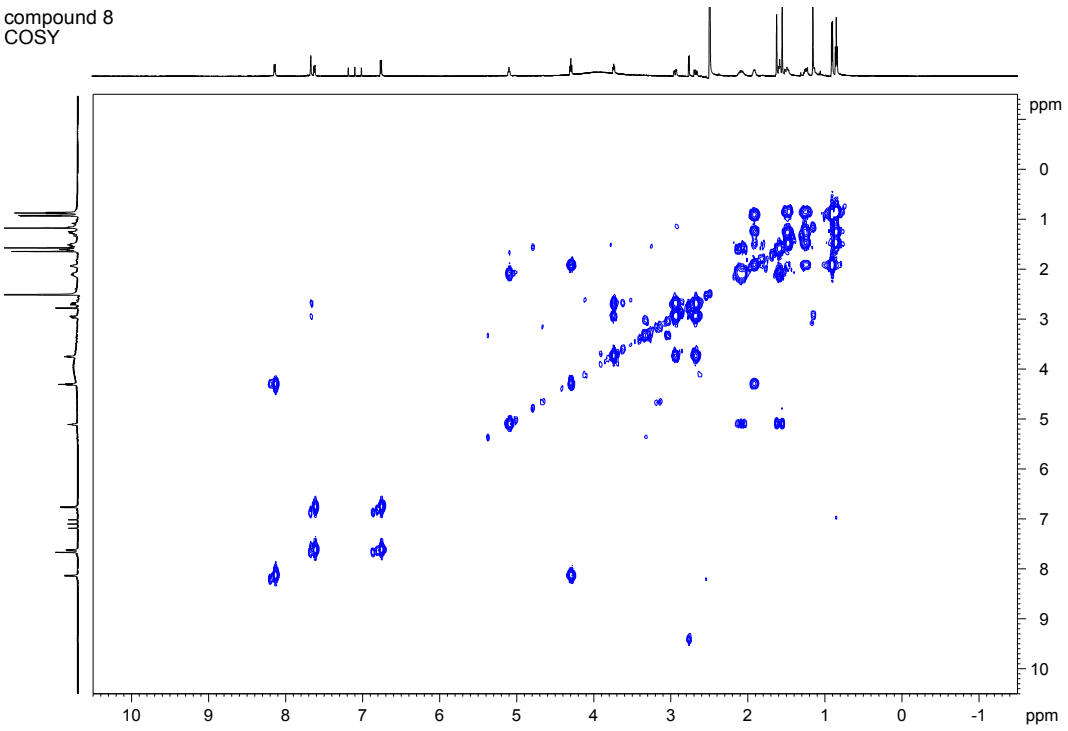

Figure S101. COSY spectrum of **8**.

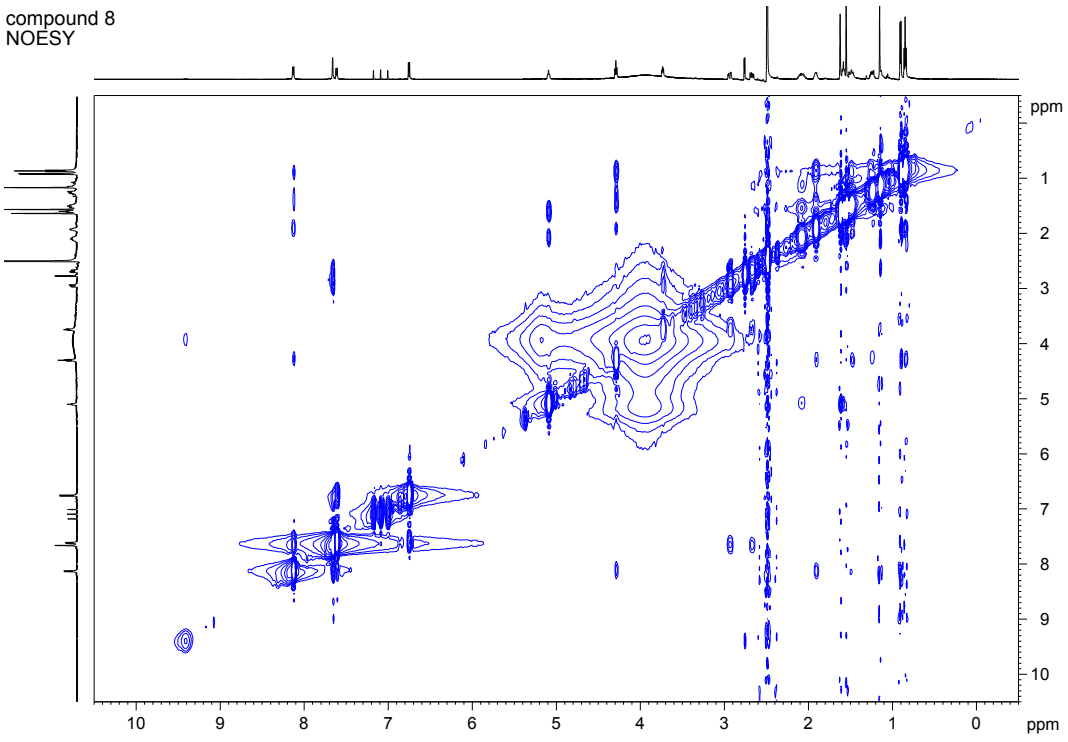

Figure S102. NOESY spectrum of **8**.

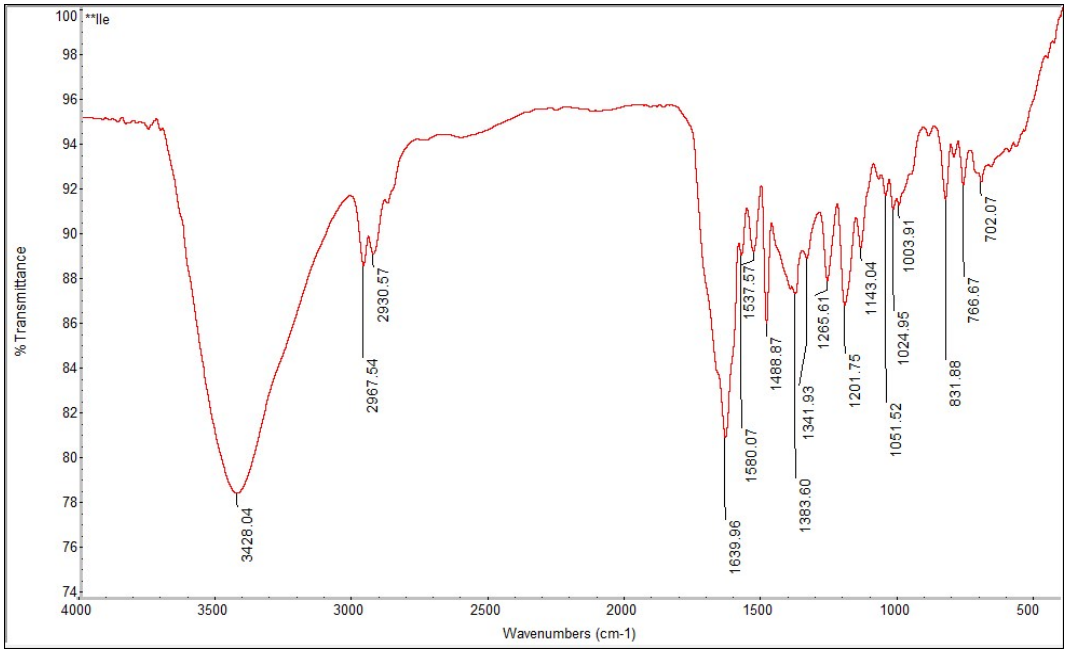

Figure S103. IR spectrum of **8**.

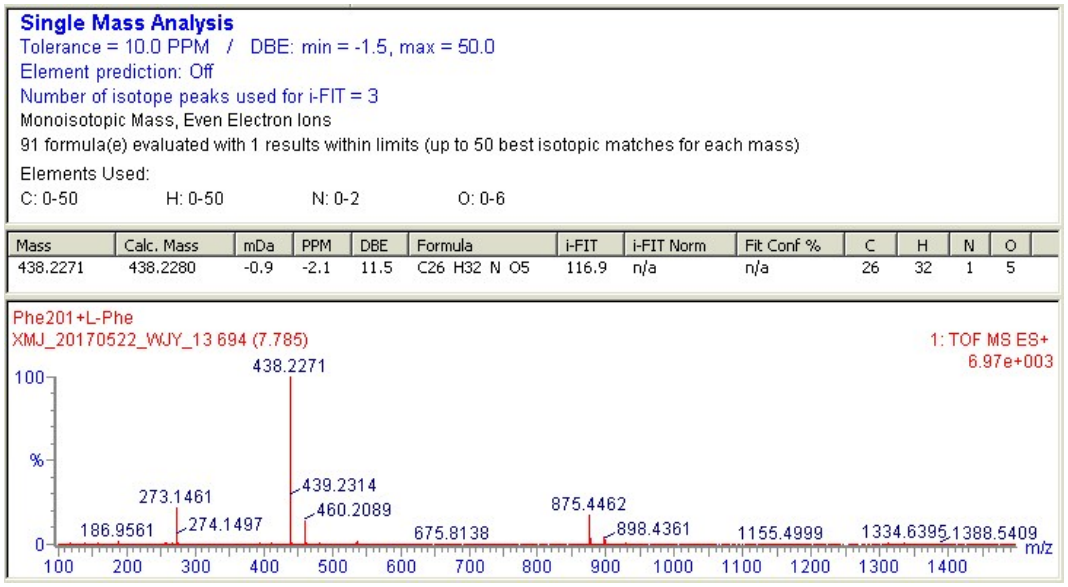

Figure S104. HR-ESI-MS analysis of **9** (Positive mode).

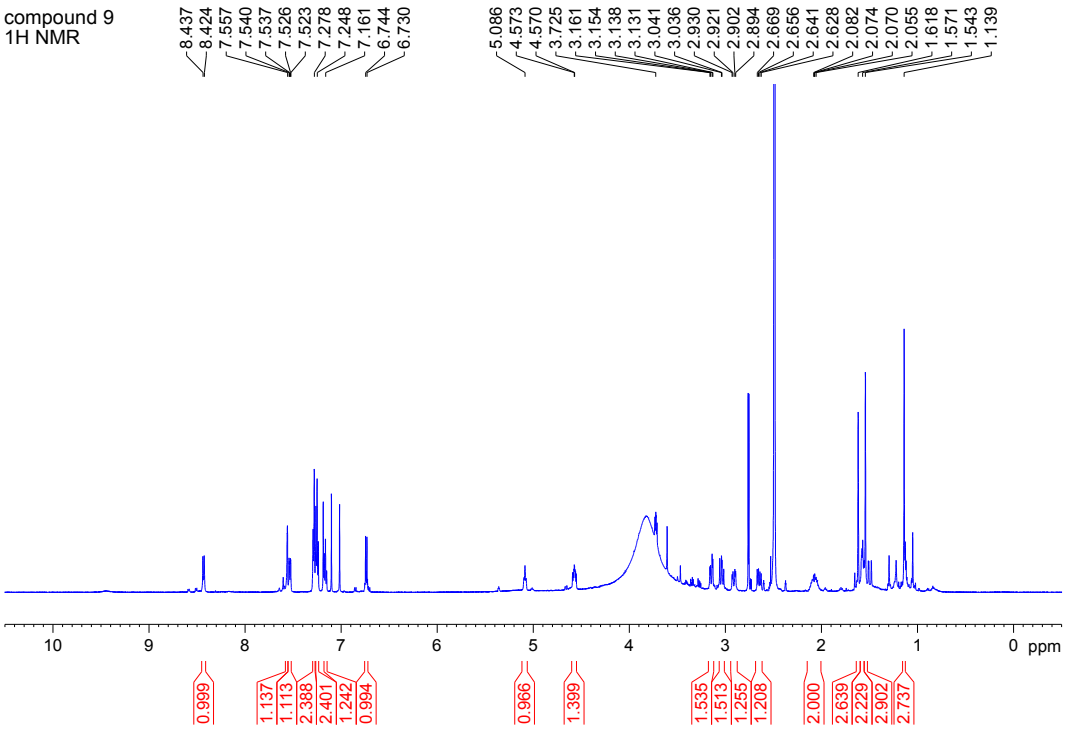

Figure S105. ^{1}H NMR (600 MHz, DMSO-d_6) spectrum of **9**.

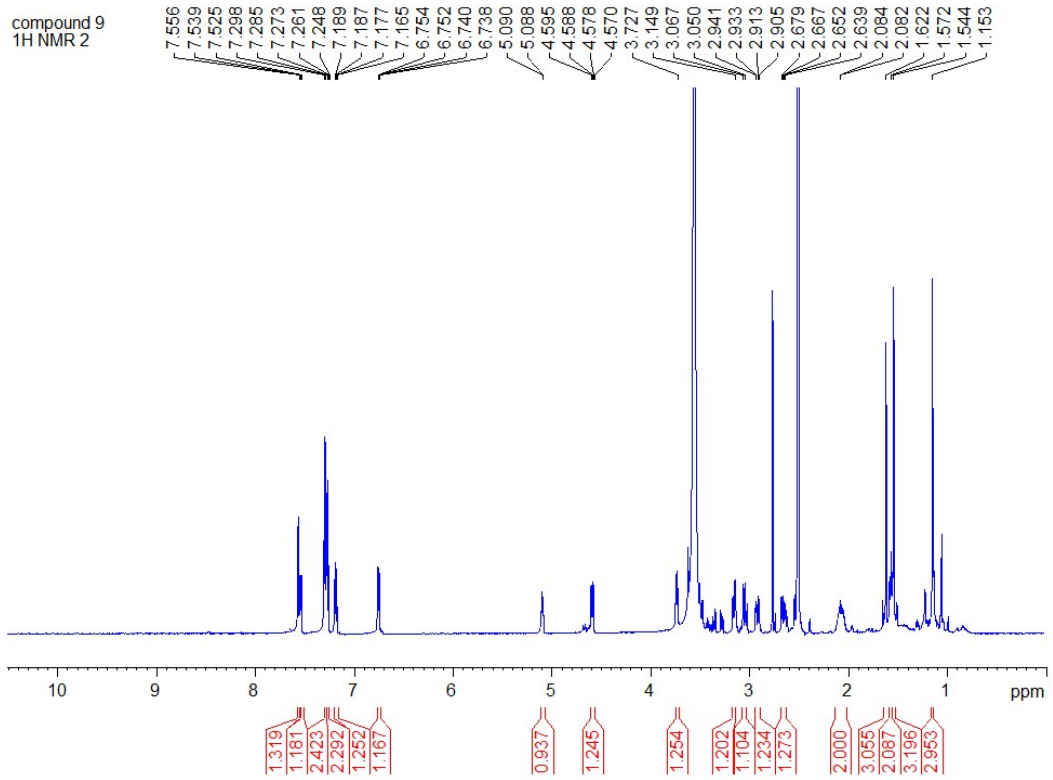

Figure S106. ^{1}H NMR (600 MHz, D_2O and DMSO-d_6) spectrum of **9**.

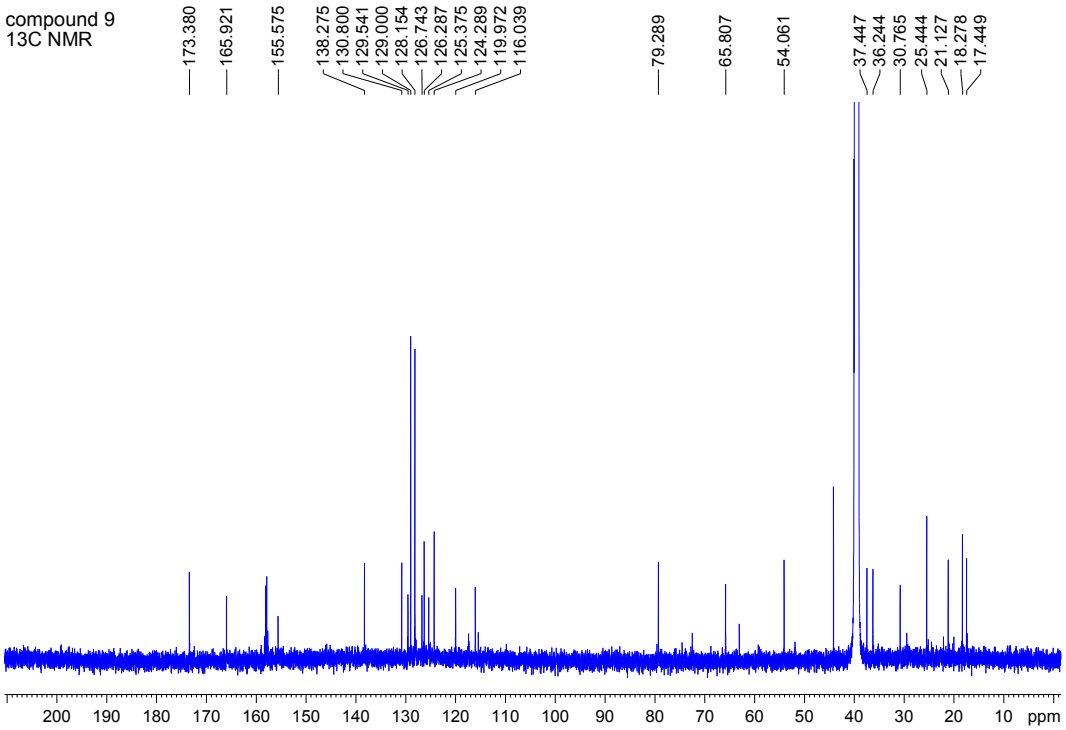

Figure S107. ^{13}C NMR (150 MHz, DMSO-d_6) spectrum of **9**.

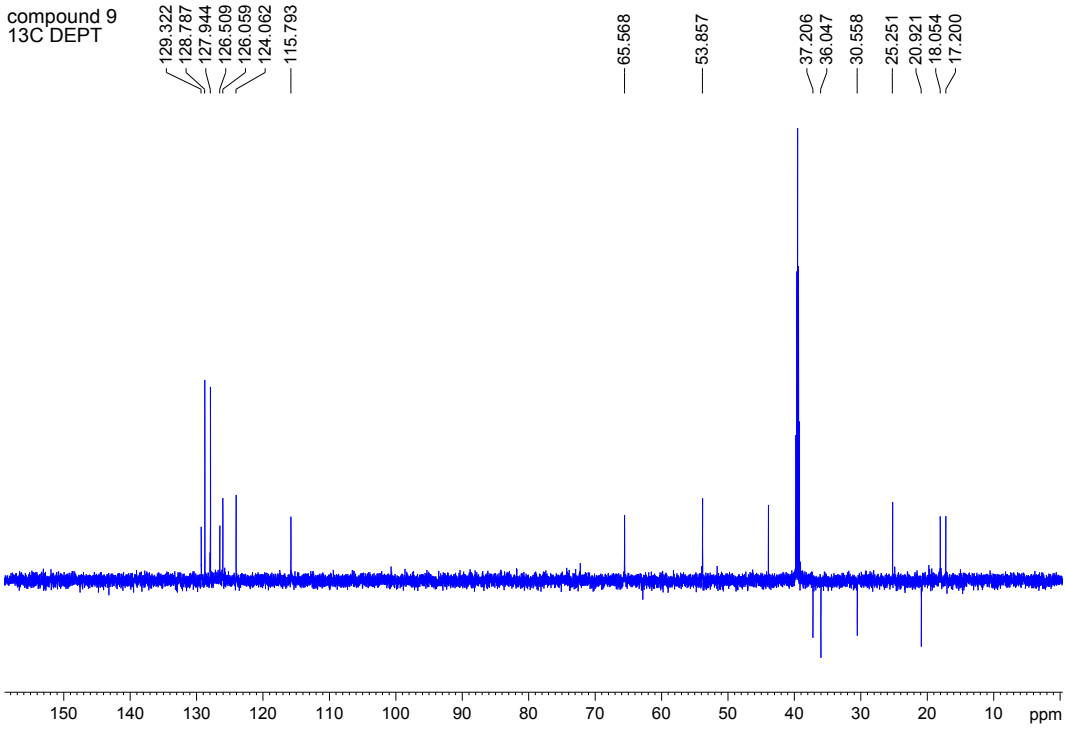

Figure S108. ^{13}C-DEPT (150 MHz, DMSO-d_6) spectrum of **9**.

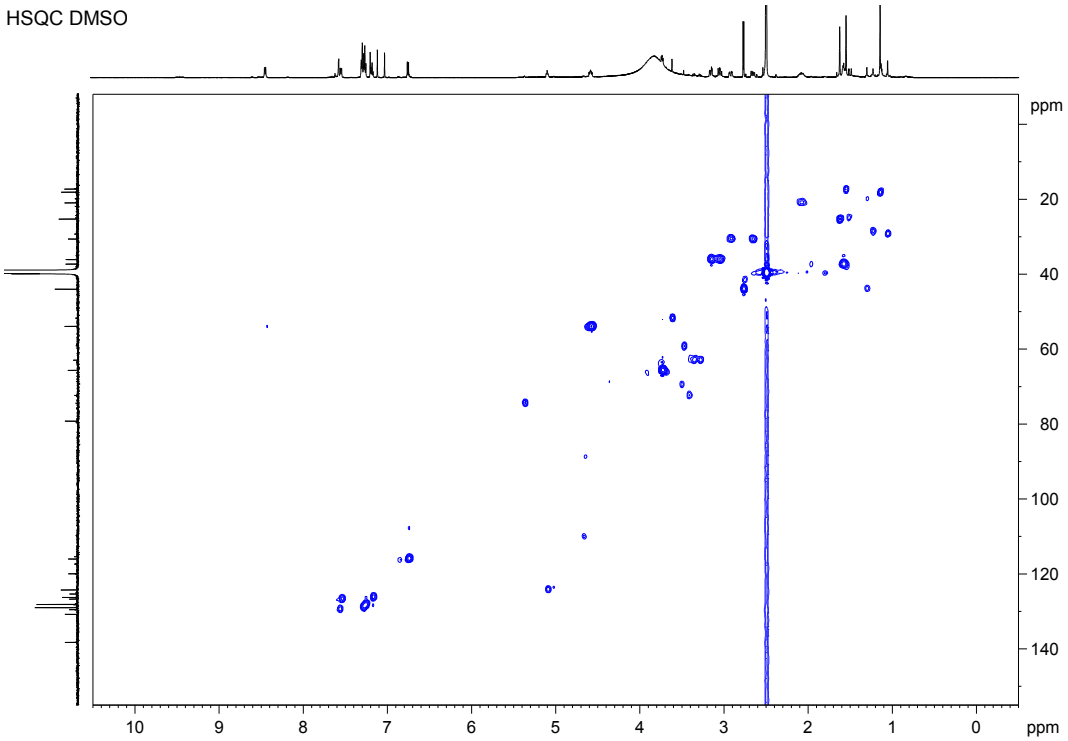

Figure S109. HSQC spectrum of **9**.

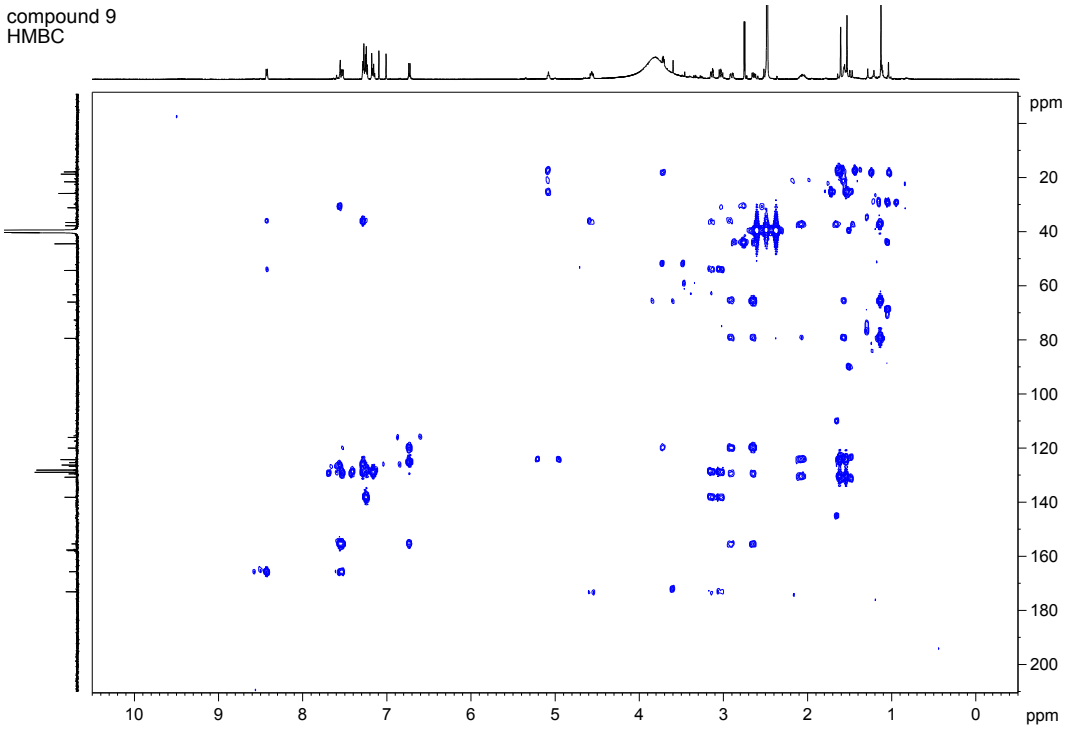

Figure S110. HMBC spectrum of **9**.

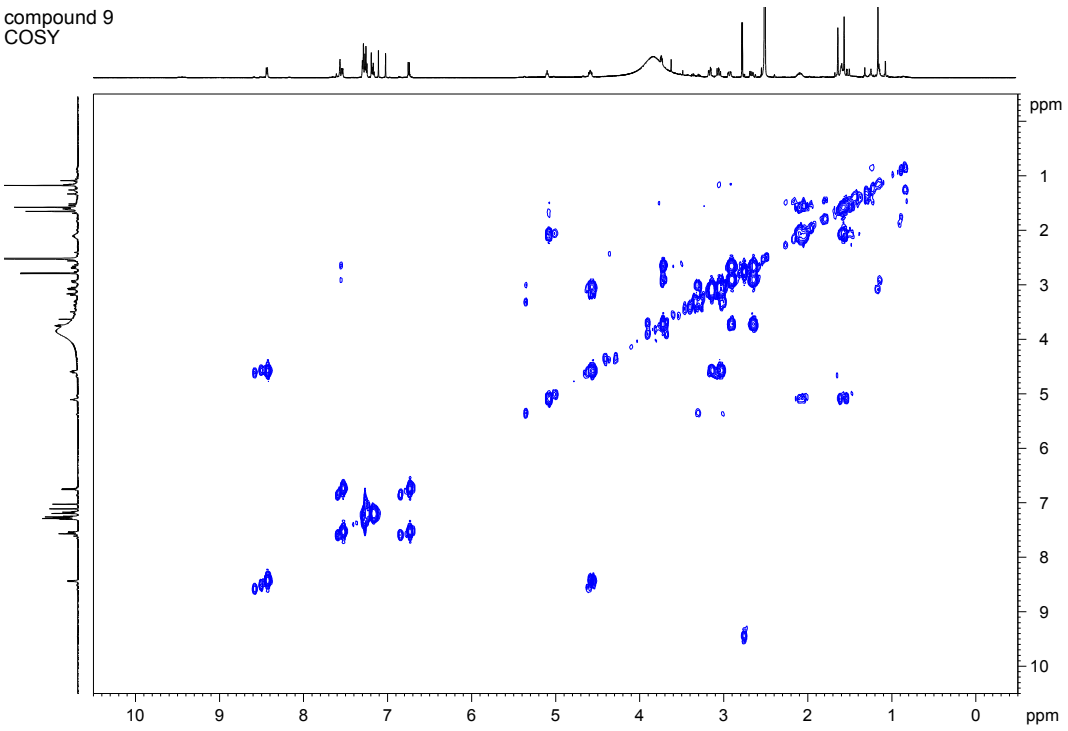

Figure S111. COSY spectrum of **9**.

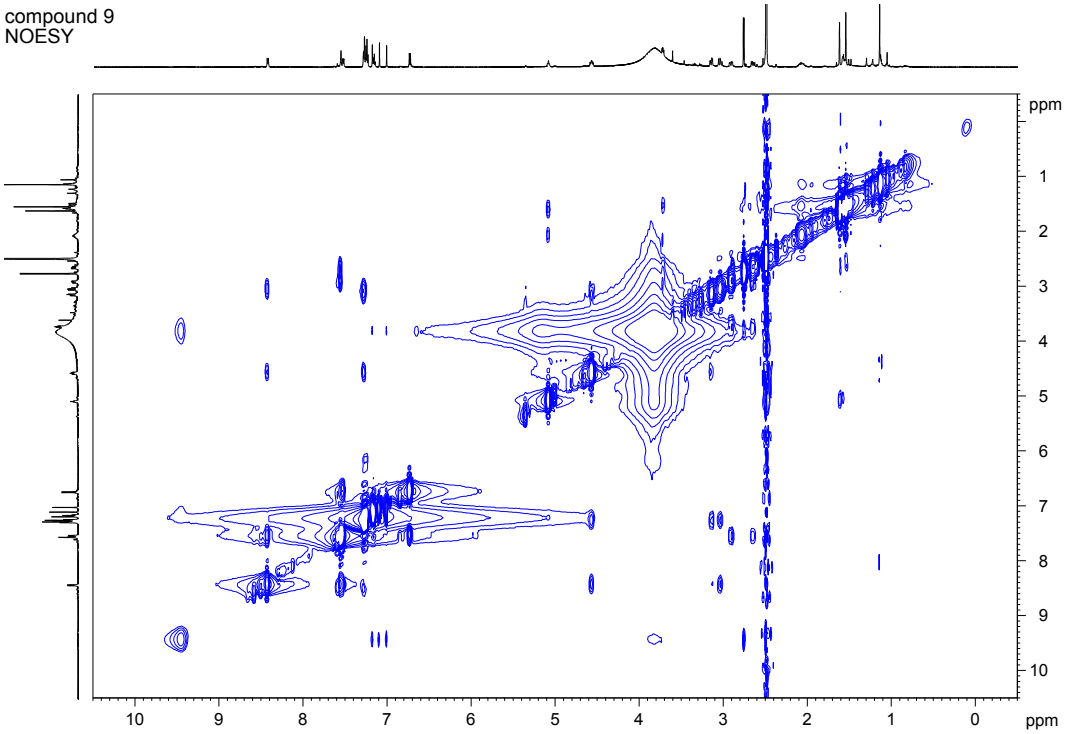

Figure S112. NOESY spectrum of **9**.

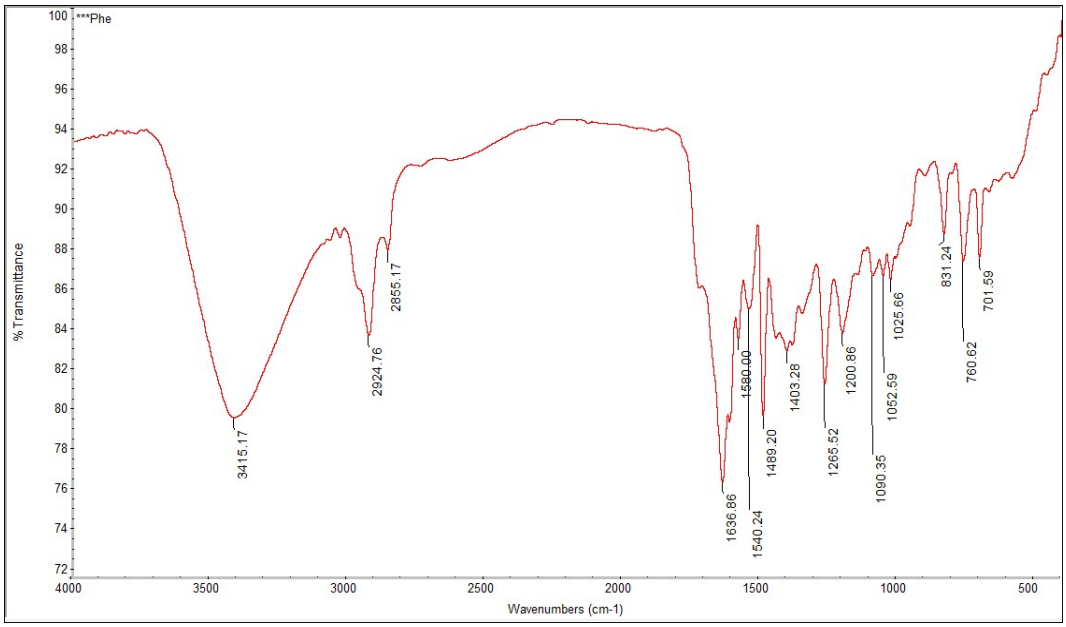

Figure S113. IR spectrum of **9**.

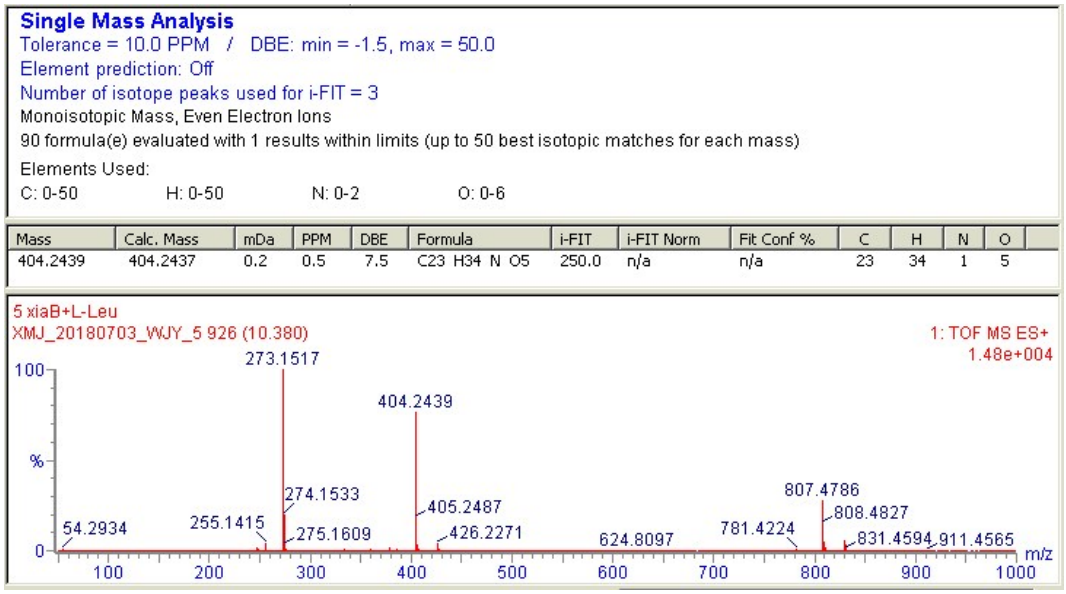

Figure S114. HR-ESI-MS analysis of **10** (Positive mode).

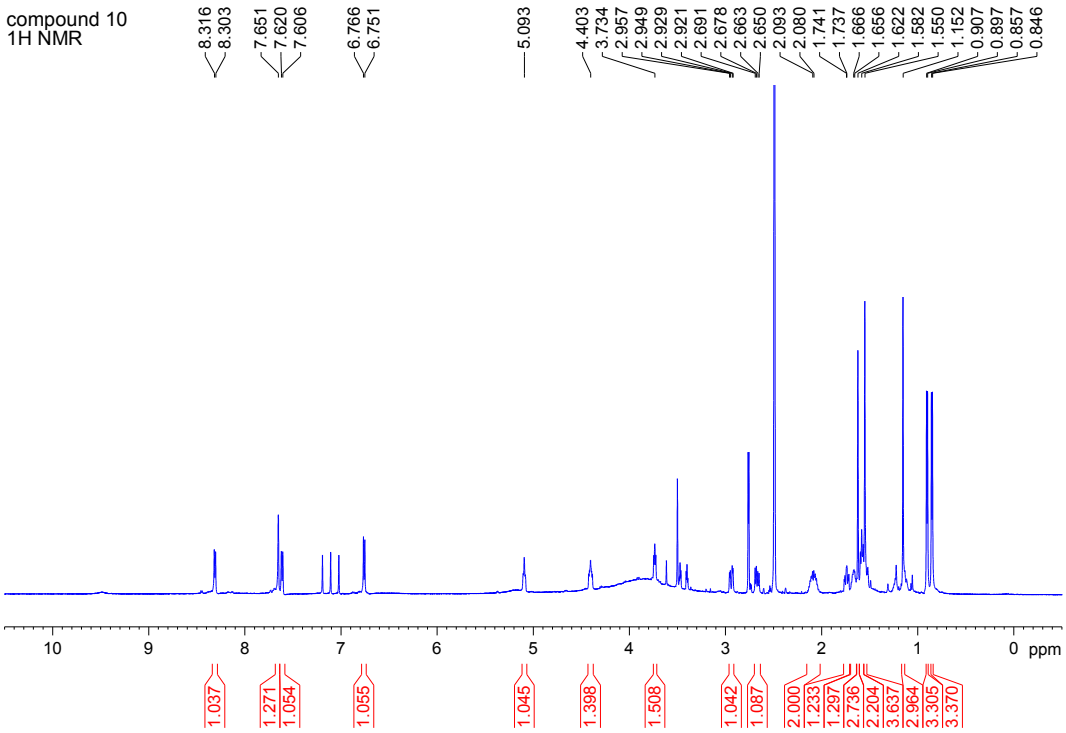

Figure S115. ^{1}H NMR (600 MHz, DMSO-d_6) spectrum of **10**.

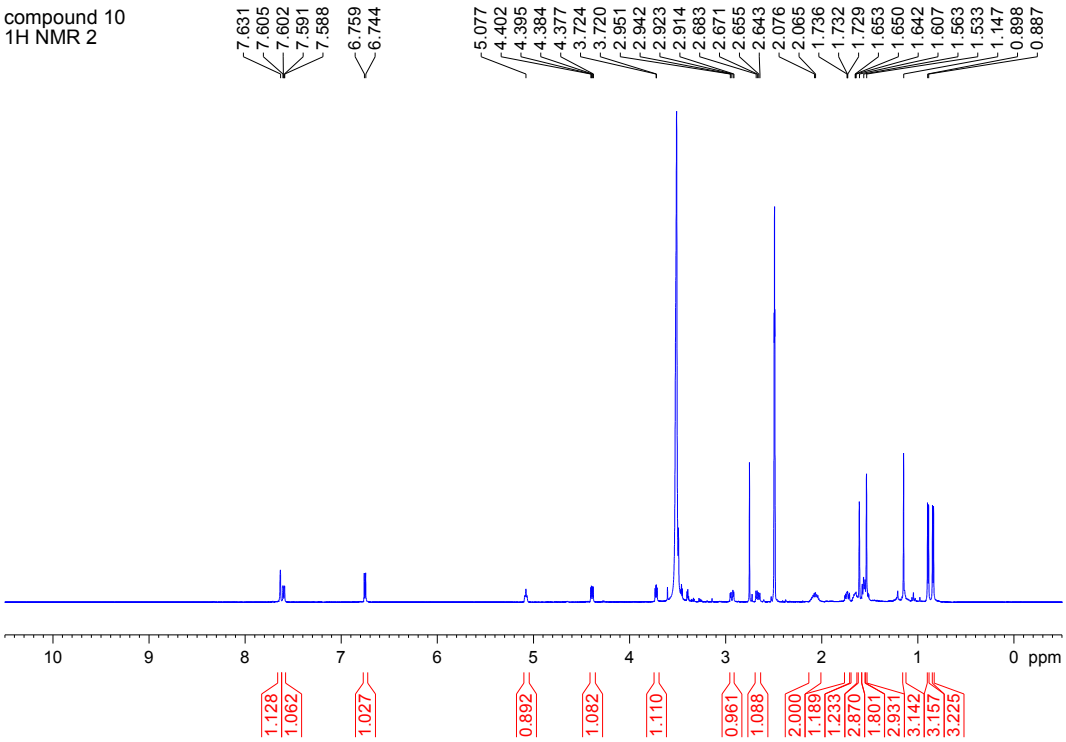

Figure S116. ^{1}H NMR (600 MHz, D_2O and DMSO-d_6) spectrum of **10**.

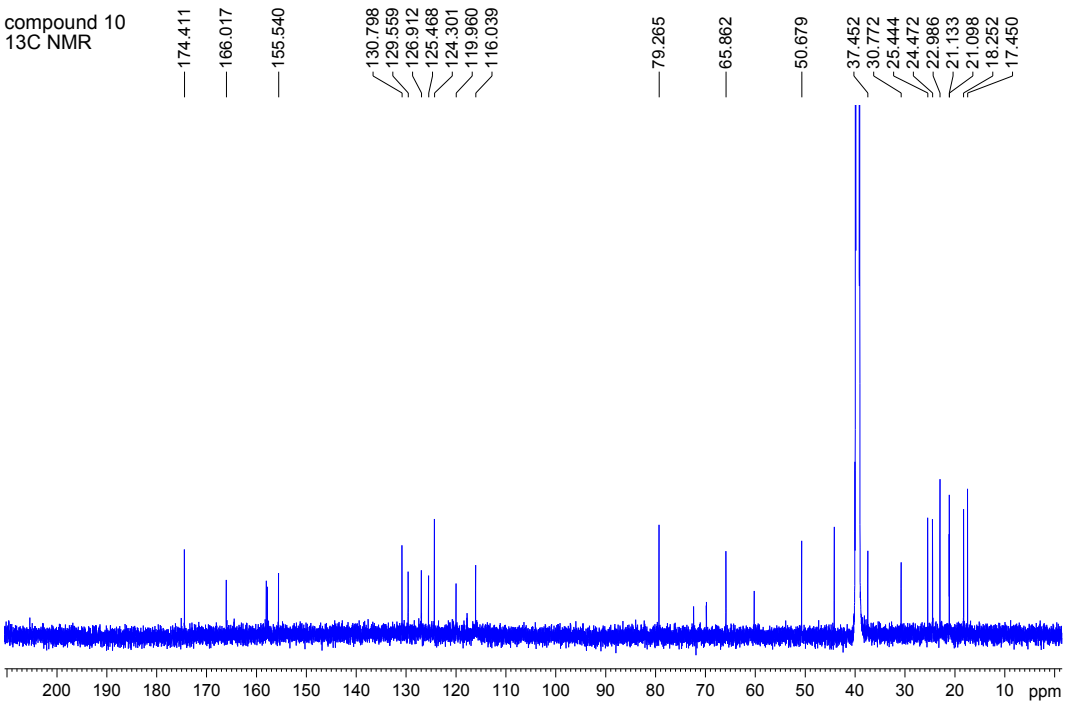

Figure S117. ^{13}C NMR (150 MHz, DMSO-d_6) spectrum of **10**.

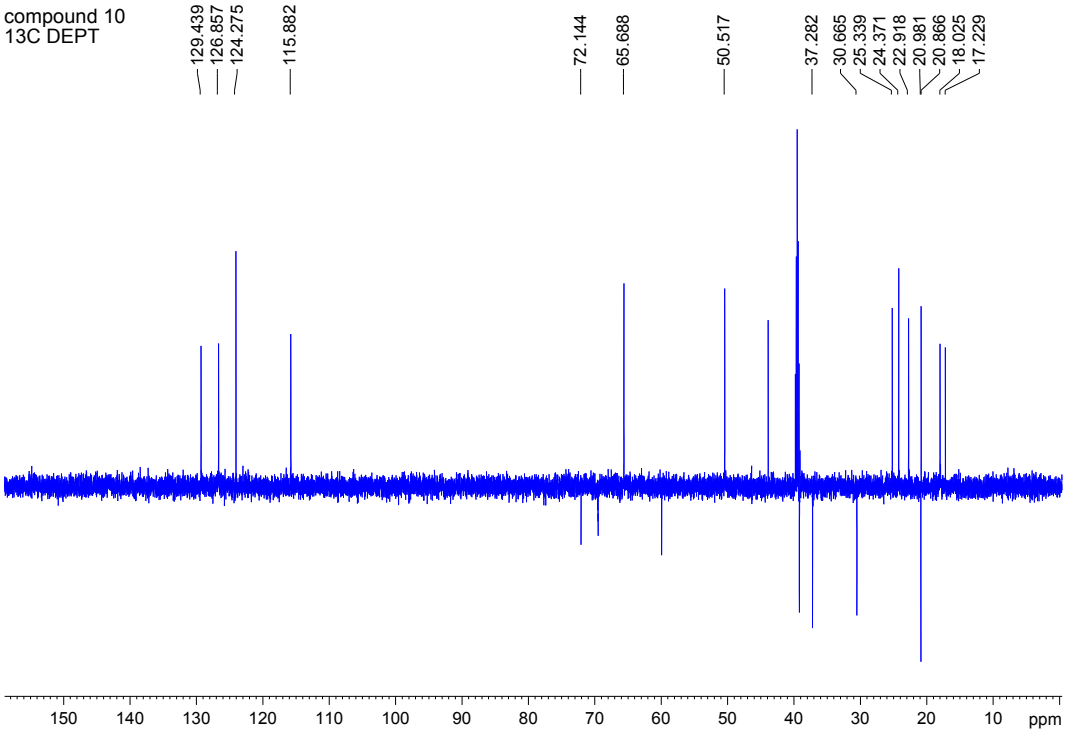

Figure S118. ^{13}C-DEPT (150 MHz, DMSO-d_6) spectrum of **10**.

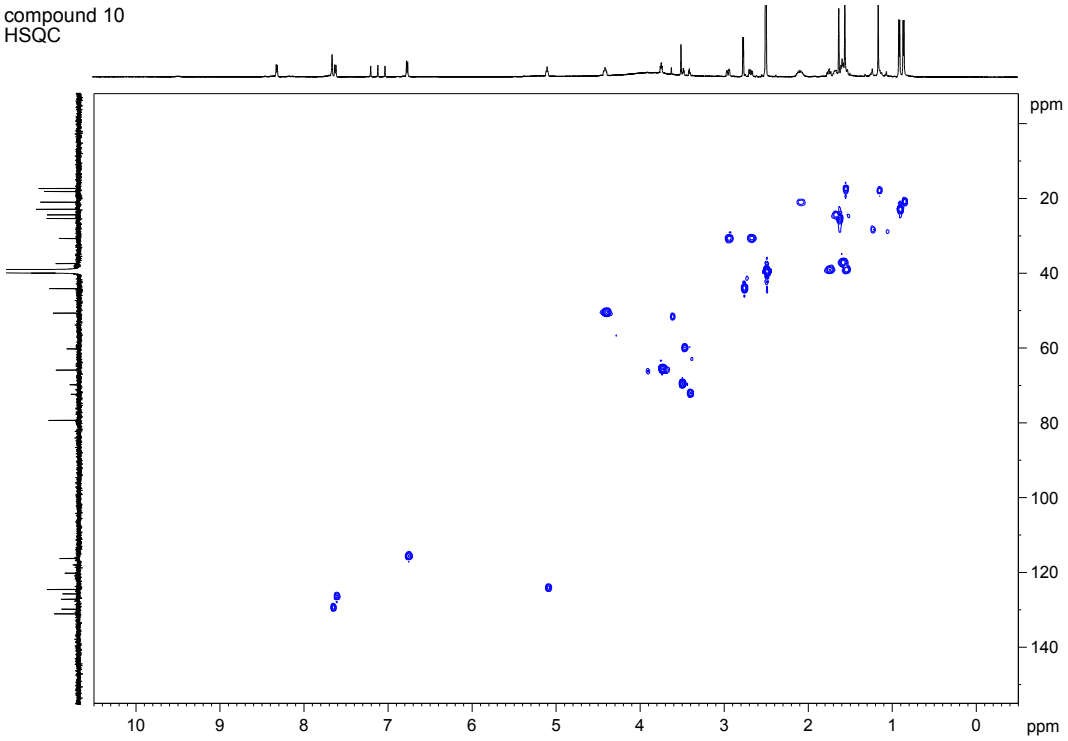

Figure S119. HSQC spectrum of **10**.

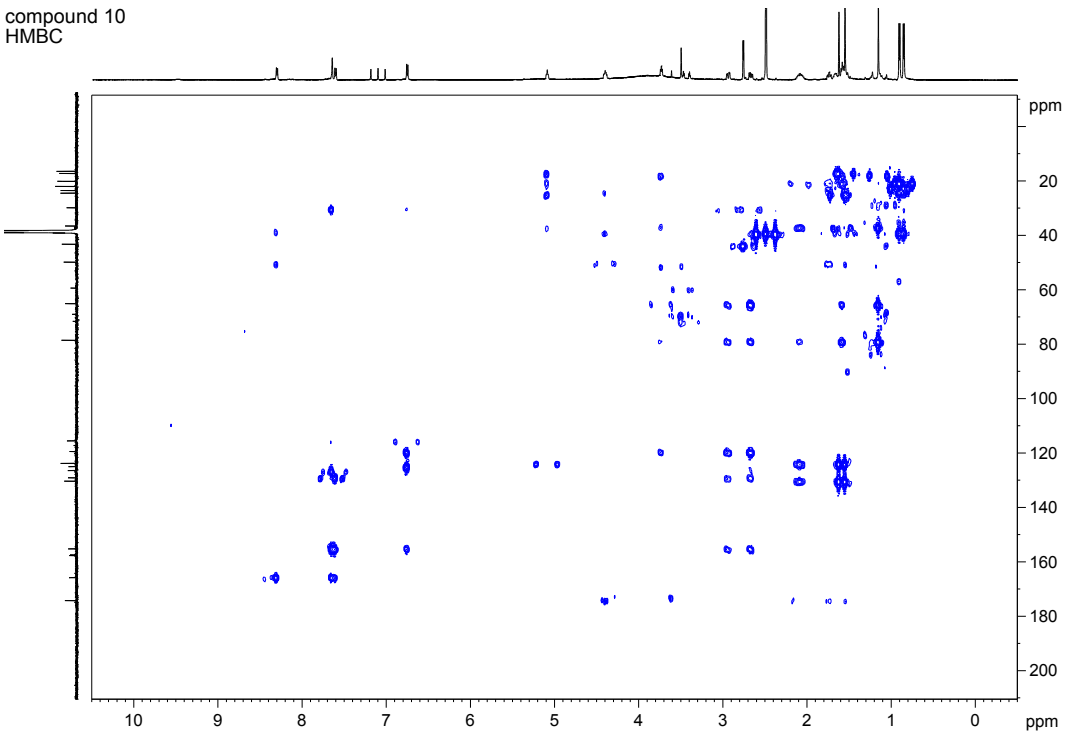

Figure S120. HMBC spectrum of **10**.

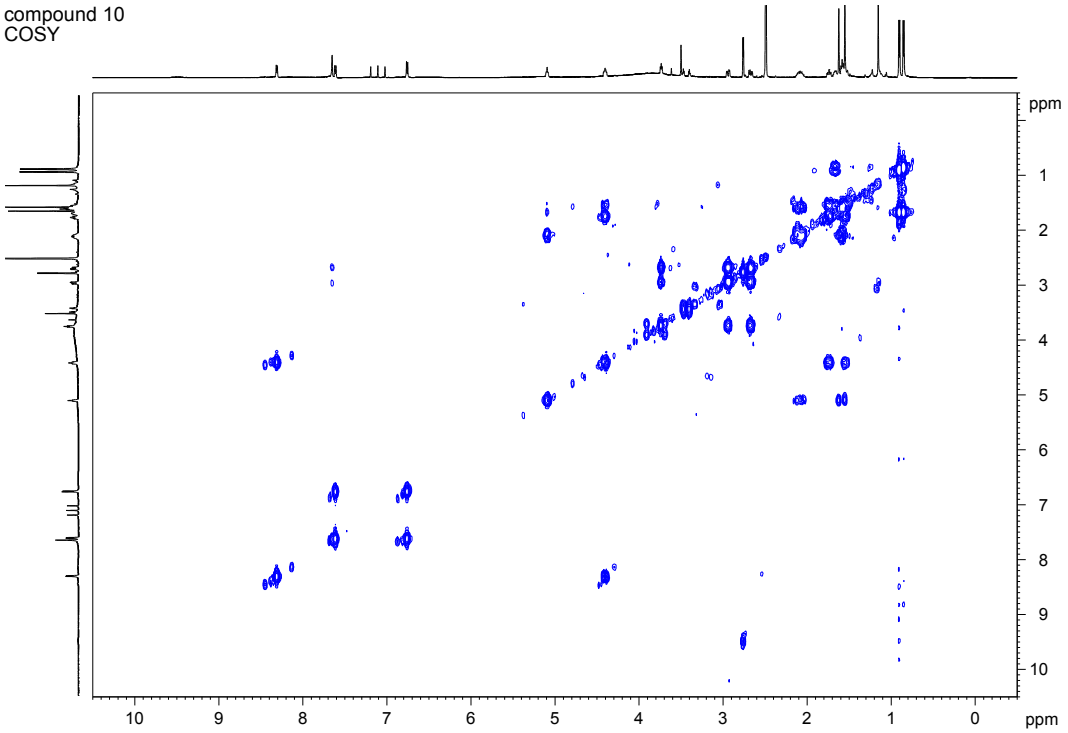

Figure S121. COSY spectrum of **10**.

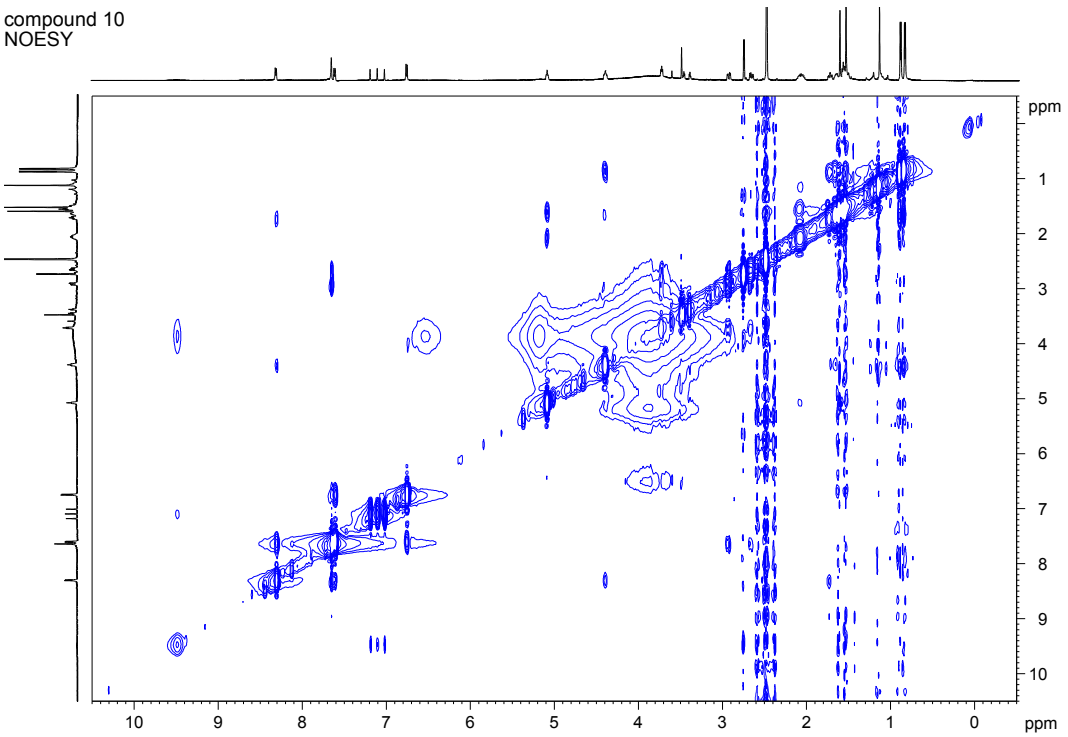

Figure S122. NOESY spectrum of **10**.

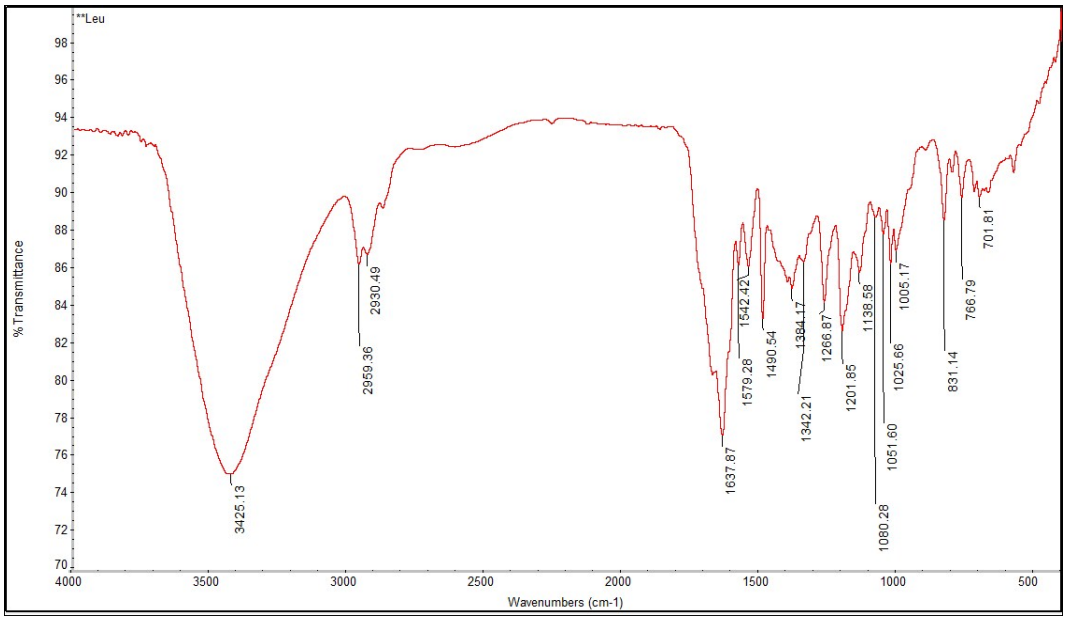

Figure S123. IR spectrum of **10**.

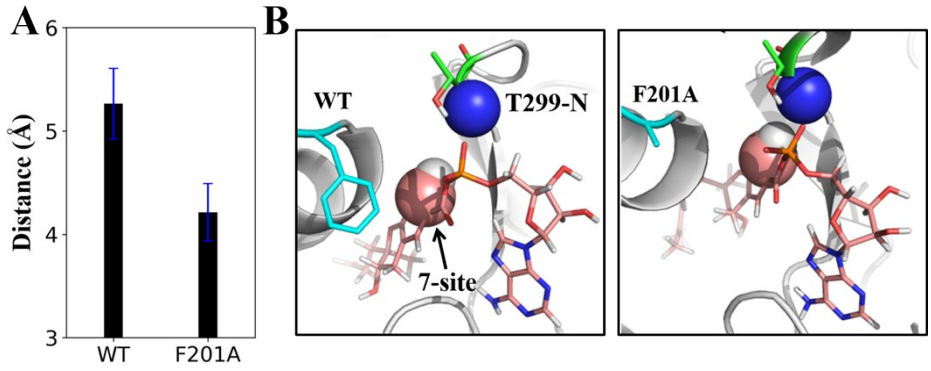

Figure S124. The F201A variant undermines the tolerance of XimA towards the 7-site substitutions of the acyl donor.

(A) Average distance between the 7-site C atom of the intermediate and the T299 N atom during the MD simulations for WT and F201A systems, the standard errors are also indicated. (B) Representations structures derived from the MD simulations for each system, in which the 7-site C-H group and T299-N atom are shown in sphere models.

Table S1. Secondary structures of XimA and its site-directed mutants estimated from CD spectrum.

Protein	α-Helix (%)	β-Sheet (%)	β-Turn (%)	Random coil (%)
XimA	8.0	33.6	22.3	33.6
F201A	18.4	21.9	23.3	32.5
F201C	19.6	27.2	22.6	33.8
F201M	16.4	28.6	21.8	32.9
F201N	19.6	27.1	22.7	33.9
F201Q	18.6	27.1	21.2	32.6
F201S	20.6	18.9	22.3	33.4
F201T	21.2	21.8	23.2	32.9
Y296A	9.4	32.3	23.1	34.6
T299A	9.5	33.0	23.1	35.0
R390A	9.1	33.2	22.9	34.2
D375A	8.8	27.2	22.3	39.9
K492A	8.6	29.5	23.0	37.7

Table S2. [1]H NMR data of compounds **1-5**.

Position	1	2*	3*	4	5
1	--	--	--	--	--
2	--	--	--	--	--
3	3.74, dd (7.7, 5.0)	3.74, m	3.74, m	3.73, m	3.73, m
4	2.67, dd (16.7, 7.7)	2.68, dd (16.7, 7.9)	2.67, dd (16.7, 7.9)	2.67, dd (16.7, 7.9)	2.65, dd (16.7, 7.9)
	2.94, dd (16.7, 5.0)	2.94, dd (16.7, 5.0)	2.94, dd (16.7, 4.8)	2.94, dd (16.7, 4.8)	2.90, m
4a	--	--	--	--	--
5	7.64, brs	7.64, brs	7.62, brs	7.64, brs	7.56, brs
6	--	--	--	--	--
7	7.60, dd (8.6, 1.6)	7.60, brd (8.5)	7.58, brd (8.5)	7.60, dd (8.6, 1.6)	7.54, dd (8.4, 2.0)
8	6.77, d (8.6)	6.76, d (8.5)	6.76, d (8.5)	6.76, d (8.6)	6.74, d (8.4)
8a	--	--	--	--	--
9	1.58, m	1.58, m	1.58, m	1.58, m	1.58, m
10	2.08, m	2.09, m	2.09, m	2.08, m	2.07, m
11	5.09, t (7.0)	5.09, t (7.0)	5.09, t (7.0)	5.09, t (7.3)	5.09, t (7.0)
12	--	--	--	--	--
13	1.55, s	1.55, s	1.55, s	1.55, s	1.55, s
14	1.62, s	1.62, s	1.62, s	1.62, s	1.62, s
15	1.15, s	1.15, s	1.15, s	1.15, s	1.14, s
1′	--	--	--	--	--
2′	8.08, d (8.0)	8.12, d (8.0)	8.57, t	8.39, d (7.1)	8.35, d (8.0)
3′	4.32, dd (8.0, 6.3)	4.43, m	3.86, d (5.8)	4.37, dq (7.3, 7.1)	4.48, m
4′	--	--	--	--	--
5′	4.01, dq (6.8, 6.3)	3.76, m		1.36, d (7.3)	2.92, m
					3.00, dd (14.0, 4.5)
6′	1.16, d (6.8)				--
7′					7.06, d (8.4)
8′					6.62, d (8.4)
9′					--
10′					6.62, d (8.4)
11′					7.06, d (8.4)

Measured in DMSO-d_6. δ values are given in ppm.

*These two samples contain impurity.

Table S3. ^{1}H NMR data of compounds **6-10**.

Position	6	7	8	9	10
1	--	--	--	--	--
2	--	--	--	--	--
3	3.74, dd (7.9, 5.0)	3.72, dd (7.9, 5.0)	3.73, dd (7.9, 5.0)	3.72, dd (7.9, 5.0)	3.73, brt (6.5)
4	2.67, dd (16.7, 7.9)	2.64, dd (16.7, 7.9)	2.67, dd (16.7, 7.9)	2.65, dd (16.7, 7.9)	2.67, dd (16.7, 7.9)
	2.94, dd (16.7, 5.0)	2.90, dd (16.7, 5.0)	2.94, dd (16.7, 5.0)	2.91, dd (16.7, 5.0)	2.94, dd (16.7, 4.9)
4a	--	--	--	--	--
5	7.66, brs	7.57, brs	7.66, brs	7.56, brs	7.65, brs
6	--	--	--	--	--
7	7.62, dd (8.5, 1.8)	7.55, dd (8.5, 2.0)	7.61, brd (8.6)	7.53, dd (8.4, 2.0)	7.61, brd (8.6)
8	6.74, d (8.5)	6.73, d (8.5)	6.75, d (8.6)	6.74, d (8.4)	6.76, d (8.6)
8a	--	--	--	--	--
9	1.58, m	1.57, m	1.58, m	1.57, m	1.58, m
10	2.09, m	2.07, m	2.09, m	2.07, m	2.09, m
11	5.09, t (7.0)	5.09, t (7.0)	5.09, t (7.0)	5.09, t (7.0)	5.09, t (7.0)
12	--	--	--	--	--
13	1.55, s	1.54, s	1.55, s	1.54, s	1.55, s
14	1.62, s	1.62, s	1.62, s	1.62, s	1.62, s
15	1.15, s	1.14, s	1.15, s	1.14, s	1.15, s
1′	--	--	--	--	--
2′	8.12, d (8.0)	8.35, d (8.0)	8.13, d (8.0)	8.43, d (8.0)	8.31, d (7.8)
3′	4.25, t (7.6)	4.62, m	4.29, t (7.6)	4.57, m	4.40, m
4′	--	--	--	--	--
5′	2.15, m	3.17, dd (14.8, 9.8)	1.91, m	3.04, dd (14.0, 10.0)	1.54
		3.26, dd (14.8, 4.5)		3.15, dd (14.0, 4.5)	1.74, brs
6′	0.95, d (6.8)	--	0.90, d (6.8)	--	1.66, m
7′	0.93, d (6.8)	7.17, d (2.0)	1.25, m	7.24-7.29	0.90, d (6.5)
			1.49, m		
8′		10.79, brs	0.85, t (7.4)	7.24-7.29	0.85, d (6.5)
9′		--		7.16, t (7.6)	
10′		7.30, d (8.0)		7.24-7.29	
11′		7.04, t (7.5)		7.24-7.29	
12′		6.97, t (7.5)			
13′		7.58, d (8.0)			
14′		--			

Measured in DMSO-d_6. δ values are given in ppm.

Table S4. ^{13}C NMR data of compounds **1**-**5**.

Position	1	2*	3*	4	5
1	--	--	--	--	--
2	79.3, C	79.3, C	79.3, C	79.3, C	79.3, C
3	65.9, CH	65.9, CH	65.8, CH	65.9, CH	65.8, CH
4	30.8, CH_2	30.8, CH_2	30.8, CH_2	30.8, CH_2	30.8, CH_2
4a	120.1, C	120.0, C	120.1, C	119.9, C	120.0, C
5	129.7, CH	129.5, CH	129.5, CH	129.6, CH	129.6, CH
6	125.6, C	125.5, C	125.4, C	125.4, C	125.4, C
7	127.0, CH	126.8, CH	126.6, CH	126.9, CH	126.7, CH
8	116.2, CH	116.1, CH	116.1, CH	116.1, CH	116.0, CH
8a	155.8, C	155.6, C	155.6, C	155.5, C	155.5, C
9	37.5, CH_2	37.5, CH_2	37.5, CH_2	37.5, CH_2	37.5, CH_2
10	21.2, CH_2	21.1, CH_2	21.1, CH_2	21.1, CH_2	21.1, CH_2
11	124.4, CH	124.3, CH	124.3, CH	124.3, CH	124.3, CH
12	130.9, C	130.8, C	130.8, C	130.8, C	130.8, C
13	17.5, CH_3	17.5, CH_3	17.4, CH_3	17.4, CH_3	17.4, CH_3
14	25.5, CH_3	25.5, CH_3	25.5, CH_3	25.4, CH_3	25.5, CH_3
15	18.3, CH_3	18.3, CH_3	18.3, CH_3	18.2, CH_3	18.3, CH_3
1′	166.0, C	166.0, C	166.1, C	165.7, C	165.9, C
2′	--	--	--	--	--
3′	59.1, CH	55.5, CH	41.1, CH_2	48.0, CH	54.4, CH
4′	172.3, C	172.1, C	171.5, C	174.4, C	173.5, C
5′	66.7, CH	61.3, CH_2		16.9, CH_3	35.5, CH_2
6′	20.2, CH_3				128.2, C
7′					129.9, CH
8′					114.9, CH
9′					155.8, C
10′					114.9, CH
11′					129.9, CH

Measured in DMSO-d_6. δ values are given in ppm.

*These two samples contain impurity.

Table S5. ^{13}C NMR data of compounds **6-10**.

Position	6	7	8	9	10
1	--	--	--	--	--
2	79.3, C	79.3, C	79.3, C	79.3, C	79.3, C
3	65.9, CH	65.9, CH	65.9, CH	65.8, CH	65.9, CH
4	30.8, CH_2	30.8, CH_2	30.8, CH_2	30.8, CH_2	30.8, CH_2
4a	119.9, C	120.0, C	119.9, C	120.0, C	120.0, C
5	129.7, CH	129.6, CH	129.7, CH	129.5, CH	129.6, CH
6	125.6, C	125.5, C	125.5, C	125.4, C	125.5, C
7	127.1, CH	126.8, CH	127.1, CH	126.7, CH	126.9, CH
8	116.0, CH	116.0, CH	116.0, CH	116.0, CH	116.0, CH
8a	155.5, C	155.6, C	155.5, C	155.6, C	155.5, C
9	37.5, CH_2	37.5, CH_2	37.5, CH_2	37.4, CH_2	37.5, CH_2
10	21.1, CH_2	21.1, CH_2	21.1, CH_2	21.1, CH_2	21.1, CH_2
11	124.3, CH	124.3, CH	124.3, CH	124.3, CH	124.3, CH
12	130.8, C	130.8, C	130.8, C	130.8, C	130.8, C
13	17.5, CH_3	17.5, CH_3	17.5, CH_3	17.4, CH_3	17.5, CH_3
14	25.4, CH_3	25.5, CH_3	25.4, CH_3	25.4, CH_3	25.4, CH_3
15	18.3, CH_3	18.3, CH_3	18.3, CH_3	18.3, CH_3	18.3, CH_3
1′	166.4, C	165.9, C	166.2, C	165.9, C	166.0, C
2′	--	--	--	--	--
3′	58.2, CH	53.5, CH	57.0, CH	54.1, CH	50.7, CH
4′	173.3, C	173.7, C	173.4, C	173.4, C	174.4, C
5′	29.5, CH	26.7, CH_2	35.7, CH	36.2, CH_2	39.2, CH_2
6′	19.3, CH_3	110.5, C	15.6, CH_3	138.3, CH	24.5, CH
7′	18.8, CH_3	123.5, CH	25.1, CH_2	128.2, CH	23.0, CH_3
8′		--	11.0, CH_3	129.0, CH	21.1, CH_3
9′		136.1, C		126.3, CH	
10′		111.4, CH		129.0, CH	
11′		120.9, CH		128.2, CH	
12′		118.3, CH			
13′		118.2, CH			
14′		127.2, C			

Measured in DMSO-d_6. δ values are given in ppm.

Table S6. Strain and plasmid information.

Strain	Description	Source/reference
E. coli DH5α	General cloning host	Takara
E. coli Rosetta(DE3)	Host for expression of proteins	Takara
Streptomyces xiamenensis 318	Used for extracting genome DNA for *ximA*	Reference[15]
rL185A	*E. coli* Rosetta(DE3) containing L185A	This study
rF244A	*E. coli* Rosetta(DE3) containing F244A	This study
rF270A	*E. coli* Rosetta(DE3) containing F270A	This study
rT295A	*E. coli* Rosetta(DE3) containing T295A	This study
rV304A	*E. coli* Rosetta(DE3) containing V304A	This study
rF201A	*E. coli* Rosetta(DE3) containing F201A	This study
rY296A	*E. coli* Rosetta(DE3) containing Y296A	This study
rT299A	*E. coli* Rosetta(DE3) containing T299A	This study
rD375A	*E. coli* Rosetta(DE3) containing D375A	This study
rR390A	*E. coli* Rosetta(DE3) containing R390A	This study
rK492A	*E. coli* Rosetta(DE3) containing K492A	This study
rF201C	*E. coli* Rosetta(DE3) containing F201C	This study
rF201M	*E. coli* Rosetta(DE3) containing F201M	This study
rF201N	*E. coli* Rosetta(DE3) containing F201N	This study
rF201Q	*E. coli* Rosetta(DE3) containing F201Q	This study
rF201S	*E. coli* Rosetta(DE3) containing F201S	This study
rF201T	*E. coli* Rosetta(DE3) containing F201T	This study
Plasmid	Description	Source
pET28a	*kan*, P_{T7}, His-tag	Novagen
pL185A	pET28a derivative carrying *L185A*	This study
pF244A	pET28a derivative carrying *F244A*	This study
pF270A	pET28a derivative carrying *F270A*	This study
pT295A	pET28a derivative carrying *T295A*	This study

pV304A	pET28a derivative carrying *V304A*	This study
pF201A	pET28a derivative carrying *F201A*	This study
pY296A	pET28a derivative carrying *Y296A*	This study
pT299A	pET28a derivative carrying *T299A*	This study
pD375A	pET28a derivative carrying *D375A*	This study
pR390A	pET28a derivative carrying *R390A*	This study
pK492A	pET28a derivative carrying *K492A*	This study
pF201C	pET28a derivative carrying *F201C*	This study
pF201M	pET28a derivative carrying *F201M*	This study
pF201N	pET28a derivative carrying *F201N*	This study
pF201Q	pET28a derivative carrying *F201Q*	This study
pF201S	pET28a derivative carrying *F201S*	This study
pF201T	pET28a derivative carrying *F201T*	This study

Table S7. Synthetic primers for cloning and site-specific mutation of XimA.

Primers	Sequence (5'-3', the mutated codons are underlined)
XimA-F	CGCGGATCCATGCGTCAGGAACATCGTGTCGAC (BamHI)
XimA-R	CGCAAGCTTTTAAGTGCGTGGAGCATTAGAAGC (HindIII)
L185A-F	CGTGCACCAGGTGCGGTTTCTGGTCCGGAT
L185A-R	ATCCGGACCAGAAACCGCACCTGGTGCACG
F244A-F	GTGACCGTTCTGGCTGCTCAGCCGTCCTTT
F244A-R	AAAGGACGGCTGAGCAGCCAGAACGGTCAC
F270A-F	GTTCGCCAGGCAGCTTGCGCAGGTGAAGTA
F270A-R	TACTTCACCTGCGCAAGCTGCCTGGCGAAC
T295A-F	CGTCTGCTGAACGCCTACGGTACGACCGAA
T295A-R	TTCGGTCGTACCGTAGGCGTTCAGCAGACG
V304A-F	GAAGCAGGTGCCGCAGCTGTAGGCCCACCT
V304A-R	AGGTGGGCCTACAGCTGCGGCACCTGCTTC

F201A-F	TCTCGTATGTACGCCGTGGGTGGTCTGTCT
F201A-R	AGACAGACCACCCACGGCGTACATACGAGA
Y296A-F	CGTCTGCTGAACACCGCCGGTACGACCGAA
Y296A-R	TTCGGTCGTACCGGCGGTGTTCAGCAGACG
T299A-F	ACCTACGGTACGGCCGAAGCAGGTGCCGTA
T299A-R	TACGGCACCTGCTTCGGCCGTACCGTAGGT
D375A-F	TGGTGGCCAACTGGCGCTCTGGCGTCTATC
D375A-R	GATAGACGCCAGAGCGCCAGTTGGCCACCA
R390A-F	GTACACGCGCATGGTGCTCTGGACGATATT
R390A-R	AATATCGTCCAGAGCACCATGCGCGTGTAC
K492A-F	AACGGCAATGGCGCACTGCTGCGTCGCGTT
K492A-R	AACGCGACGCAGCAGTGCGCCATTGCCGTT
F201C-F	TCTCGTATGTACTGCGTGGGTGGTCTGTCT
F201C-R	AGACAGACCACCCACGCAGTACATACGAGA
F201M-F	TCTCGTATGTACATGGTGGGTGGTCTGTCT
F201M-R	AGACAGACCACCCACCATGTACATACGAGA
F201N-F	TCTCGTATGTACAACGTGGGTGGTCTGTCT
F201N-R	AGACAGACCACCCACGTTGTACATACGAGA
F201Q-F	TCTCGTATGTACCAAGTGGGTGGTCTGTCT
F201Q-R	AGACAGACCACCCACTTGGTACATACGAGA
F201S-F	TCTCGTATGTACTCCGTGGGTGGTCTGTCT
F201S-R	AGACAGACCACCCACGGAGTACATACGAGA
F201T-F	TCTCGTATGTACACCGTGGGTGGTCTGTCT
F201T-R	AGACAGACCACCCACGGTGTACATACGAGA
N490A-F	CTGCCACGTAACGGCGCTGGCAAACTGCTG
N490A-R	CAGCAGTTTGCCAGCGCCGTTACGTGGCAG

Reference

(1) McQuade, T. J.; Shallop, A. D.; Sheoran, A.; DelProposto, J. E.; Tsodikov, O. V.; Garneau-Tsodikova, S. *Anal. Biochem.* **2009,** *386*, 244-250.
(2) Kumar, S.; Stecher, G.; Tamura, K. *Mol. Biol. Evol.* **2016,** *33*, 1870-1874.
(3) Zhang, H. K.; Gao, S. H.; Lercher, M. J.; Hu, S. N.; Chen, W. H. *Nucleic Acids Res.* **2012,** *40*, W569-W572.
(4) Waterhouse, A.; Bertoni, M.; Bienert, S.; Studer, G.; Tauriello, G.; Gumienny, R.; Heer, F. T.; de Beer, T. A. P.; Rempfer, C.; Bordoli, L.; Lepore, R.; Schwede, T. *Nucleic Acids Res.* **2018,** *46*, W296-W303.
(5) Thornburg, C. K.; Wortas-Strom, S.; Nosrati, M.; Geiger, J. H.; Walker, K. D. *Biochemistry* **2015,** *54*, 6230-6242.
(6) Morris, G. M.; Huey, R.; Lindstrom, W.; Sanner, M. F.; Belew, R. K.; Goodsell, D. S.; Olson, A. J. *J. Comput. Chem.* **2009,** *30*, 2785-2791.
(7) Van der Spoel, D.; Lindahl, E.; Hess, B.; Groenhof, G.; Mark, A. E.; Berendsen, H. J. C. *J. Comput. Chem*. **2005,** *26*, 1701-1718.
(8) Hornak, V.; Abel, R.; Okur, A.; Strockbine, B.; Roitberg, A.; Simmerling, C. *Proteins* **2006,** *65*, 712-725.
(9) Wang, J. M.; Wolf, R. M.; Caldwell, J. W.; Kollman, P. A.; Case, D. A. *J. Comput. Chem*. **2004,** *25*, 1157-1174.
(10) Case, D. A.; Cheatham, T. E.; Darden, T.; Gohlke, H.; Luo, R.; Merz, K. M.; Onufriev, A.; Simmerling, C.; Wang, B.; Woods, R. J. *J. Comput. Chem.* **2005,** *26*, 1668-1688.
(11) Berendsen, H. J. C.; Postma, J. P. M.; van Gunsteren, W. F.; Hermans, J. *Dordrecht* **1981,** 331-342.
(12) Essmann, U.; Perera, L.; Berkowitz, M. L.; Darden, T.; Lee, H.; Pedersen, L. G. *J. Chem. Phys.* **1995,** *103*, 8577-8593.
(13) Hess, B.; Bekker, H.; Berendsen, H. J. C.; Fraaije, J. *J. Comput. Chem.* **1997,** *18*, 1463-1472.
(14) Bussi, G.; Donadio, D.; Parrinello, M. *J. Chem. Phys.* **2007,** *126*, 7.
(15) Xu, J.; Wang, Y.; Xie, S. J.; Xu, J.; Xiao, J.; Ruan, J. S. *Int. J. Syst. Evol. Microbiol.* **2009,** *59*, 472-476.